MASTER

A new regenerator for a Stirling cryocooler

Dolmans, P.C.

Award date:
2005

A NEW REGENERATOR FOR A STIRLING CRYOCOOLER

P.C. Dolmans
July 2005

A NEW REGENERATOR FOR A STIRLING CRYOCOOLER

P.C. Dolmans
July 2005

Under supervision of:
Ir. D.W.J. Willems (Stirling Cryogenics & Refrigeration BV)
Prof. Dr. A.T.A.M. de Waele (Eindhoven University of Technology)

Summary

Stirling Cryogenics & Refrigeration BV produces cryocoolers, based on the Stirling cycle. The heart of these cryocoolers is the regenerator in which heat is stored and released during the cycle. The current regenerator consists of stacked stainless steel screens. The goal of this research is to improve this regenerator. Improvement can be either a better performance or a reduction in production costs.

An alternative for the screen regenerator is a regenerator of sintered stainless steel particles. Two different sintered materials are tested in a so-called Stirling Economy machine. The main difference between the two materials is the particle size. The minimum temperature and the cooling power at different temperatures are determined.

Compared to the screens, the cooling power of the Economy at 77 K is 30-40 % less with the sintered materials. The efficiency is 50 % less. The difference in performance between the two sintered materials is only small. A regenerator with a combination of the different sintered materials delivers a comparable cooling power with a slightly higher efficiency.

The pressure drop across the regenerator is significantly higher with the sintered materials. This is the main reason for the lower performance of the sintered materials compared to the screens. The pressure drop is higher in these materials because non-linear effects play a much larger role than in a regenerator with stacked screens.

A direct replacement of the screen regenerator by a regenerator of sintered material does not give the same performance, but first results are hopeful. For an improved performance with the sintered materials, the regenerator geometry has to be further optimized.

A powerful design tool for the machine and all its components, is the Stirling model. This model combines theory with empirical coefficients for flow resistance, heat exchange, and heat conduction. In this research an approach is found to model the sintered metal materials.

Based on the Stirling model and on minimization of entropy production, combined with recent literature, some opportunities for regenerator improvement are discovered. A suggestion to improve the performance is to create a regenerator with perforated plates or cylindrical tubes. Another way is to create a regenerator with smaller flow channels at the cold side and larger flow channels at the warm side. None of these suggestions have been tested.

Another recommendation for the future is to test a regenerator in which the screens are rolled instead of stacked. Assumed is that the performance will be the same, but production costs will be reduced significantly.

Pier Dolmans / July 2005

Preface

"We will show practically that bundles of wire are capable of exerting more force than shiploads of coal" John Ericsson 1855

The quote above is a first recognition of the value a regenerator can have for a Stirling type machine. Its capability to store great amounts of heat significantly improves the performance of the machine. Therefore the regenerator is the heart of the machine. The goal of this research is to improve this heart of the machine, a beautiful challenge.

This research is my graduation project at the Eindhoven University of Technology (TU/e). The research is performed at Stirling Cryogenics & Refrigeration BV, Worlds largest producer of Stirling type cryocoolers. I would like to thank all the people at Stirling for the great support they have given me during my 10 months of research. Special thanks for Daniel Willems who has guided me during the whole period of my research. The research is supported by the Low Temperature group of the department of Applied Physics at the TU/e. Therefore I would also like to thank the people of this group for the great cooperation. Special thanks for professor De Waele for his great support and his sharp view.

Some of the information in the original report is confidential. In this version of my report, all confidential information is left out.

Pier Dolmans / July 2005

Index

1 Introduction

1.1 Stirling Cryogenics & Refrigeration BV

The main activity of Stirling Cryogenics & Refrigeration BV (Stirling) is finding innovative solutions to cool down gasses and fluids to temperatures as low as 20 K. For this purpose Stirling has developed high quality refrigeration systems to liquefy gasses and to cool down gasses, fluids and complete processes. The central element in all plants developed by Stirling is the Stirling cryogenerator, operating according to the principles of the Stirling cycle.
Stirling has installed over 4000 systems worldwide. The systems are used in artificial insemination centers, high temperature superconductivity laboratories, process industry, hospitals, observatories, amusement parks, at universities and for many other purposes.
Stirling develops and assembles standard as well as custom made systems. After production, Stirling installs the systems at location and takes care of the maintenance service. In 1998 cryogenic know-how is combined in the Stirling Consulting Group. This business unit supports companies with engineering consultancy in the fields of thermodynamics, mechanics and fluid dynamics.
Stirling has over 50 years of experience in developing cryogenic systems, before 1990 under the wings of "Nederlandse Philips Bedrijven BV", afterwards as a company on its own. More information about the activities of Stirling Cryogenics & Refrigeration BV can be found on: www.Stirling.nl

1.2 The regenerator as the heart of the Stirling cryogenerator

As stated before, the Stirling cryogenerator operates according to the principles of the Stirling cycle. The Stirling cycle involves alternately compressing and expanding a fixed quantity of a (nearly ideal) gas in a closed cycle. The compression takes place at room temperature and the expansion is performed at the required low temperature. Compression and expansion take place in different spaces of the Stirling cryogenerator. The ideal Stirling cycle comprises four phases:

1) Isothermal compression
2) Isochoric displacement and cooling
3) Isothermal expansion
4) Isochoric displacement and re-heating

During phase 1 the heat generated by the compression is taken out of the cycle by a heat exchanger (cooler) to keep it isothermal. During phase 2 the volume is kept constant (isochoric) and the gas is pushed through a regenerator by a displacer. During this phase heat is stored in the regenerator material (matrix). Phase 3 is the phase during which the actual cold production takes place by expanding the gas in the cold volume. The cold produced is taken out of the cycle by a second heat exchanger and during phase 4 (isochoric) the gas is pushed back through the regenerator and takes up the stored heat again.

The heart of the Stirling cryogenerator is the regenerator in which heat is stored during one half of the cycle and is released during the other half. The performance of the machine is mainly dependent on the quality of the regenerator. The thermodynamic and hydrodynamic properties of a regenerator usually are extremely complicated. In its most extreme form in an ideal regenerator:

1) The heat capacity of the matrix is infinite.
2) The heat contact between the gas and the matrix is perfect.
3) The gas in the regenerator is an ideal gas.
4) The flow resistance of the matrix is zero.
5) The axial thermal conductivity (through the matrix and the gas) is zero.

In practice none of these requirements can be fulfilled completely. To get the best performance, a regenerator is needed that combines approaches to these requirements in the best possible way.

The current regenerator used by Stirling, is a regenerator filled with stacked screens. The purpose of this research is to improve the current regenerator. This improvement can be a better performance of the machine, or a significant reduction of the production costs of the regenerator. First in section 2 more information is presented about the physical principles of the Stirling cycle and the regenerator. Section 3 gives an overview of recent developments in regenerator technology and possibilities for improvement of the current regenerators used in the Stirling cryogenerators. To model the complete machine and its individual components, the Stirling model has been developed. In section 4 this powerful design tool will be described. With the Stirling model and by minimizing the total entropy production, design calculations are performed for possible new regenerator geometries and materials. This is presented in section 5. Tests are performed with a new type of regenerator, made of sintered stainless steel particles. In section 6 the experimental setup for these tests is described. The results of the tests are presented in section 7. Finally, in section 8 the conclusions from this research are presented and recommendations for the future are given.

2 Theory

2.1 The ideal Stirling cycle

A so-called Stirling cooler operates according to the principles of the Stirling cycle. Gas is compressed at room temperature and expanded at a low temperature where the actual cooling of an application takes place. An ideal Stirling cooler is presented schematically in figure 2.1.

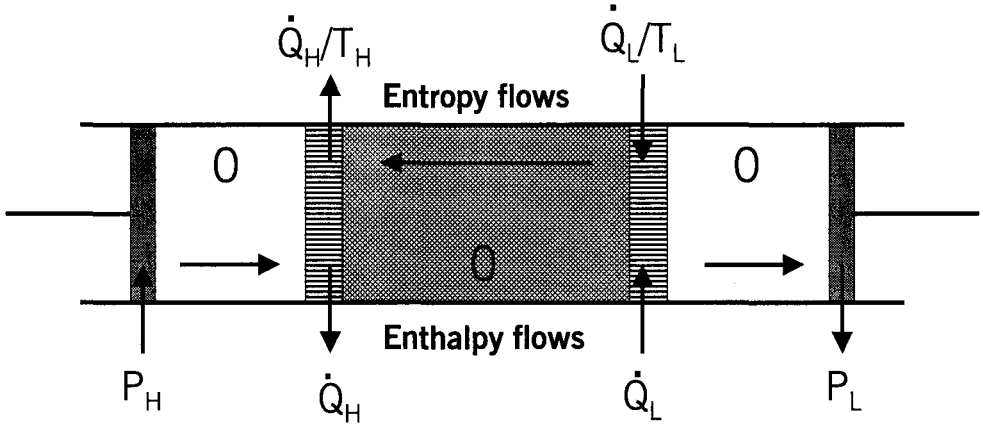

Figure 2.1: *Schematic picture of an ideal Stirling cooler. From left to right, the system comprises one piston at room temperature (T_H), a compression space, a warm heat exchanger, a regenerator, a cold heat exchanger, an expansion space, and a piston at low temperature (T_L). Also shown are the average entropy and enthalpy flows through the system during one operating cycle.*

The ideal Stirling cooler can be divided into three parts:

1) A piston at room temperature (warm piston), a compression space and a warm heat exchanger. In this part of the cooler the compression of the gas takes place. The thermal contact with the surroundings at temperature T_H is supposed to be ideal so the compression is isothermal.

2) An ideal regenerator which can store heat from the gas during one half of the Stirling cycle and can give back the same amount of heat during the other half of the cycle. The requirements for an ideal regenerator are presented in section 1.2.

3) A cold heat exchanger, an expansion space and a piston at low temperature (cold piston). In this part of the cooler the expansion of the gas takes place and the work performed on the cold piston during this expansion is supposed to be recovered. The thermal contact with the application at temperature T_L is supposed to be ideal so the expansion is isothermal.

An ideal Stirling cycle during steady state, can be divided into four phases that are schematically presented in figure 2.2a. Figure 2.2b is a pV-diagram of an ideal Stirling cycle. The four individual phases are described below:

1) Isothermal compression. The warm piston moves to the right and an amount of work P_H is performed on the gas. The cold piston is kept at the same position, in contact with the regenerator, so all of the compression takes place in the compression space.

The process is isothermal so an amount of heat Q_H is given off to the surroundings through the warm heat exchanger.

2) Isochoric displacement and cooling. Both pistons move to the right and the gas is forced to pass the regenerator. The total gas volume remains constant. During this phase, heat is stored in the regenerator. The gas enters the regenerator at room temperature T_H and leaves it at the low temperature T_L.

3) Isothermal expansion. The gas expands and the cold piston moves to the right. The warm piston is kept at the same position, in contact with the regenerator, so all of the expansion takes place in the expansion space. The process is isothermal so an amount of heat Q_L is taken up from the application. The work P_L exerted on the cold piston during this phase is recovered.

4) Isochoric displacement and re-heating. Both pistons move to the left and the gas is forced back through the regenerator. During this phase heat is taken up from the regenerator. The gas enters the regenerator at the low temperature T_L and leaves it at room temperature T_H. At the end of this phase the state is the same as at the start of phase 1.

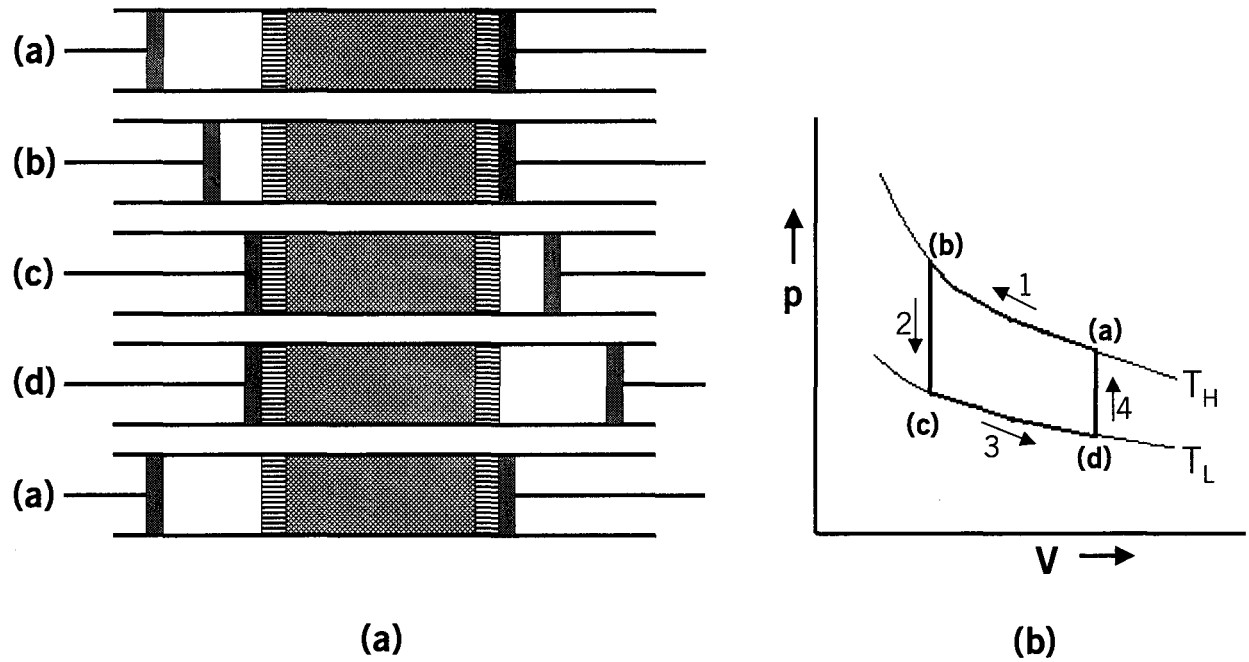

(a) (b)

Figure 2.2 a: *The four phases of an ideal Stirling cycle: Isothermal compression (a to b), isochoric displacement and cooling (b to c), isothermal expansion (c to d), and isochoric displacement and re-heating (d to a).*
Figure 2.2b: *The four phases (1 to 4) of an ideal Stirling cycle presented in a pV-diagram.*

The ideal Stirling cycle can be described by the first and second law of thermodynamics,

$$\dot{U} = \sum_k \dot{Q}_k + \sum_k \overset{*}{\dot{H}}_k - \sum_k p_k \dot{V}_k + P \quad \text{and} \tag{2.1}$$

$$\dot{S} = \sum_k \frac{\dot{Q}_k}{T_k} + \sum_k \overset{*}{\dot{S}}_k + \sum_k \dot{S}_{ik} \; ; \quad \dot{S}_{ik} \geq 0 . \tag{2.2}$$

In equation 2.1 (first law), U is the internal energy of the system. Q_k are amounts of heat transferred to and from the system at the different boundaries of the system, labeled with index "k". Heat flows are counted positive if heat flows from outside into the system. H_k is the enthalpy of the mass flows into the system. The third term on the right represents the work exerted on the system due to a change in volume. Finally, P takes into account all other forms of work done on the system by its environment. A dot ($\dot{}$) on top of a symbol means the rate of change of that property and an asterisk (*) means the flow into the system. In equation 2.2 (second law), S is the total entropy of the system. T_k represent the temperatures at which the heat flows enter or leave the system and S_{ik} are the irreversible entropy production rates inside the system.

If the ideal Stirling cycle is considered for the different parts of the ideal Stirling cooler (steady state, time averaged values), the first law reduces to

$$P_H = \dot{Q}_H , \tag{2.3}$$

for the system consisting of the warm piston, the compression space and the warm heat exchanger. For the system consisting of the cold heat exchanger, the expansion space and the cold piston, the first law reduces to

$$P_L = \dot{Q}_L . \tag{2.4}$$

The enthalpy flow through an ideal regenerator is zero. In an ideal regenerator no irreversible processes take place, so the entropy production inside an ideal regenerator is zero. The second law for the ideal Stirling cooler reduces to

$$\frac{\dot{Q}_H}{T_H} = \overset{*}{\dot{S}}_r = \frac{\dot{Q}_L}{T_L} . \tag{2.5}$$

In equation 2.5, S_r is the entropy flow through the regenerator. The entropy and enthalpy flows in an ideal Stirling cycle are presented in figure 2.1. If equations 2.3 to 2.5 are combined, this results in the following coefficient of performance (*COP*) that equals the Carnot *COP*:

$$COP = \frac{\dot{Q}_L}{P} = \frac{T_L}{T_H - T_L} . \tag{2.6}$$

In deriving equation 2.6 it is assumed that the power exerted by the gas on the cold piston is recovered, so total power consumption of the system $P = P_H - P_L$. The descriptions given in this section are based on [1].

2.2 The real Stirling cycle

The cold piston as described in the previous section is not very practical and in many coolers (also at Stirling) it is avoided by using a displacer instead of a cold piston. A displacer is a piston which function is to move the gas back and forth between the cold and the warm end of the cooler. Its motion is synchronized with the motion of the piston and is typically 90° out of phase. The idealized displacer type Stirling cycle is represented schematically in figure 2.3.

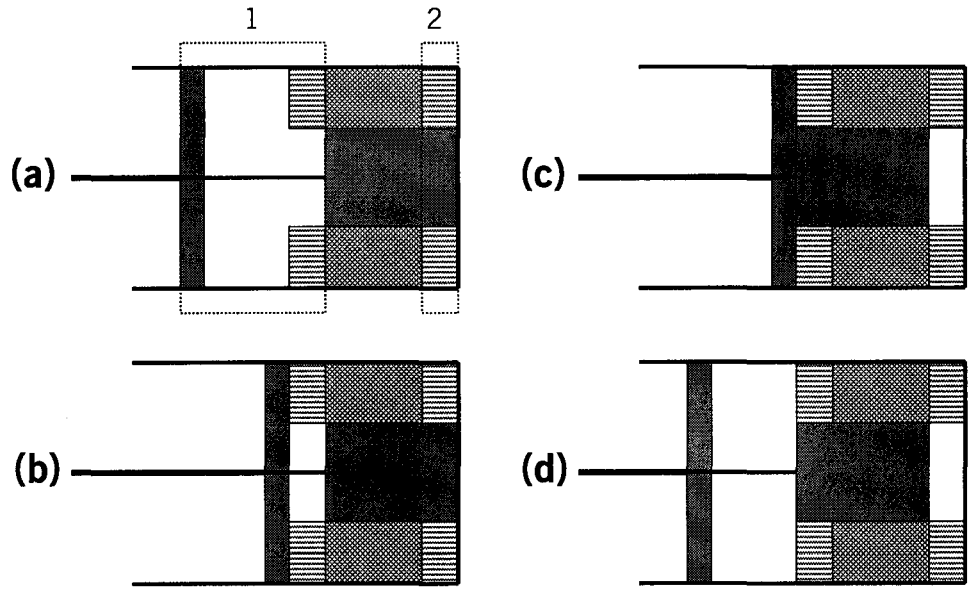

Figure 2.3: *The four phases of a displacer type Stirling cycle: Isothermal compression (a to b), isochoric displacement and cooling (b to c), expansion (c to d,) and isochoric displacement and re-heating (d to a). During isothermal expansion part of the gas already flows through the regenerator to the warm end of the cooler, reducing the maximum cooling power.*

Again the idealized Stirling cycle can be divided into four phases, starting with all of the gas in the compression space at room temperature. Schematically this is represented in figure 2.3.

1) Isothermal compression. An amount of work P_H is performed on the piston and it moves to the right while the position of the displacer is fixed. To get isothermal compression, an amount of heat Q_H is given off to the surroundings at the warm heat exchanger.

2) Isochoric displacement and cooling. The displacer moves to the left while the position of the piston is fixed. The gas is forced through the regenerator, giving off a certain amount of heat. The gas enters the regenerator from the left at room temperature T_H and leaves it at the right at the low temperature T_L.

3) Expansion. The piston moves to the left while the position of the displacer is fixed. The gas expands isothermally, so heat Q_L is taken up from the application. In contrast with the two-piston system described in section 2.1, not all the expansion of the gas takes place in the expansion space. Part of the gas flows back through the regenerator to the compression space, taking up heat from the regenerator. There it expands isothermally, taking up heat from the warm heat exchanger, reducing the net amount of heat Q_H given off to the surroundings at this location.

4) Isochoric displacement and re-heating. The displacer moves to the right while the position of the piston is fixed. The cold gas is forced to pass the regenerator, taking up the rest of the stored heat. The gas enters the regenerator at the low temperature T_L and leaves it at room temperature T_H. At the end of this phase, the state is the same as at the start of phase 1.

Starting again with the first law (equation 2.1) in steady state, it reduces to

$$P_H = \dot{Q}_H - \overset{*}{H}_D \tag{2.7}$$

for the system consisting of the warm piston, the compression space and the warm heat exchanger (indicated with "1" in figure 2.3). For the system consisting of the cold heat exchanger and the expansion space (indicated with "2" in figure 2.3), the first law reduces to

$$\dot{Q}_L = \overset{*}{H}_D . \tag{2.8}$$

Because the enthalpy flow through an ideal regenerator is zero, an enthalpy flow through the displacer (H_D) has to be introduced in equation 2.7 and 2.8 to fulfill the first law. In an ideal regenerator no irreversible processes take place, so the entropy production inside an ideal regenerator is zero. The second law for the ideal displacer Stirling cooler reduces to

$$\frac{\dot{Q}_H}{T_H} = \overset{*}{S}_r = \frac{\dot{Q}_L}{T_L} . \tag{2.9}$$

If equations 2.7 to 2.9 are combined, the *COP* again equals Carnot (equation 2.6).

In a real Stirling cooler, the movement of the piston and the displacer is not divided into discrete steps. A typical movement is a sinusoidal movement in which the displacer is out of phase with the piston at a fixed angle. Therefore the compression does not take place completely in the compression space, nor does the expansion take place completely in the expansion space. This causes that less heat Q_L is taken up from the cold heat exchanger during one cycle than in the ideal case, giving a lower cooling power. The influence of a non-ideal regenerator is discussed in the next section.

2.3 The regenerator

Introduction

Most commonly used in Stirling coolers are regenerator matrices made of stacks of metal screens or small metal spheres packed together. Typical wire sizes of the screens are 25-50 μm, with aperture widths of 50-100 μm. The spheres have typical diameters of 100-200 μm. One characteristic of a regenerator matrix is the filling factor f, defined as the ratio of the volume occupied by the matrix material to the total volume of the regenerator. Because the flow channels through a matrix of screens or spheres are not uniform, a characteristic measure for the diameter of the flow channels has to be defined. This measure is called the hydraulic diameter d_h, which for a porous medium is defined as

$$d_h = \frac{4(1-f)}{F}. \tag{2.10}$$

In equation 2.10, F is the heat-exchanging surface of the matrix per unit of volume. For perfectly stacked screens with wire diameter d_w, d_h is given by

$$d_h = \frac{(1-f)d_w}{f}. \tag{2.11}$$

A real regenerator does not satisfy the requirements of the ideal regenerator mentioned in section 1.2, so entropy is produced inside the regenerator. Making use of the definitions of f, d_h and F, the entropy production in a non-ideal regenerator can be described.

Entropy production

In a non-ideal regenerator, a net enthalpy flow takes place through the regenerator, reducing the *COP* of the cooler. The enthalpy flow is caused by the imperfect heat exchange between gas and matrix and the finite heat capacity of the matrix. Therefore the temperature of the gas flowing through the regenerator during the second phase of the cycle has a higher temperature than the matrix and the gas flowing back during the fourth phase has a lower temperature than the matrix, causing a net enthalpy flow during each cycle [2].
Besides this, in a non-ideal regenerator entropy is produced. Four different irreversible processes cause this entropy production: axial thermal conduction through the gas, axial thermal conduction through the matrix, flow resistance of the matrix, and imperfect heat exchange between the gas and the matrix. The rest of this section will be focused on the different entropy production terms given in equation 2.12 to 2.15 [3]:

$$\frac{d\dot{S}_{cg}}{dl} = (1-f)A_r \frac{N_u \lambda_g}{T_g^2}\left(\frac{dT_g}{dl}\right)^2 \quad \text{(conduction through the gas)}, \tag{2.12}$$

$$\frac{d\dot{S}_{cm}}{dl} = fA_r \frac{C_k \lambda_m}{T_r^2}\left(\frac{dT_m}{dl}\right)^2 \quad \text{(conduction through the matrix)}, \tag{2.13}$$

$$\frac{d\dot{S}_f}{dl} = z_r \frac{\eta \overset{*}{n}^2 V_m^2}{A_r T_g} \text{ (flow resistance of the matrix), and} \tag{2.14}$$

$$\frac{d\dot{S}_{hx}}{dl} = \beta A_r \frac{(T_m - T_g)^2}{T_m T_g} \quad \text{(imperfect heat exchange).} \tag{2.15}$$

In equations 2.12 to 2.15, $d\dot{S}/dl$ is the entropy production rate per unit of length; A_r is the cross-sectional area of the regenerator and z_r is the characteristic flow impedance of the matrix. N_u (Nusselt number) is a dimensionless number that is proportional with the convectional heat exchange. The Nusselt number in equation 2.12 is a correction for the effective thermal conduction in the gas. The heat-conduction coefficient in the gas is given by λ_g, λ_m is the heat conduction coefficient of the matrix material and C_k the conduction degradation coefficient of the matrix. T is the local temperature of the gas (g) or the matrix (m), η is the gas viscosity, $\overset{*}{n}$ the molar flow rate and V_m the molar volume of the gas. The volumetric heat exchange parameter β can be written as

$$\beta = \alpha F = F \frac{\lambda_g N_u}{d_h}. \tag{2.16}$$

In Equation 2.16, α is the surface heat exchange coefficient. For stacked screens, cylindrical tubes (d_h = diameter tube) and stacked spheres (diameter d), F is respectively

$$F = 4\frac{(1-f)}{d_h} \tag{2.17a}$$

for screens and tubes and

$$F = 6\frac{f}{d} \tag{2.17b}$$

for spheres.
In [2] an expression is derived for the change of the gas temperature in a regenerator, based on conservation of energy

$$\begin{aligned} \frac{(1-f)}{V_m} C_p \frac{\partial T_g}{\partial t} = &-\frac{\overset{*}{n}}{A_r} C_p \frac{\partial T_g}{\partial l} - \frac{\overset{*}{n}}{A_r}\left(V_m - T_g\left(\frac{\partial V_m}{\partial T_g}\right)_p\right)\frac{\partial p}{\partial l} + \\ &\frac{(1-f)}{V_m} T_g \left(\frac{\partial V_m}{\partial T_g}\right)_p \frac{\partial p}{\partial t} + \beta(T_m - T_g) + \frac{\partial}{\partial l}\left(\lambda_g \frac{\partial T_g}{\partial l}\right) \end{aligned} \tag{2.18}$$

In equation 2.18, C_p is the molar specific heat of the gas. For an ideal gas the pre-factor of the $\partial p/\partial l$ term in equation 2.18 is zero and the pre-factor of $\partial p/\partial t$ is equal to (1-f), which is zero if zero void volume is assumed in the regenerator. With some general assumptions equation 2.18 can be rewritten. These assumptions are: the regenerator material has an infinitely high heat capacity so the matrix temperature is not a function of time, neither is the local gas temperature; T_m is a linear function of length and the axial thermal conduction through the gas is zero. Equation 2.18 can then be simplified to equation 2.19. With equations 2.16 and 2.19,

equation 2.15 for entropy production due to imperfect heat exchange, is written as equation 2.20:

$$(T_m - T_g) = \frac{C_p \overset{*}{n}}{\beta A_r} \cdot \frac{dT_g}{dl}, \tag{2.19}$$

$$\frac{d\dot{S}_{hx}}{dl} = \frac{d_h}{A_r F} \frac{C_p{}^2 \overset{*2}{n}}{\lambda_g N_u T_m T_r} \left(\frac{dT_g}{dl} \right)^2. \tag{2.20}$$

The advantage of equation 2.20 above 2.15 is that the unknown ($T_m - T_g$) term has disappeared. To be able to calculate the different entropy production terms in a regenerator, all the individual parameters have to be determined for the specific regenerator. The Nusselt number is defined as:

$$N_u = \frac{\alpha d_h}{\lambda}. \tag{2.21}$$

If there is no adequate information about α, *Nu* for stacked screens can be approached with [4]

$$N_u = 0.68 R_e{}^{0.6} P_r{}^{0.33}. \tag{2.22}$$

In equation 2.22, R_e and P_r are defined as:

$$R_e = \frac{\rho \bar{v} d_h}{\eta}, \tag{2.23}$$

$$P_r = \frac{\eta \rho}{\lambda}, \tag{2.24}$$

with ρ the density of the gas and $\bar{v}$ the average flow-velocity of the gas.

NPH and NTU related to the entropy production

In literature (for example [5]) dimensionless expressions are commonly used for the pressure drop and heat exchange in a regenerator: *NPH* (Number of Pressure Heads) and *NTU* (Number of Transfer Units) respectively. These expressions are given in equations 2.25 and 2.26 [5]:

$$NPH = \frac{\Delta p}{0.5 \rho \bar{v}^2}, \tag{2.25}$$

$$NTU = \frac{\alpha A_w}{C_p \overset{*}{n}} = \frac{N_u}{R_e Pr} \frac{4L}{d_h}. \tag{2.26}$$

In equation 2.25, Δp is the pressure drop across the regenerator and $\bar{v}$ is the average gas velocity inside the regenerator, given by equation 2.27. In equation 2.26, A_w is the total heat exchanging surface of the matrix.

$$\bar{v} = \frac{V_m \overset{*}{n}}{(1-f)A_r}. \tag{2.27}$$

If there is a temperature gradient across the regenerator, V_m is not constant so an average value should be used. For a regenerator, the total entropy production due to flow resistance is:

$$\dot{S}_f = \frac{\Delta p \overset{*}{V}}{T}. \tag{2.28}$$

In equation 2.28, T is the average temperature of the gas in the regenerator matrix and $\overset{*}{V}$ is the volume flow through the matrix. With equations 2.25 and 2.27 this can be written as

$$\dot{S}_f = NPH \frac{\rho \overset{*}{V}^3}{2TA_r^2(1-f)^2}. \tag{2.29}$$

For a certain volume flow at a certain average temperature, *NPH* has to be reduced to reduce the entropy production due to flow friction.

According to [5], *NTU* can also be written as

$$NTU = \frac{\Delta T}{\Delta T_m}. \tag{2.30}$$

This is because the heat transferred from the fluid to the matrix during one half of the cycle is

$$Q = \overset{*}{n} C_p \Delta T = \alpha A_w \Delta T_m. \tag{2.31}$$

In equations 2.30 and 2.31, ΔT is the total temperature difference across the regenerator ($T_H - T_L$) and ΔT_m is the average temperature difference between the matrix and the gas. From equation 2.15 for the local entropy production due to imperfect heat exchange, the total entropy production can be approximated by equation 2.32 with the assumption that T_m is close tot T_g:

$$\dot{S}_{hx} \cong \beta A_r L \frac{\Delta T_m^{\ 2}}{T^2} = \frac{\dot{Q}_{hx} \Delta T_m}{T^2}. \tag{2.32}$$

In equation 2.32, $\dot{Q}_{hx}$ is the heat exchange rate between the gas and the matrix. If equations 2.30 and 2.32 are combined, equation 2.33 gives a relation between the entropy production due to imperfect heat exchange and *NTU*:

$$\dot{S}_{hx} = \frac{1}{NTU} \frac{\dot{Q}_{hx} \Delta T}{T^2}. \tag{2.33}$$

Equation 2.33 states that for a certain heat exchange rate at a certain average temperature and temperature difference between warm and cold, *NTU* has to be increased to reduce the entropy production due to imperfect heat exchange. In section 3.3 this will be discussed further.

3 Recent developments

3.1 Introduction

In this chapter, recent literature will be reviewed to get an overview of the latest developments in regenerator technology. Because the physical theory about regenerators is very complicated, assumptions have to be made to simplify the theory and to support proposed improvements for the regenerator. Many different sources of literature are used to write the section below so assumptions may differ slightly within this section. First in section 3.2 some information will be given about recent research into the traditional regenerators filled with stacked screens or spherical particles. Section 3.3 will treat some recent developments in using different matrix geometries and in section 3.4 the use of different matrix materials will be described.

3.2 Stacked screen and metal sphere regenerators

Pressure Drop

During the last decades, regenerators for cryocoolers have been studied extensively, either theoretically or experimentally. Theoretical or numerical models of the regenerator involve empirical coefficients based on steady state experimental data. Even though (numerical) models are used in regenerator analysis, the physical phenomenon is still complex and not yet completely understood for oscillating flow and pulsating pressure conditions that occur in actual cryocoolers. Recent work has focused on measuring the regenerator characteristics under real operating conditions to get a clear insight into the physical phenomena of the regenerator [6 - 8]. One of the conclusions is that the friction factor in the regenerator matrix based on steady flow calculations, underestimates the friction factor under real oscillating flow conditions. The lower the cold end temperature of the cryocooler, the larger the difference is. At liquid nitrogen temperatures and an operating frequency of 50 Hz, the value of the cycle-averaged pressure drop in an oscillating flow can be up to 6 times higher than in a steady flow at the same Reynolds number [7]. Also is revealed that the operating frequency has little effect on the pressure drop across the regenerator and that the pressure drop amplitude depends linearly on the mass flow rate at the warm end. On the other hand, phase shift characteristics between the pressure drop and the mass flow rate at the warm end, strongly depend on the oscillatory frequency [6]. Different dimensionless correction formulas are derived for the friction factor and the phase shift in stacked screen regenerators under real operating conditions [7 - 9].

The conclusion from [6 – 9] is that the pressure drop in different regenerators has to be compared under real operating conditions, because of the large difference in behavior between steady and oscillating flows.

Heat Conduction

The optimized design of regenerators takes into account the axial thermal conduction through the matrix. The thermal conduction through matrices of stacked screens and packed spheres can be represented by a thermal conductivity degradation factor [10]. This factor is the ratio of the total matrix axial thermal conductivity to the thermal conductivity of a solid bar of the same material with the same total cross section. The smaller the factor is, the smaller the losses due to axial thermal conduction are in the regenerator. When the gas in the matrix is helium at a pressure of 10 to 25 bar, sintered stainless steel screen matrices (wire thickness of 35.6 μm) are compared to matrices in which the stacked screens are not sintered. Measured conductivity degradation factors of the sintered and non-sintered matrices are 0.18 and 0.12 respectively. The cold end of the regenerator is kept at a temperature of 80 K and the warm end at 300 K. Another type of regenerator that is tested is a regenerator filled with lead spheres (diameter 102 ± 13 μm) that were non-bonded or bonded by an epoxy material. The measured conductivity degradation factors of the bonded and non-bonded matrices are 0.12 and 0.08 respectively. Below 10 bar, measurements as function of the helium gas pressure, indicate that most of the conduction between the individual wires or spheres is through the helium gas within a few microns of the contact point rather than directly through the contact. For pressures below 10 bar and the used sizes of the flow channels between the matrix material, the flow is in the region of molecular flow. The heat transfer in the helium gas is proportional to gas pressure as is the conductivity degradation factor. For helium pressures between 10 and 25 bar, the flow is in the viscous flow region and the heat transfer in the helium gas is not dependent of pressure, neither is the conductivity degradation factor. Bonding the layers by sintering or with a thinned epoxy increases the conduction across the contact points, but this conduction remains small compared to the conduction through the helium gas near the boundary.

The conclusion is that increased conduction caused by bonding or sintering is small enough to not significantly degrade the performance of regenerative cryocoolers under the operating conditions described above.

Performance

A way to determine the performance of a regenerator is to define a regenerator performance factor R_{pf} [11],

$$R_{pf} = \frac{\alpha A_w}{\partial p / \partial x}. \tag{3.1}$$

In equation 3.1, α is the matrix convection coefficient, a measure of the heat exchange between the gas and the matrix; A_w is the total regenerator matrix surface area and $\partial p / \partial x$ is the pressure drop per unit length. For different regenerators the R_{pf} is calculated [11]. Some of the tested regenerators consisted of single screens cut to the regenerator dimensions and then stacked together. Some of them were produced using a new manufacturing technique. Layers of screen are stacked and then bonded by sintering, creating laminates of 20-30 screens. The sintered laminates are cut to the dimensions of the regenerator and are piled up to fill the final regenerator. This significantly reduces the costs of the manufacturing process with respect to stacking individual screens.

From the described tests [11] is concluded that cooling power is linearly dependent on R_{pf}. One of the advantages of piling up the laminates is that the use of laminates with different hydraulic diameters in different temperature regions, might give a better approach of the optimal performance of the regenerator. Another idea to improve the flow and heat exchange characteristics, is to design a regenerator with different cross sections in the different temperature regions [12].

3.3 Different matrix geometries

In addition to a large heat capacity of the matrix material and a small axial thermal conduction of the matrix, good regenerator performance also requires very good heat transfer between the fluid and the matrix and at the same time a low pressure drop across the regenerator. As stated before, these are conflicting requirements. Most present day regenerators consist of beds of spheres or stacked screens. Other geometries like parallel plates, square channels, crossed rods and etched foil are recent developments in regenerator technology. A comparison of the thermal attributes of different heat transfer surfaces shows a large potential to improve traditional regenerators with respect to ratio between pressure drop and heat transfer [5]. To describe the pressure drop in a certain length of the regenerator, the dimensionless term "number of pressure heads" *NPH* is introduced. The quality of heat transfer can be described with the dimensionless principle of "number of transfer units" *NTU* (see also section 2.3). According to [5], the suitability of a geometrical configuration for use in a regenerator can be related to the ratio *NPH/NTU*:

$$\frac{NPH}{NTU} = \frac{C_w R_e P_r}{4 N_u}, \tag{3.2}$$

$$C_w = \frac{2 \Delta p d_h}{\rho \bar{v}^2 L}. \tag{3.3}$$

In equations 3.2 and 3.3, C_w is the friction factor of a certain geometry and Δp is the pressure drop over the length L of the regenerator. Together with N_u, C_w has to be determined experimentally or can be found in literature for certain existing geometries [11]. As stated in section 3.1 care has to be taken with values of C_w determined for steady flow because these can differ significantly from values under real operating conditions. For some geometries, the values of *NPH/NTU* are pictured in figure 3.1 [5]. In figure 3.1 can be seen that etched foil, square channels or parallel plates theoretically give a lower ratio than the stacked screens or packed spheres. However, in practice it is difficult to construct a fine structure with these geometries. Another difficulty is reducing the axial thermal conduction, which is very high for example in a parallel plate geometry.

A note about the use of *NPH/NTU* should be made. Both are related to the entropy production in the regenerator. Minimizing their ratio however, is not the same as minimizing the total entropy production in a regenerator. If for example *NPH* and *NTU* are both chosen very large, their ratio might still be small, but the entropy production due to pressure drop is very large (section 2.3). Also neither *NPH*, nor *NTU* is a pure geometrical characteristic of the regenerator. Both are dependent on the mass flow through the regenerator and comparing the ratio of *NPH/NTU* of one regenerator to the ratio of another, can only be useful under the same flow conditions. At a fixed mass flow the R_{pf} (equation 3.1) is proportional to the inverse ratio *NTU/NPH*. In [11] is shown that the R_{pf} of a regenerator is linearly proportional to the performance of the cryocooler under

the same flow conditions. This confirms that comparing *NPH/NTU* for different regenerator geometries only makes sense under these specific conditions. In most of the reviewed literature however, this ratio is used, as can be seen in the rest of this section.

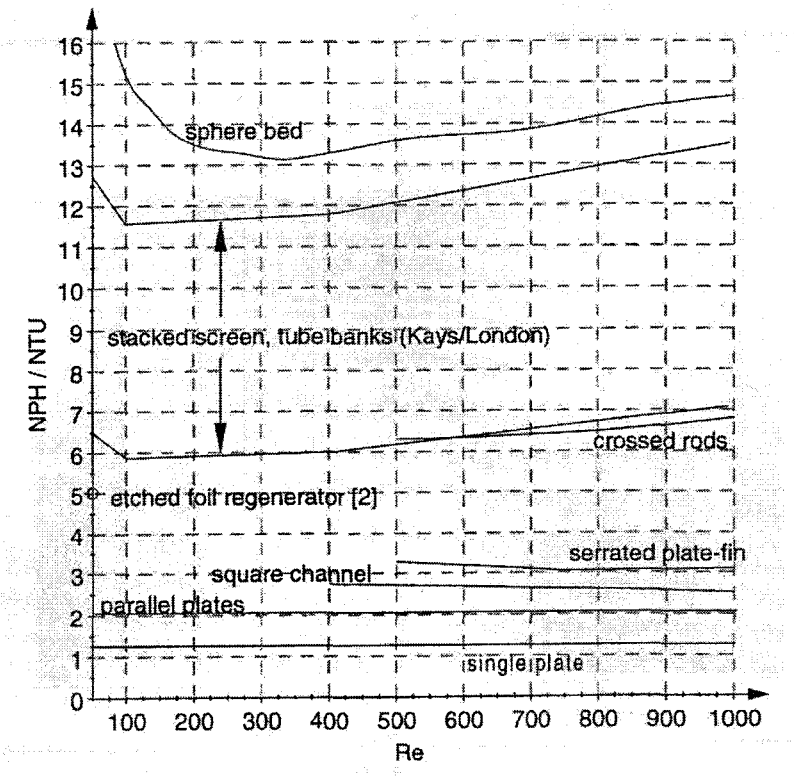

Figure 3.1: *Ratio of NPH/NTU for different regenerator geometries as a function of the Reynolds number. Typical Reynolds numbers in a regenerator at cryogenic temperatures are below 200.*

Elliptical matrix elements

Recent systematic numerical research [5] has identified what an ideal inner geometry of a regenerator should look like. It turned out that two main parameters of a matrix geometry have substantial influence on the ratio of *NPH/NTU*: the aspect ratio (thickness to length) of a single element and the ratio of the mean flow area to the minimum flow area within the matrix. Sudden changes in flow velocity (acceleration/deceleration) dramatically increase the pressure drop. Therefore elliptical shapes with the long side in the flow direction (figure 3.2a) theoretically perform better than round shapes. By winding elliptical wires of phosphor bronze around a core (with a certain spacing) a regenerator with an elliptical geometry is produced and tested [14]. Despite the predictions, the no-load low temperature and the cooling performance of a screen regenerator are not reached. The main reason given for this is that the hydraulic diameter of the flow channels might be too large for the two prototypes tested. The main challenge is to develop a technology to fabricate appropriate matrices with this new geometry.

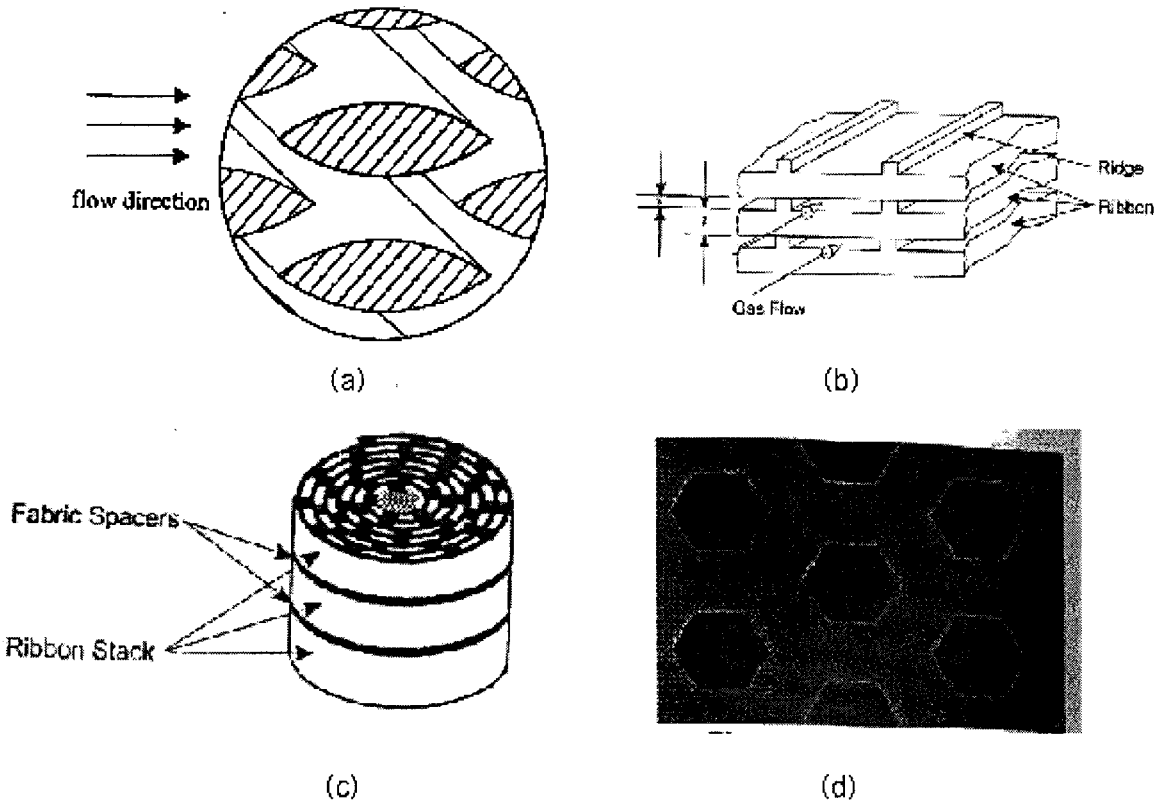

Figure 3.2: *Different regenerator geometries: a) Elliptical matrix elements, b) Square Channel geometry, c) Regenerator made of rolled ribbons with the same geometry as pictured in figure 3.2b, in which the individual rolls of ribbon are separated by small spacers, and d) Perforated plate produced with the LIGA process.*

Parallel flow channels

Another promising geometry is one of parallel rectangular flow-channels, approaching a parallel plate geometry. (figure 3.2b) In literature a production technique is presented to construct a thin foil of polyimide in which wide rectangular channels are formed by a photolithographic process [15]. The foil is then wound around a mandrel with the length of the channels in the flow direction. Polyimide has a thermal conductivity that is over an order of magnitude lower than that of stainless steel (small axial thermal conduction) and a relatively high heat capacity. The filling factor of this new geometry is 0.67, which is much higher than that of screen matrices (around 0.34), making it more compact for equivalent heat storage capacity. Computer calculations [15] predict a considerable improvement of the performance for this new geometry. A regenerator with this geometry is constructed, construction costs being relatively low. Despite the predicted improvement, the constructed regenerator did not approach the performance of a stainless steel screen regenerator. No plausible explanation is given but the conclusion can be drawn that finding a proper production method for rectangular flow channel matrix geometries is very difficult. A comparable experiment has been performed for regenerators used at very low temperatures (<10K), made of neodymium (Nd) [16]. Instead of using one rolled foil, several strips of ribbon are wound around a mandrel, spaced by very small spacers (figure 3.2c). At every spacing between the rolled ribbons, the flow is re-distributed and bad thermal contact exists, reducing the axial thermal conductivity. Small porosities (1 - *f*) can be reached and with appropriate spacing between the ribbons, low pressure drops can be achieved. Two regenerators

are produced with the ribbon (porosities of 0.15 and 0.20) and are tested in a refrigerator. The tested ribbon-regenerator with the highest porosity performed better than one with a matrix of packed Nd spheres. Furthermore, the testing indicates that higher performance gains can be achieved in comparison with spherical beds if the ratio of *NPH/NTU* is further optimized. In addition to a better cooling performance, two other advantages over spheres are presented. Producing the ribbon should cost less than producing spheres, primarily because little material is wasted during production. In the process of manufacturing spheres from bulk material, only 15 to 30% of the spheres is of useful size. The other advantage that ribbon has over spheres is reliability while operating in a refrigerator. No particles can get loose and "leak out".
Another technique for manufacturing microchannel structures that is proposed is based on producing a solid block with straight microchannels from rods of regenerator material and a filler [17]. First, thin rods (about 100 μm) are produced of a filler material and a binder, coated with regenerator material (e.g. Er_3Ni) and the same binder. Then bundles are formed of the rods. Finally, the binder and the filler material is removed from the structure by heat treatment, leaving behind a structure of small micro-channels. With this production method structures of any material can be formed with porosities varying from 1-95% and channel diameters in the range from a few microns to a few millimeters. Again no experimental testing is reported. A disadvantage in parallel flow channels can be that the flow is not uniformly distributed over the different flow channels. Also has to be noted that in the case of laminar flow, heat exchange between the gas and the wall only takes place in the boundary layer, reducing *NTU*. Therefore the channel diameter has to be small enough, increasing *NPH*.

Perforated plates

Another matrix geometry that predicts a better performance than matrices made of screens or spheres, is a perforated plate geometry [18]. In this geometry, perforated plates are separated by small spacing rings, which decrease axial thermal conduction and allow a better flow distribution. If the plate thickness is much larger that the hydraulic diameter of a perforated flow channel, the heat transfer and pressure drop characteristics can be approximated by internal tube flow, which has a much lower *NPH/NTU* ratio than stacked screens or packed spheres. With the perforated plate geometry a much lower porosity can be reached (as low as 5%) which should lead to a lower ratio of *NPH/NTU* and thus a better regenerator performance. With a regenerator simulation program [18], regenerator performance for perforated plate geometries is simulated for several porosities. The computer simulation indicates that a reduction in porosity yields a net improved performance. According to the simulations, the perforated plate geometry holds promise for at least a factor two improvement in refrigeration power. The difficulty is to find a proper manufacturing technique for the perforated plate geometry. In [19] some more calculations are given that indicate the better performance of a perforated plate geometry. A production technique is tested that is based on extrusion technology. A sacrificial material fills the channels that are later used as flow channels and a mold is filled with the regenerator material (e.g. stainless steel). Afterwards the sacrificial material is removed by use of a suitable chemical etch and the material is cut into slices. No tests in a real regenerator are presented.
To achieve an optimal ratio of heat transfer/pressure drop in a regenerator, a length to hydraulic diameter ratio of 10-20 is needed. A method to produce micro-channel regenerators with this required ratio, is the LIGA micromachining process [20]. The LIGA process, developed at the Institute for Microstructure Technology (IMT-FzK) in Karlsruhe, Germany, is a three-step process comprised of X-ray lithography, electroforming and molding. Typical plates for regenerator use would be about 1 mm thick, perforated with 20-40 μm holes (figure 3.2d). Very low porosities can be reached (10-15%), decreasing the *NPH/NTU* ratio. An analytical comparison for low

temperatures (10-30K) is made between a regenerator filled with lead spheres (d_h = 56 μm) and parallel plates of lead (d_h = 20-30 μm). The simulation indicates that an improvement by a factor 3-4 is possible with this new geometry.

Etched foil

The last geometry that will be described in this section, is an etched foil geometry with flow passages perpendicular to the direction of flow [21 - 23] (figure 3.3). Although having a relatively high porosity (53-80%), the etched foil geometry predicts a lower NPH/NTU ratio than stacked screens and packed spheres. To create the etched foil, thin strips (30-125 micron) of material (e.g. stainless steel, phosphor bronze or lead) are etched from two sides, leaving a pattern of channels in the flow direction with bypasses perpendicular to the flow improving the flow distribution in the matrix. Etched foil geometries can be approximated with parallel plate flow characteristics. The foil can be rolled around a mandrel to form a cylindrical regenerator. A regenerator produced this way has been tested in a cryocooler. Under the same operating conditions, it reached lower temperatures and delivered more cooling power than when equipped with a stacked screen regenerator.

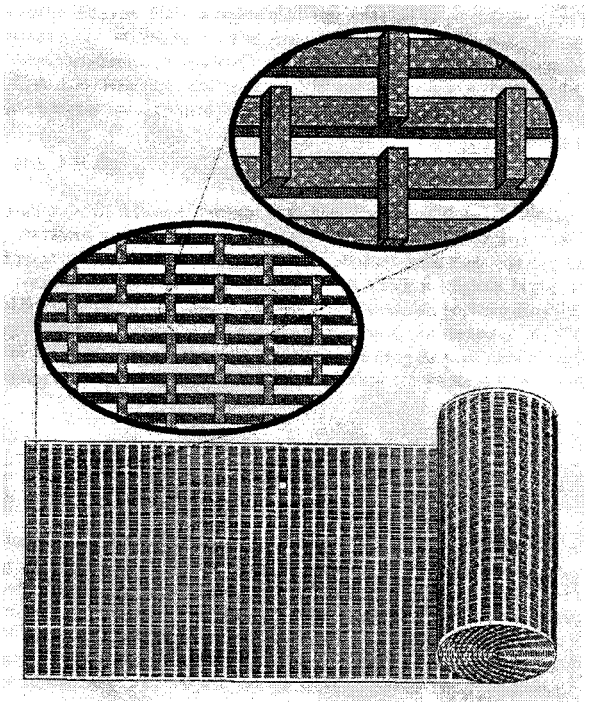

Figure 3.3: *The etched foil geometry with bypasses perpendicular to the plane of flow. The foil is rolled around a mandrel to create a regenerator.*

3.4 Different matrix materials

With modern production methods it is possible to produce spherical particles from many different materials, including rare-earth metals. The main advantage of using rare-earth metals is that some of them have a higher specific heat than conventional regenerator materials (e.g. lead and stainless steel), in the temperature range of 15-85K. This is due to the low magnetic ordering temperatures of these materials and the increased specific heat around this temperature. In figure 3.4 the specific heats of stainless steel, lead and erbium are given for a temperature range of 10-300K [24] [25]. As can be seen, stainless steel - most commonly used in a single stage cryocooler - has a higher specific heat than lead at temperatures above 70K. In two stage coolers, cooling down to 20K, lead is commonly used as matrix material. Figure 3.4 indicates that erbium has even better abilities to store heat at these low temperatures.

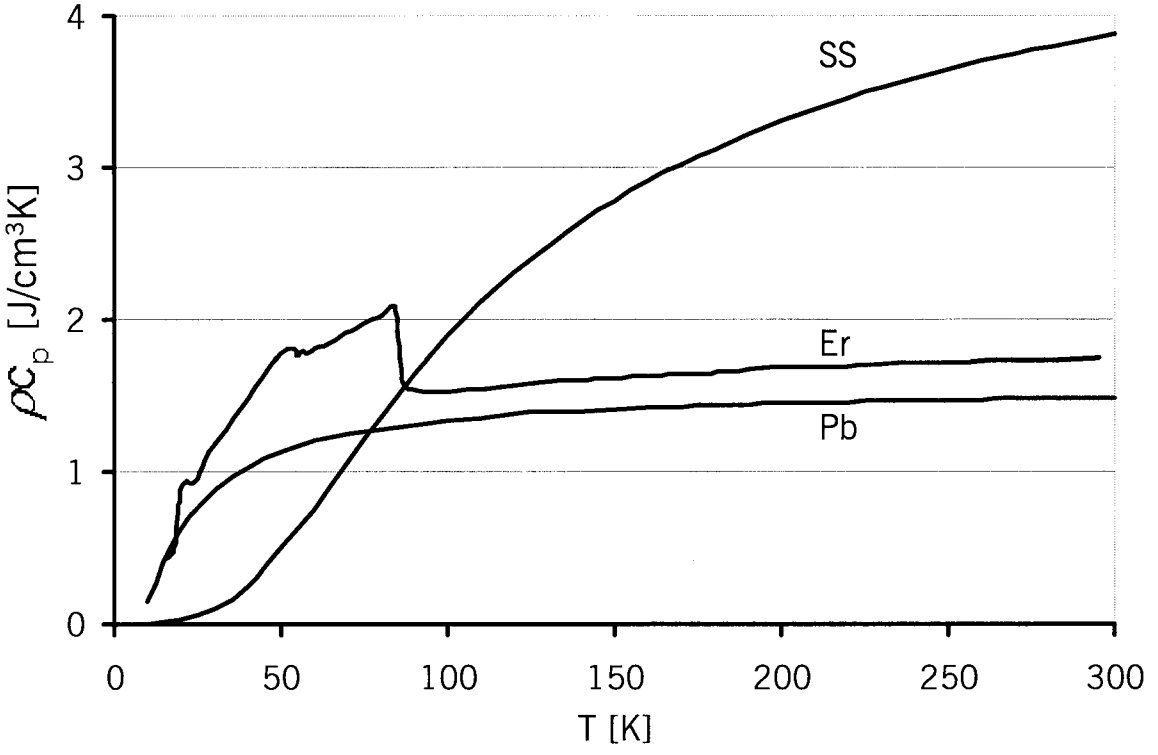

Figure 3.4: *Volumetric specific heat of erbium, stainless steel, and lead. For temperatures between 15 and 85K erbium has the highest volumetric specific heat.*

At Ames Laboratory in Ames, Iowa, erbium (Er) and some Er-based alloys are produced as spherical particles of 100 μm [26] [27]. In a specially developed test machine, pure erbium powder is tested as regenerator material and the first test results are promising. Compared to lead powder of the same size, the cooler with the erbium reaches a lower no-load temperature. The magnetic contribution to the heat capacity arises from the magnetic ordering process itself and this can give rise to either a very narrow heat capacity peak for a first order magnetic transformation or a modestly broader lambda-like peak for a second order magnetic transition. A third kind of heat capacity peak is known as a Schottky anomaly and is quite broad. Pure erbium has a sharp peak at 19K, a smaller one at 25K and two broader peaks at 52 and 88K. A sharp peak in the heat capacity however, is not very useful because it occurs in a narrow temperature range. If this peak would be stretched out over a wider temperature range, overall heat capacity in the temperature range of 10 to 90K can be increased. By adding impurities to the erbium,

this effect can be reached. Most commercially available erbium already contains such impurities and also the data used for figure 3.4 show flattened peaks at the temperatures stated above, indicating the presence of impurities. Adding different volume-percentages of Praseodymium (Pr) increases the heat capacity in different temperature regions. In the temperature region of 25-40K for example $Er_{73}Pr_{27}$ gives the best results, while in the range of 10-25K $Er_{50}Pr_{50}$ has the highest heat capacity [28]. Other advantages of Er-based alloys over lead stated in [28] are it not being as toxic as lead, its lower thermal conductivity (one order of magnitude) and its tensile strength being larger (one order of magnitude). Intermetallic compounds of lanthanides (like Er and Pr) and regular metals (like Ni) are very brittle, alloys of pure lanthanides however are quite ductile. Therefore they are easy to handle and can readily be fabricated into spheres, wires and foils. A recently developed technique to produce small spherical particles (40-300 μm) is the Plasma Rotating Electrode Process (PREP) [29]. With this technique, powder is produced by controllably melting the end of a round bar of the chosen material with a plasma torch, while the bar is rapidly rotating about its longitudinal axis. The molten metal is centrifugally ejected from the surface of the bar and forms droplets that solidify to form spherical powder particles. Because of the contactless melting, very "clean" powder can be produced and because the droplets are dispersed and move radially away from each other, the powder is almost perfectly spherical and satellite free. The particle size is controlled by the rotation speed of the bar.

A radically different approach of the use of Er-based alloys in a regenerator matrix is not using spherical particles at all [30]. Intermetallic compounds of rare earth and regular metals generally are very brittle. The use of spherical particles increases the tensile strength and fracture toughness of the materials, reducing the chances of particle desintegration in regenerator use. Spherical particles however are relatively expensive to produce because sophisticated manufacturing techniques are necessary. The brittleness of intermetallic compounds simplifies the production of fine, irregularly shaped particles by simple crushing and sieving. Particles like this can be used to fill a regenerator. To avoid frictional contact between the individual particles, causing particle desintegration, the entire regenerator has to be bonded with a diluted epoxy mixture. Poor thermal contact in the point contacts the individual particles reduces the axial thermal conductivity. A regenerator filled with Er_3Ni and $ErNi_{0.9}Co_{0.1}$ produced in this way (effective particle diameter 200-300 μm) is tested in a two-stage GM refrigerator and a lower minimum temperature is reached than when using lead spherical particles (300 μm) in the same refrigerator. After 250 hours of continuous operation no degradation of the refrigerator performance was noticed.

The conclusion from section 3.3 and 3.4 is that a lot of new developments for regenerator geometry and matrix materials are described in literature. However, converting model predictions for better performance to a real regenerator that actually performs better in a real refrigerator in many cases remains a difficult challenge. Also the fact that a lot of suggestions for regenerator improvement are much more expensive than the currently used screens or spheres, makes it very difficult to find improvements that are commercially attractive.

In Appendix A, a list of companies that are contacted during this research is presented. Information about the company and which products they can deliver is given, as well as prices (if known) and contact information.

4 The Stirling model

4.1 Introduction

To predict the performance of the cryogenerators produced at Stirling, a powerful simulation model has been developed, which from now on will be called the Stirling model. The model is a one-dimensional model based on conservation of mass, momentum and energy in the different parts of the cooler. All properties are assumed to be first order harmonically varying quantities. Another approximation is that the mass and energy calculations are decoupled from the momentum calculation. Therefore temperature profiles and thermal losses are calculated independently from the pressure drop [31 - 33].

During decades of research at Philips, the model has been improved to a powerful design tool for the cryogenerators. Not only does it incorporate all the important physical processes, it is also calibrated with extensive measurements. From these measurements empirical relations for pressure drop, heat transfer, thermal conduction, etc. are derived for the different components of the actual machines. Therefore the Stirling model accurately predicts the performance (cooling power and efficiency) of the complete machine, as well as the thermal losses and pressure drops inside the individual components. In section 4.2, the structure of the Stirling model will be described. Section 4.3 will be focused on the losses inside the regenerator only. Section 4.4 will describe a typical input and output file of the computer model and finally section 4.5 will be about the adaptations that have to be made to include an extra regenerator geometry or material into the model.

4.2 Model structure

In the Stirling model the machine is divided into a number of control volumes. Figure 4.1 is a schematic representation of these different volumes. The machine is divided into a compression space, a warm heat exchanger, a regenerator, a cold heat exchanger and an expansion space. Furthermore several void volumes are defined, volumes that are not swept by the compression or the expansion piston. The compression and expansion space are considered adiabatic (no heat exchange with the surroundings) and the rest of the volumes are considered isothermal (constant temperature). In figure 4.2 the flow chart of the Stirling model is presented. The entire model has several nested loops. The innermost loop is the iteration loop for undisturbed pressure (pressure before flow losses are taken into account), mass flow and temperature. The initial temperature profile in the regenerator is assumed linear. For the phase of the undisturbed pressure profile and the mass flow in the rest of the machine, the movement of the expansion piston (displacer) is used as a reference. The volume of the expansion (V_E) and compression space (V_C) is respectively

$$V_E(t) = \frac{1}{2} V_{E0}(1 + \cos(\omega t)) \quad \text{and} \tag{4.1}$$

$$V_C(t) = \frac{1}{2} V_{C0}(1 + \cos(\omega t - \phi)) . \tag{4.2}$$

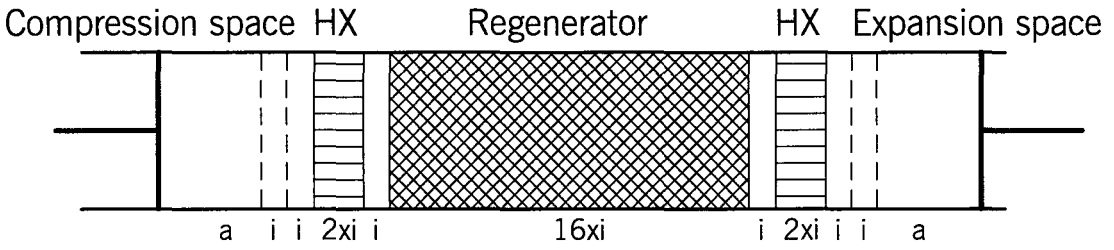

Figure 4.1: *The Stirling model divides the cooler into several control volumes: The compression space, the warm heat exchanger, the regenerator, the cold heat exchanger, and the expansion space. Furthermore several void volumes are defined. An index 'i' denotes a volume considered isothermal and an index 'a' denotes an adiabatic volume.*

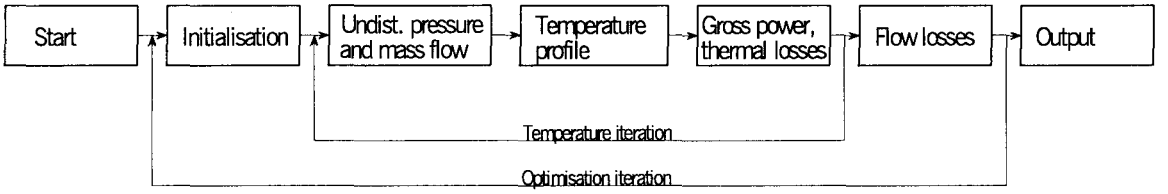

Figure 4.2: *Flow chart of the Stirling model. After initialization of the input parameters, first the temperature profile in the regenerator is calculated from the undisturbed pressure and mass flow. Then the pressure drop is calculated. Finally the model gives an output for the cooling power of the machine, the power input and the losses in the individual components.*

In equations 4.1 and 4.2, V_{E0} and V_{C0} are the maximum values of respectively the (adiabatic) expansion- and compression space. The angular frequency of both pistons (compression and expansion) is ω and ϕ is the phase difference between them. The undisturbed pressure is given by

$$p(t) = p_m(1 - \varepsilon\cos(\omega t + \theta)\,. \tag{4.3}$$

In equation 4.3, p_m is the average pressure in the machine, ε is the relative pressure amplitude and θ is the phase difference between the movement of the expansion piston and the pressure. Calculations of the undisturbed pressure are based the fact that the total mass in the machine is conserved

$$m_{tot} = \frac{p}{R}Y\left(\sum_i \frac{V}{T} + \sum_a \frac{V}{T}\right). \tag{4.4}$$

Equation 4.4 is the ideal gas law with a correction factor Y for real gas behavior. R is the molar ideal gas constant, which is 8.3145 J/molK. With the undisturbed pressure, the undisturbed mass flow is calculated, being the time derivative of the mass. This results in an equation for the undisturbed mass flow in the different control volumes "j" of the system,

$$\dot{m}_j(t) = m_{0j}\sin(\omega t + \theta - \gamma_j)\,. \tag{4.5}$$

In equation 4.5, m_{0j} is the mass flow amplitude and γ_j the phase shift between pressure and mass flow for the different control volumes. After determining the undisturbed pressure and mass flow, the temperature profile and thermal losses inside the heat exchangers, regenerator and cylinders are calculated, using conservation of energy. Because the undisturbed pressure and mass flow depend on the temperature distribution, the calculation is repeated until the changes in temperature are below a specified value (iteration).

With the final temperature profile and mass flow, the pressure drop over each component is calculated. This pressure drop is considered as a correction to the undisturbed pressure. The undisturbed mass flow is only corrected for its phase difference with the pressure. With this corrected pressure distribution the mass flows, thermal losses and the temperature profile are calculated one more time. The output of the model finally gives the cooling power of the machine, the required power input, the flow losses and the thermal losses inside the regenerator and the other components of the machine. The next section will be focused on the thermal losses inside the regenerator.

4.3 Regenerator losses

Energy flow

Thermal losses occur at different locations inside the machine. By far the largest contribution to the total thermal loss is caused by the imperfectness of the regenerator. This results in an energy flow through the regenerator, consisting of an enthalpy flow and a heat flow due to conduction. The Stirling model takes into account five different terms that contribute to this energy flow. The terms are derived in [34], in the text below only the final equations are presented.

1) The Φ-effect

The Φ-effect is caused by the finite heat capacity of the regenerator matrix. The enthalpy flow caused by this effect (I_1) is proportional to the ratio of the specific heat of the gas in the expansion space and the total specific heat of the regenerator,

$$I_1 = (1 - \rho c_T)\Phi_E Q_E , \tag{4.6}$$

$$\Phi_E = (1 - f)\rho_E \frac{c_p}{c_r} , \tag{4.7}$$

$$c_r = f\rho_m c_m + (1 - f)\rho_g c_p . \tag{4.8}$$

In equation 4.6, c_T is the throttling coefficient of the gas, given by $(\partial h/\partial p)_T$, in which h is the local enthalpy of the gas. The local density is given by ρ, Q_E is the cooling power and ρ_E is the density of the gas in the expansion space. The specific heat of the gas at constant pressure is expressed by c_p and c_r is the total specific heat of the regenerator (matrix + gas). From equation 4.6 to 4.8 can be seen that the Φ-effect is small if the specific heat of the matrix is much larger than the specific heat of the gas in the expansion space.

2) The Joule-Thomsoneffect

The Joule-Thomsoneffect is a non-ideal gas effect, caused by the pressure drop across the regenerator. Due to expansion, the gas is cooled or heated isenthalpically (throttling effect). Whether the gas cools or heats, depends on the sign of the local throttling coefficient c_T, which is zero for an ideal gas. The enthalpy flow caused by this effect (I_2) is represented by

$$I_2 = c_T \rho_E P_E . \tag{4.9}$$

3) Heat transfer losses

The heat transfer coefficient between the gas and the matrix is finite, therefore not all the heat inside the gas is transferred to the matrix. If there is a temperature gradient across the gas inside the matrix, at a certain point in the regenerator, the temperature of the gas flowing from warm to cold is at a higher temperature than the gas flowing back. This causes a net enthalpy flow (I_3) through the regenerator,

$$I_3 = \frac{c_p \overset{*}{m} \Delta T}{\Lambda + 2 - \Omega}. \tag{4.10}$$

In equation 4.10, ΔT is the temperature difference across a control volume of the regenerator. Λ equals NTU in equation 2.26 and Ω is a dimensionless empirical correction factor. From equation 4.10 can be seen that if the heat transfer is good (large Λ), this term gives a small contribution to the total enthalpy flow.

4) The pressure-effect

This effect is caused by the finite heat transfer coefficient and heat capacity in combination with the pressure oscillations inside the gas. The contribution to the total enthalpy flow of this effect (I_4) is defined by

$$I_4 = -r_n \cdot \varsigma \cdot I_1 , \tag{4.11}$$

$$r_n = \frac{8}{\pi} \frac{\Gamma_r}{\Lambda}, \tag{4.12}$$

$$\varsigma = -\frac{\sqrt{1-e^2}}{\tan\gamma}. \tag{4.13}$$

In equation 4.12, Γ_r is the ratio of the total heat capacity of the matrix to the heat capacity of the gas passing through during half a cycle. The larger this ratio is, the larger the value I_4. Because γ has a negative value, I_4 is a negative contribution to the total thermal loss. If the pressure and mass flow are out of phase by 90°, $\tan\gamma = -\infty$ and I_4 goes to zero.

5) Heat conduction through the regenerator

This term is proportional to the heat conduction coefficient of the regenerator λ_r, the cross sectional surface area of the regenerator A_r and the temperature gradient across a control volume of the regenerator, $\partial T/\partial x \approx \Delta T/\Delta l$. The value of λ_r, is empirically determined and is a combination of the matrix thermal conductivity and the thermal conductivity in the gas. The contribution to the energy flow (I_5) is defined as

$$I_5 = -\lambda_r A_r \frac{\Delta T}{\Delta l}. \tag{4.14}$$

Conduction through the regenerator wall is calculated separately from the thermal losses inside the regenerator.

The result of the five effects introduced above is a total energy flow I_{tot},

$$I_{tot} = I_1 + I_2 + I_3 + I_4 + I_5. \tag{4.15}$$

Calculation of the temperature profile

To calculate the temperature profile, the regenerator is divided into eight sections. Figure 4.1 shows a regenerator divided into 16 control volumes, but for temperature calculations, pairs of two bordering volumes are assumed to have the same temperature profile. The thermal regenerator losses can be divided into two groups: losses that are dependent on the local temperature gradient (heat transfer and heat conduction) and losses that are not. With this fact, two parameters can be defined:

$$A(i) = I_1(i) + I_2(i) + I_4(i), \tag{4.16}$$

$$B(i) = \frac{\Delta T(i)}{I_3(i) + I_5(i)}. \tag{4.17}$$

In equation 4.16 and 4.17, i (= 1...8) is the index for the considered section of the regenerator. With equation 4.16 and 4.17, I_{tot} can be written as

$$I_{tot}(i) = A(i) + \frac{\Delta T(i)}{B(i)}. \tag{4.18}$$

In a stationary situation, the total energy flow should be the same through each control volume. (first law of thermodynamics, equation 2.1) Therefore,

$$A(8) + \frac{\Delta T(8)}{B(8)} = A(7) + \frac{\Delta T(7)}{B(7)} = \ldots = A(1) + \frac{\Delta T(1)}{B(1)}. \tag{4.19}$$

This results in:

$$\Delta T(i) = \left(A(8) + \frac{\Delta T}{B(8)} - A(i) \right) B(i) \quad , \quad (i = 1...8). \tag{4.20}$$

The total temperature difference across the regenerator is

$$\Delta T_r = \sum_{i=1}^{8} \Delta T(i) = A(8) \sum_{i=1}^{7} B(i) + \frac{\Delta T(8)}{B(8)} \sum_{i=1}^{7} B(i) - \sum_{i=1}^{7} A(i)B(i) + \Delta T(8). \tag{4.21}$$

If the total temperature gradient across the regenerator is fixed, the temperature gradient across section 8 can be calculated:

$$\Delta T(8) = \frac{\left(\Delta T_r + \sum_{i=1}^{7} A(i)B(i) - A(8)\sum_{i=1}^{7} B(i)\right)B(8)}{\sum_{i=1}^{8} B(i)}. \qquad (4.22)$$

After this temperature difference is determined, the temperature differences across section 1 to 7 can be calculated with equation 4.20. With this new temperature profile, the undisturbed pressures and mass flows are recalculated as well as the thermal losses. The iteration stops when equation 4.19 is fulfilled, giving the final temperature profile in the regenerator.

Flow losses

After calculation of the temperature profile, the undisturbed pressure, mass flow and thermal losses, the pressure drop across a section of the regenerator (length Δl) is calculated:

$$\Delta p = C_w \frac{1}{2}\rho v^2 \frac{\Delta l}{d}. \qquad (4.23)$$

Equation 4.23 is a general equation for the pressure drop in which C_w is the friction factor, depending on the geometry of the flow resistance and often also on the flow velocity and the viscosity of the gas (R_e). C_w has been determined empirically for different geometries used in the Stirling model. The diameter d used in combination with this C_w is the thickness of a wire or the diameter of a sphere used in the regenerator matrix. The empirical relations for C_w are

[confidential] (screens), (4.24)

[confidential] (spheres), (4.25)

$$R_{ef} = \frac{4}{3} R_{es}. \qquad (4.26)$$

In equation 4.26, R_{es} is calculated (equation 2.23) with the velocity the gas would have if the regenerator would be empty ($f = 0$). Because the Stirling model uses d instead of d_h to calculate R_{es}, some confusion might arise. In the equations below R_{es}, the Reynolds number used by the Stirling model (in the empty regenerator with d instead of d_h), is compared to the R_e defined by equation 2.23:

$$R_{es} = \frac{\dot{m} d}{\eta A_r} = f \frac{\dot{m} d_h}{\eta (1-f) A_r} = f \frac{\rho \bar{v} d_h}{\eta} = f R_e \qquad \text{(screens)}, \qquad (4.27)$$

$$R_{es} = \frac{\dot{m} d}{\eta A_r} = \frac{3f}{2} \frac{\dot{m} d_h}{\eta (1-f) A_r} = \frac{3f}{2} \frac{\rho \bar{v} d_h}{\eta} = \frac{3f}{2} R_e \qquad \text{(spheres)}. \qquad (4.28)$$

To get to equations 4.27 and 4.28, equations 2.10, 2.17 and 2.27 are used.

The velocity through a flow resistance in a control volume, is proportional to the mass flow. A pressure drop across a control volume, will increase the pressure at one side and decrease it on the other side. Pressure drop is in phase with velocity and mass flow so it will not be in phase with the undisturbed pressure (equation 4.5). A pressure drop therefore will result in a change in pressure amplitude, as well as an additional phase shift between pressure and mass flow. This

effect is called the Stigter-effect. For each control volume, the effect of a pressure drop across that volume on the pressure in the other volumes is calculated. Finally the flow losses are expressed in a term of power loss. This loss is calculated as a change in work done by the compression and the expansion piston,

$$\Delta P = \frac{\omega}{2\pi} \oint \Delta p dV \,. \tag{4.29}$$

In equation 4.29, Δp is the pressure difference in the compression and the expansion space and dV is determined from equations 4.1 and 4.2.

The Stirling model takes into account a lot more small effects in the different components of the Stirling machine, but if it is used as a designing model, it is not necessary to explain every detail. All these effects are described in [34]. Because of this detail, in the next section an input and output file of the computer model are discussed, describing the most important input and output parameters.

4.4 Model input and output

[confidential]

4.5 Adjusting the Stirling model

[confidential]

5 Design calculations

5.1 Introduction

Calculations have been performed to predict the performance of new regenerator designs. By minimizing the entropy production inside the regenerator, the most ideal regenerator can be obtained. In section 5.2 some entropy calculations are shown for the conventional regenerator of the Stirling SPC-1, consisting of a matrix of stacked stainless steel screens. In section 5.3, the current production technique is compared to a new technique, which consists of rolling the screens instead of stacking them. If a proper construction technique is used, this new regenerator design is expected to reduce the production costs of the regenerator. Another regenerator design that is expected to reduce the production costs significantly, is a matrix of sintered stainless steel particles. In section 5.4 design calculations for this new regenerator matrix a are presented. In the Stirling model, the flow channels in the porous medium will be modeled as small cylindrical tubes.

5.2 Minimizing the entropy production

In section 2.3 the different entropy production terms inside a regenerator are introduced. For the calculations in this section, the equations for heat conduction through the gas and the matrix (2.12 + 2.13), flow resistance (2.14) and heat exchange (2.20) will be used. When the exact values of the input parameters are unknown, correct estimations have to be made. In table 5.1 the values of the input parameters for the conventional Stirling SPC-1 regenerator are presented.

Table 5.1: *The input values for entropy production calculations are presented for the Stirling SPC-1 regenerator. In the last column, comment is given on how the values are acquired. For values that are temperature dependent, information is given about the literature where the used values are found.*

Parameter	Value	Comment
f	-	Determined by weighing the matrix and measuring the matrix volume. With the density of stainless steel, the filling factor is calculated.
A_r	-	A regenerator with uniform cross section is assumed.
L_r	-	This is the total length of the matrix.
d_h	68 μm	Calculated with equation 2.11.
F	-	Calculated with equation 2.10, d_h = 68 μm.
dT/dl	-	A linear temperature profile is assumed, as well as $T_g = T_m$. The estimation is based on T_H = 320K and T_L = 70K.
C_k	0.15	This conductivity degradation factor is an average from literature. [10]
z_r	$2.0 \cdot 10^{10}$ m^{-2}	Measured with a static pressure drop experiment at room temperature, atmospheric pressure and R_e around 1. For oscillating flow, the flow impedance might be higher by a factor 2-6. [6, 7]

$\lambda_{g,m}$ η	W/Km kg/sm	From an internal document at Stirling Cryogenics & Refrigeration BV [24]. The values that are used are presented in Appendix D.
ρ V_m C_p	kg/m^3, m^3/mol, J/molK	From a database for cryogenic fluids, Allprops [35]. The values that are used are presented in Appendix D.
$\dot{n}$	28 mol/s	At the cold side, the average volume flow is estimated to be $V_{E0}\, 2\omega/2\pi$. With the molar volume V_m, the molar flow is calculated, which is assumed to be constant inside the regenerator.

For the calculations in this section, all the data for helium are taken at a pressure of 30 bar, a common pressure inside the Stirling SPC-1. N_u is calculated with equation 2.22, P_r = 0.7 and equation 2.23 is used for R_e. In equation 2.23 the average velocity given by equation 2.27 is used. To calculate the entropy production rates inside the regenerator, the regenerator has been divided into 26 isothermal sections of equal length. Inside each section the gas- and matrix properties are assumed to be constant. The temperatures of the 26 sections are 70, 80,...,320 K respectively.

In figure 5.1 the total entropy production rate by conduction (gas + matrix), flow resistance, and heat exchange is presented for the 26 sections. The gas and matrix data used for these calculations are presented in Appendix D. The calculations are performed with the flow impedance z_r of the matrix equal to $2.0 \cdot 10^{10}$ m^{-2} = z_{r1} and a flow impedance that is a five times larger. This because the flow impedance might be significantly higher in oscillating flow than in steady flow [6, 7]. Figures 5.2 and 5.3 show the relative contributions of the different entropy production terms at eight different temperatures.

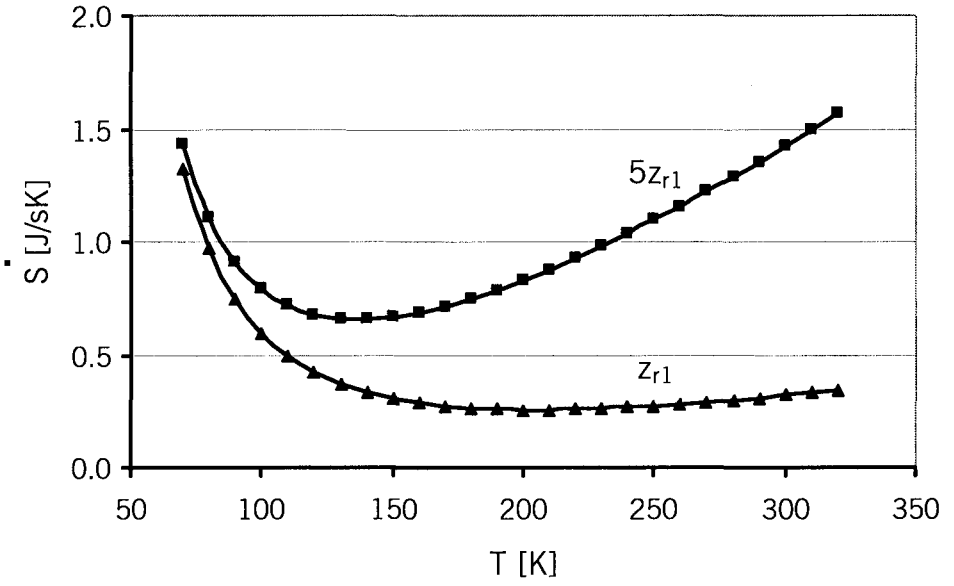

Figure 5.1: *For 26 isothermal sections of the regenerator, the total entropy production rate is calculated for two different values of the flow impedance: $z_r = z_{r1} = 2.0 \cdot 10^{10}$ m^{-2} and $z_r = 5z_{r1}$.The total entropy production rate is 10.39 J/sK for $z_r = z_{r1}$ and 25.82 J/sK for $z_r = 5z_{r1}$.*

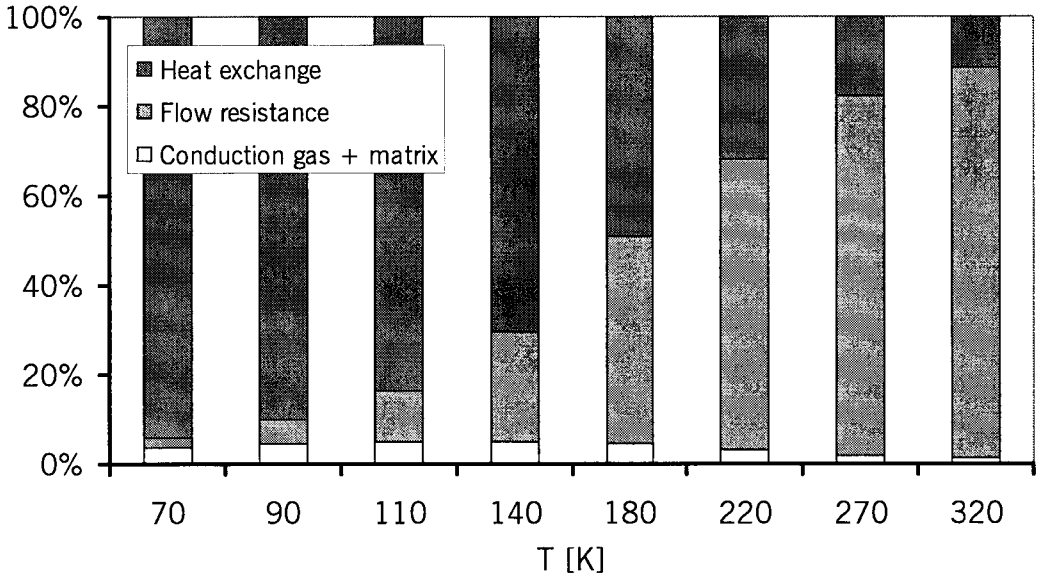

Figure 5.2 ($z_r = z_{r1}$)

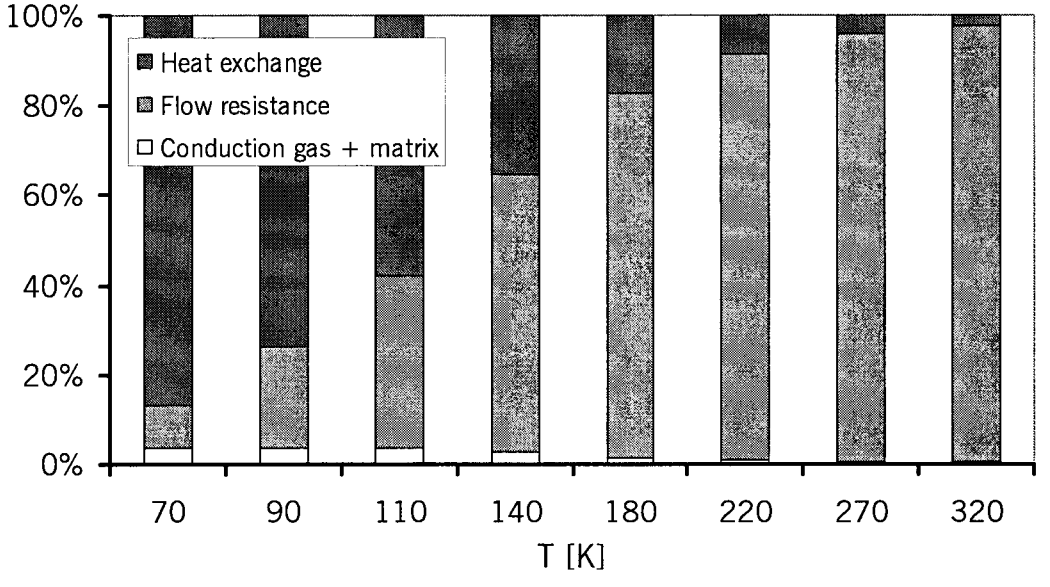

Figure 5.3 ($z_r = 5\ z_{r1}$)

Figure 5.2 and 5.3: *For eight different temperatures the relative contribution of three entropy production terms is given: conduction (gas + matrix), flow resistance, and heat exchange. In figure 5.2, $z_r = z_{r1}$ and in figure 5.3, $z_r = 5z_{r1}$. At low temperatures, the heat exchange term is the dominant term, at higher temperatures the flow resistance becomes the most important contribution to the total entropy production. Increasing the flow resistance by a factor five, strongly increases the relative contribution of this term.*

It can be seen from figure 5.1 that for $z_r = z_{r1}$, 50% of the total entropy production inside the regenerator, takes place in the first eight sections of the regenerator at the cold side. An increase of a factor five in the flow resistance causes the total regenerator entropy production to rise with a factor 2.5. This is mainly due to the significant increase of the entropy production rate in the temperature region between 140 and 320 K (figure 5.1). In figure 5.2 and 5.3 can be seen that the main part of the entropy production in this part of the regenerator is caused by the flow resistance term. This term is linearly dependent on z_r so it will increase by a factor 5 as well. In the region between 70 and 110 K, the heat exchange term still is the dominant term.

The heat exchange entropy production term is dependent on d_h and F. A regenerator with smaller hydraulic diameter and thus more heat exchanging surface per volume (equation 2.10) at the cold side, might lead to a lower entropy production in the regenerator. A smaller d_h however, will lead to a higher flow resistance. To get a better view on the influence of the hydraulic diameter on the entropy production, all the input parameters are kept the same, except d_h. In these calculations z_r is assumed to be equal to $c_z d_h^{-2}$ [3] with the proportionality constant c_z being 92 for $z_r = z_{r1}$ respectively 460 for $z_r = 5z_{r1}$. For $z_r = z_{r1}$, the dependence of the heat exchange and flow resistance entropy production term on d_h is pictured in figure 5.4 for a temperature of 70 K and 300 K.

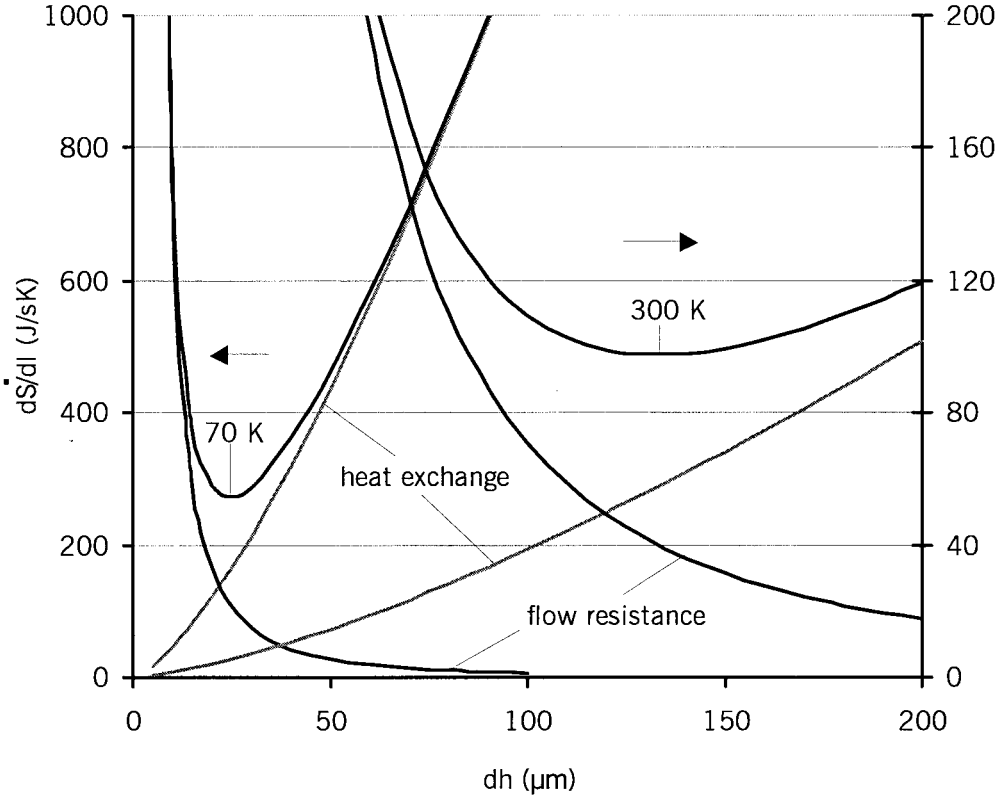

Figure 5.4: *For $z_r = z_{r1}$ and at a temperature of respectively 70 K and 300 K, the entropy production rates per unit length caused by imperfect heat exchange, flow resistance, and the sum of both are presented as a function of hydraulic diameter d_h. The scales on the right and left axis differ by a factor 5. The optimum d_h at 70 K lies around 25 μm and at 300K around 135 μm.*

In figure 5.4 it can be seen that the optimum hydraulic diameter differs significantly between the cold and the warm side of the regenerator. At 70 K the optimum d_h lies around 25 μm, while it lies around 135 μm at 300 K. The value of the minimum total entropy production rate differs

by a factor 2.8 between these two temperatures, 273 J/sKm and 98 J/sKm respectively. The optimum range at 300 K is quite broad, while it is much sharper at 70 K. With the assumptions made for this calculation, it is shown that the hydraulic diameter of 68 μm lies quite far from its optimum value, both at the cold side and at the warm side of the regenerator. This causes a 2.5 times higher entropy production rate than optimum at the cold side of the regenerator and a value that is 1.6 times the optimum value at the warm side. The absolute entropy production is largest in the coldest sections (figure 5.1), so the entropy production inside the regenerator can be decreased by decreasing the hydraulic diameter at the cold side of the regenerator. Increasing d_h at the warm side will even lower the total entropy production some more. The same calculations are performed for $z_r = 5z_{r1}$ and are presented in figure 5.5.

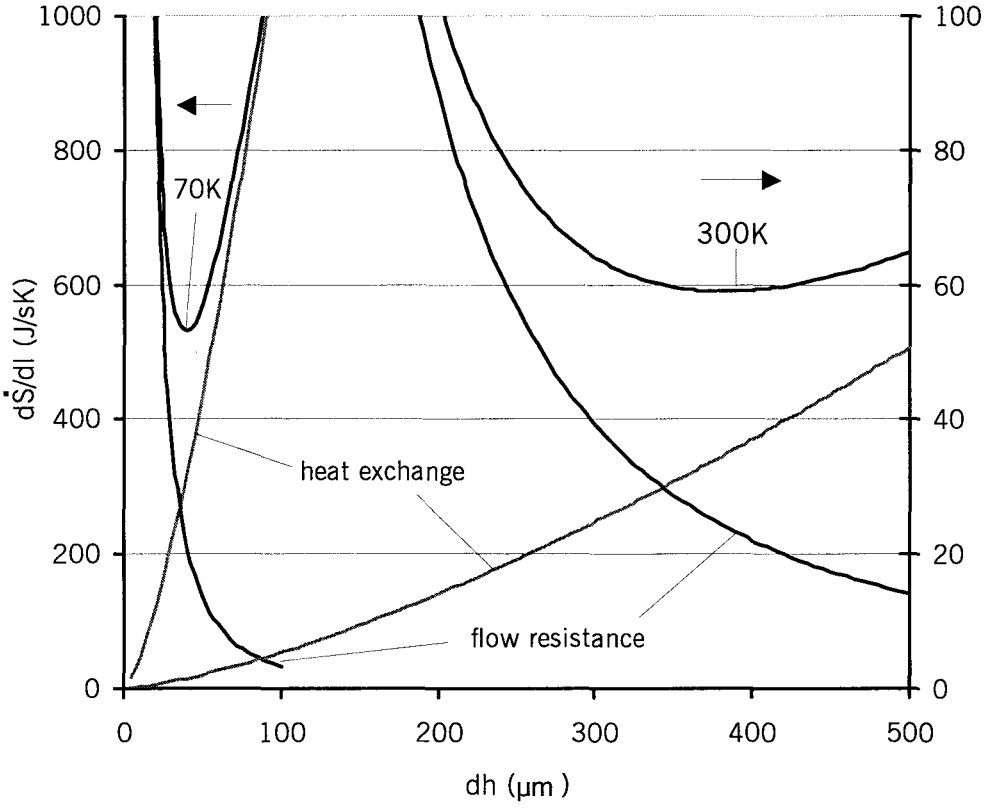

Figure 5.5: *For $z_r = 5z_{r1}$ and at a temperature of respectively 70 K and 300 K, the entropy production rates per unit length caused by imperfect heat exchange, flow resistance, and the sum of both are presented as a function of hydraulic diameter d_h. The scales on the right and left axis differ by a factor 10. The optimum d_h at 70 K is around 40 μm and at 300 K around 380 μm.*

In figure 5.5 can be seen that for $z_r = 5z_{r1}$, the optimum hydraulic diameter differs even more between the cold and the warm side of the regenerator. At 70K this optimum d_h lies around 40 μm, while it lies around 380 μm at 300K. The value of the minimum total entropy production rate differs by a factor 9 between these two temperatures, 530 J/sKm and 59 J/sKm respectively. The optimum range at 300K again is quite broad, while it is much sharper at 70K. With the assumptions made for this calculation, it is shown that the hydraulic diameter of 68 μm at the cold side of the regenerator is closer to the optimum and only gives a factor 1.4 times higher entropy production than the optimum value. At the warm side the hydraulic diameter of 68 μm now lies very far from the optimum and gives a 13 times higher entropy production than the optimum value.

Whatever the assumptions for the input parameters are, it is clear that a regenerator with uniform hydraulic diameter over its length is not ideal for minimization of the total entropy production. For example if z_r is assumed to be z_{r1} and equal to $c_z d_h^{-2}$ with $c_z = 92$, the total entropy production rate calculated inside the regenerator can be minimized to 7.07 J/sK instead of 10.39 J/sK for the current regenerator, an improvement of 32%. The regenerator then has to be divided into 26 sections of equal length (1.88 mm), varying in hydraulic diameter from 25 μm at the cold side to 120 μm at the warm side. In figure 5.6 entropy production rates of a regenerator like this are compared to a conventional SPC-1 regenerator ($z_r = z_{r1}$). If $z_r > z_{r1}$, the relative improvement can be even larger (not shown here).

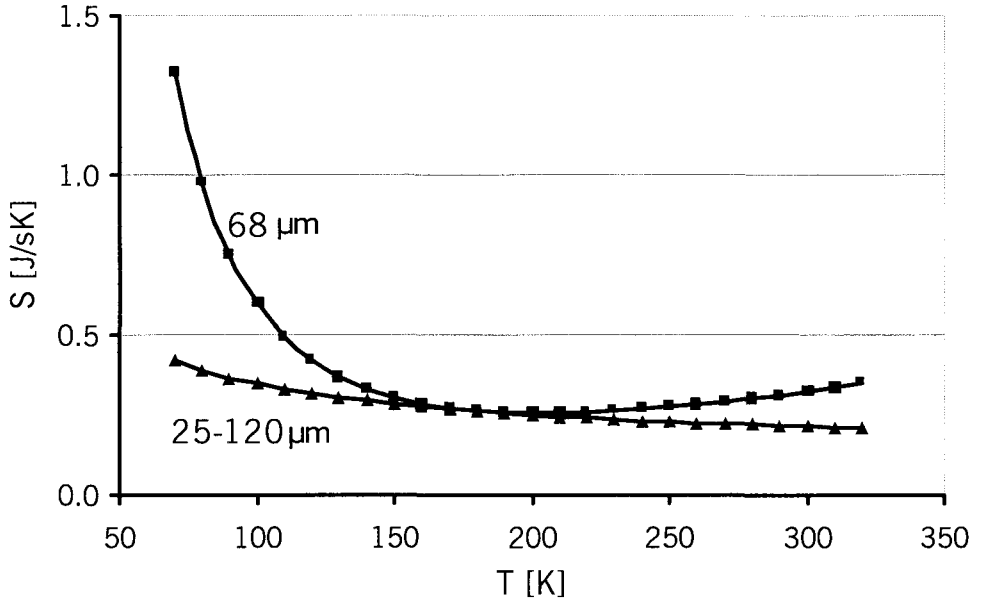

Figure 5.6: *For 26 isothermal sections of the regenerator, the total entropy production rate is calculated ($z_r = z_{r1}$). A uniform regenerator is used with $d_h = 68$ μm and one in which d_h increases from 25 μm at the cold side to 120 μm at the wam side. The total entropy production rate calculated for the regenerators is 10.39 J/sK and 7.07 J/sK respectively.*

A practical implementation of this optimization is somewhat difficult, because a lot of different screen material is needed. However, dividing the matrix into fewer sections with different hydraulic diameter, by stacking screens with different hydraulic diameter, is possible. For optimizing the performance of a complete Stirling machine, a possible new regenerator design has to be modeled with the Stirling model as well. Changes in regenerator geometry might have a negative influence on the performance in other components of the machine. Up till now no tests have been performed with a regenerator consisting of screens with different hydraulic diameters.

5.3 Regenerator matrix with rolled screens

Production of the current SPC-1 regenerator

The current regenerator of the Stirling SPC-1 is constructed of screens with a square weave pattern. Figure 5.7 is a schematic picture of one single aperture of a woven screen.

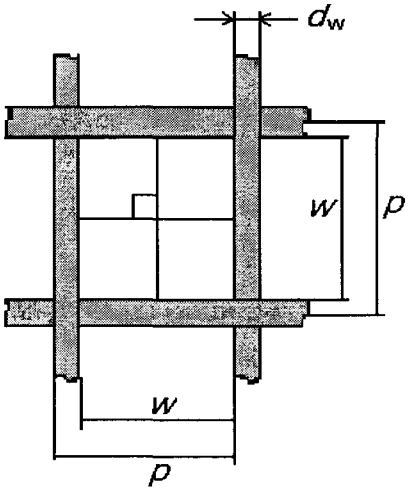

Figure 5.7: *For a screen three measures are important: The wire diameter (d_w), the aperture width (w) and the pitch (p), which is the total width of one wire and one aperture.*

After weaving, the screens are cut out to hollow circles. These screens are stacked together and are sintered. The stacking takes place without considering the orientation of the screens so no straight flow path exists in the direction of flow. Sintering is a process during which the stack of screens is heated in a vacuum space. During this process a load is applied on the stack. The sintering process bonds the screens together and takes 30 minutes.

After sintering, the package is a firm hollow cylinder of porous material. Details of this construction process are presented in Appendix E.

The current production process has two big disadvantages:

1) 57% of the screen material is considered as waste after cutting out the hollow circles. The screen material is very expensive so this is a big loss.

2) The cutting and stacking is a process that takes a lot of time and therefore is expensive.

Design of a regenerator matrix with rolled screens

To solve the disadvantages of the production process described above, a new regenerator design is proposed in this section. The concept is very simple: Instead of stacking the screens, a long strip of screen is rolled around an inner core. After tightly rolling the screens to the proper outer diameter, the screen package has to be sintered to get a firm structure. Finally, the package can be placed inside the current regenerator housing with the rubber rings. No material is wasted and the production process is very simple. The technical difficulty of this production process is

cutting out the sharp edges. Haver & Böcker (Appendix A), a German company, has the facilities to weave the screens, roll them around an inner core and sinter the package inside the final inner- and outer core. However, after doing this, the screen package is sintered onto the cores and cannot be accessed anymore to cut out the sharp edges. Another option would be rolling on a smaller inner core to a larger outer diameter, sintering with the radial application of a load and then removing the inner core. After this, the screen package has to be cut to the proper dimensions (Appendix E). A company that offers these possibilities has not been found yet. So far, the construction of a regenerator with rolled screens has not been tested, but if it will be considered in the future, some geometrical features have to be taken into account.

Flow resistance

In the ideal case in which the screens are perfectly rolled, the frontal area will look like pictured in figure 5.8. In reality, the screens will fit into each other during rolling and the package will be compressed, increasing f. The increase of f by sintering without an applied load is considered small, so the final compression factor for the screen package is the same as for the stacked screens. If the filling factor and the wire diameter are kept the same, the hydraulic diameter for the rolled and the stacked screens is equal (equation 2.11).

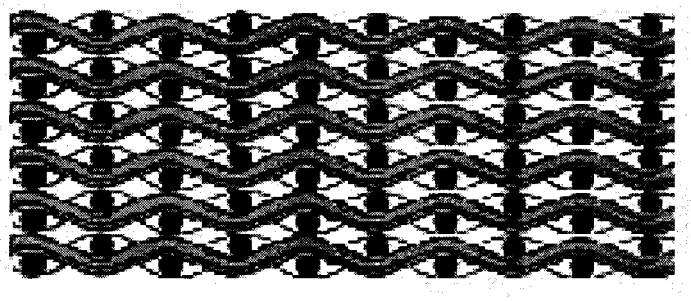

Figure 5.8: *The frontal area (perpendicular to the flow direction) of perfectly rolled screens. In reality, the screens will fit into each other and the package will be compressed by a factor 1.3.*

Next to d_h, two other geometrical parameters are assumed to determine the total flow resistance of the regenerator:

1) The minimum cross-sectional area.
A larger ratio of the maximum and minimum cross-sectional area of a flow channel inside a regenerator matrix, decreases the regenerator performance due to non linear effects in the gas [5]. Therefore the minimum and maximum cross-sectional area of a flow channel should differ as little as possible. Considering one single screen as pictured in figure 5.7 that is perpendicular to the flow direction, the minimum cross-sectional area is 44 % open for flow. If the screens are perfectly rolled like in figure 5.8, this is only 34 %, even smaller if the compression factor for rolling is taken into account.

2) The number of wires perpendicular to the flow direction.
Assumed is that a wire perpendicular to the flow, gives a much larger contribution to the total flow resistance than a wire parallel to the flow. When the screens are rolled, in one flow channel, less wires are perpendicular tot the flow.

Heat exchange

Next to d_h and F, the number of wires perpendicular to the flow direction is another geometrical factor that is assumed to influence the heat exchange between the gas and the matrix. Parallel to the flow direction, N_u is about 4 [13]. In the conventional SPC-1 regenerator, $20 < R_e < 60$ so N_u is about 2-4 for flow perpendicular to a cylindrical wire [37]. This is about the same as for parallel flow, so if the same screens are rolled, no significant change in heat exchange is expected.

Heat conduction

If the screens are rolled instead of stacked, direct thermal contact exists between the hot and the cold side of the regenerator. In the stacked matrix, thermal contact in axial direction takes place in a lot of small contact points between the individual screens. If the current screens are rolled, the total cross-sectional area for conduction in the flow direction, is 16% of the regenerator cross-sectional area. Therefore, in the Stirling model it is assumed that $\lambda_r = 0.16\lambda_m$. In figure 5.9, the calculated losses due to heat conduction (equation 4.14) are compared for a regenerator with stacked and one with rolled screens. Except for the thermal conduction, all the other parameters for the regenerator are kept the same. From figure 5.9 can be seen that the conduction loss is a factor four higher for the rolled screens. The total cooling power of the modeled Stirling SPC-1 however, only decreases by 1.5% from 1186W to 1168W. In addition to a small decrease in cooling power, the efficiency of the machine decreases from 13.7% to 13.1%.

Optimization

For an optimum geometry of rolled screens, an optimum combination has to be found for the flow resistance, heat exchange and heat conduction. Relations for these losses have to be determined empirically. A rectangular weave pattern like pictured in figure 5.10, can be of help to find the best matrix geometry. Optimization can be performed by systematically varying d_w and p as well in the direction perpendicular to the flow, as in the direction across. A weave pattern like pictured in figure 5.10 can be produced by e.g. Haver & Böcker. Up till now no further optimization has been performed.

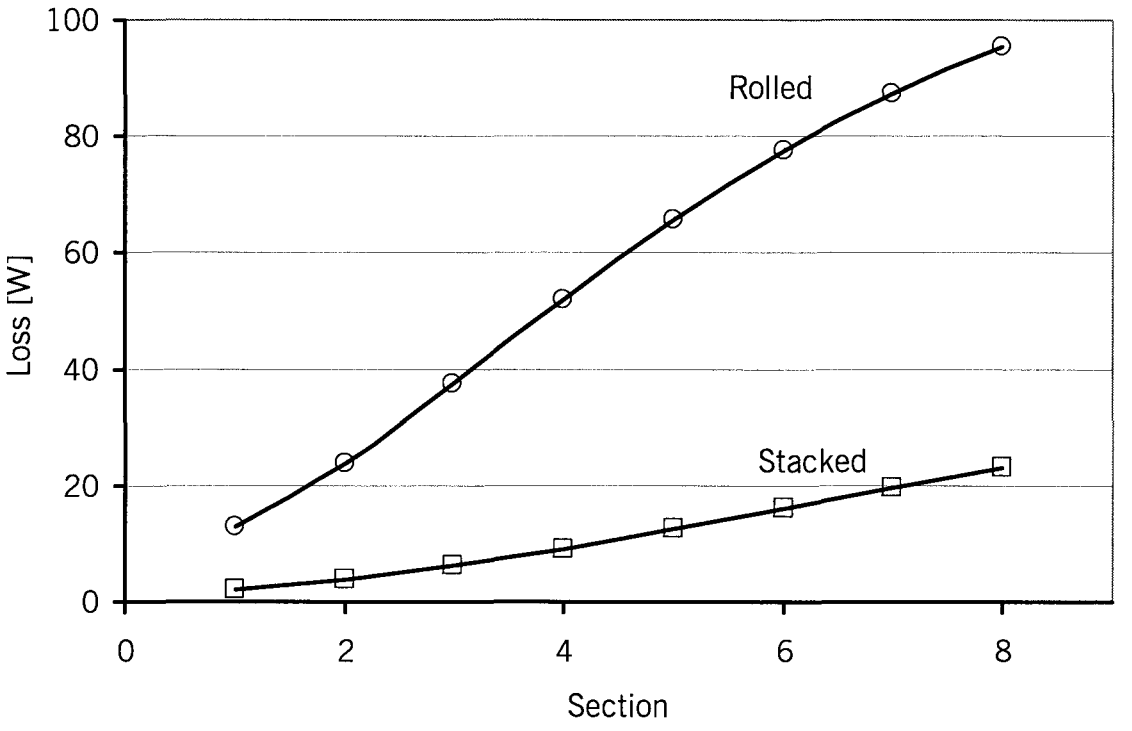

Figure 5.9: *The Stirling model has divided the regenerator into eight different sections. Section 1 is at the cold side (70 K) and section 8 at the warm side (320 K). The pressure inside the modeled SPC-1 is 30 bar. The rolled screens (circles) give a four times higher conduction loss than the stacked screens (squares). The total cooling power of the modeled machine is 1168W and 1186W and the efficiency is 13.1 % and 13.7 % for the rolled and the stacked screens respectively.*

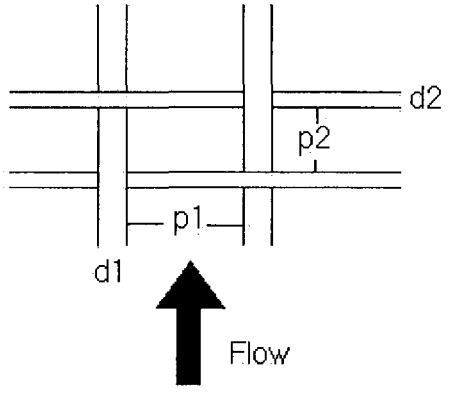

Figure 5.10: *For optimization of the rolled screen matrix geometry, wire diameters (d_1 and d_2) and pitches (p_1 and p_2) can be varied in two directions separately.*

5.4 Regenerator matrix of sintered stainless steel particles

Instead of using screens, a regenerator matrix can also be produced of small stainless steel particles sintered together. A Dutch company named I.B. Kracht BV (Appendix A) produces this kind of sintered elements, primarily for use as filter elements. An advantage of the sintered metal material is a strong reduction in production costs in comparison to screens. Another advantage is that it can be produced directly into any desired shape, also the hollow cylinder shape pictured in Appendix E. To predict the performance of a Stirling machine equipped with a regenerator of these sintered metal particles, assumptions have to be made about the pressure drop, heat exchange, and heat conduction behavior of such a regenerator. No empirical relations are known yet. Therefore the material is assumed to consist of cylindrical tubes for which the modifications to the Stirling model are given in section 4.5. First calculations are performed for laminar flow only to avoid complicated turbulent behavior. However turbulence might already occur inside this material at $R_e << 2300$, the value commonly used for the transition between laminar an turbulent flow inside cylindrical tubes. At I.B. Kracht BV pressure drop tests are performed for the different materials they produce. From the pressure drop Δp over a certain length L_r of material with a cross section A_r, the equivalent diameter of a material consisting of cylindrical tubes causing equal pressure drop is derived [20]

$$d = \sqrt{\frac{32 L_r \dot{V} \eta}{A_r \Delta p (1 - f)}} . \tag{5.1}$$

Equation 5.1 can only be used for laminar flow. A schematic picture of the model is given in figure 5.11. The number of flow channels is determined by the filling factor of the material.

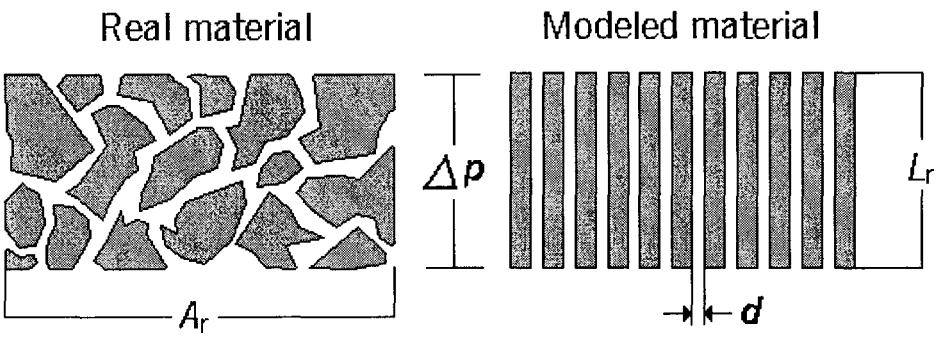

Figure 5.11: *The real material of sintered metal particles, schematically looks like pictured on the left. In the Stirling model it is modeled as cylindrical tubes, like pictured on the right. The diameter d is derived from pressure drop measurements performed at I.B. Kracht BV.*

In comparison to the cylindrical tubes, the heat exchanging surface per unit of volume of the real material is larger and the axial thermal conduction is significantly lower. This would indicate lower losses than calculated when modeling as cylindrical tubes. However the flow distribution is not uniform and more gas will flow through the wider channels in the real material. In these channels the flow losses are lower, but also the heat exchange is less. More exact relations for the pressure drop-, heat exchange-, and heat conduction behavior for a material of sintered metal particles can only be derived empirically.

I.B. Kracht BV produces the sintered material in several different qualities for stainless steel material. The different qualities are named SIKA-R 0.5 to SIKA-R 200, in which the number represents a typical particle size in μm. For some of the different qualities, material properties like f, z_r, and d are presented in table 5.2. The values of z_r are the reciprocal values of the permeability coefficient given by I.B. Kracht BV.

Table 5.2: *From information given by I.B. Kracht BV, the values of f, z_r, and d are derived and presented in columns 2 to 4 for the SIKA-R 30, 40, 50, 80 and 100 materials.*

Material	***f***	z_r $[10^{10}\ m^{-2}]$	***d*** **[μm]**
SIKA-R 30	0.57	7.1	32
SIKA-R 40	0.54	4.0	42
SIKA-R 50	0.53	2.8	49
SIKA-R 80	0.50	2.3	53
SIKA-R 100	0.48	1.7	60

For the input of the Stirling model, only the values of f and d are needed. In figure 5.12 the modeled cooling power of a Stirling "Economy" machine (SPC-1 machine with smaller displacer amplitude to reduce the cooling power) is presented for a machine with a regenerator made of sintered stacked screens and with a regenerator of the SIKA-R materials presented in table 5.2. The SIKA-R materials are modeled as cylindrical tubes. Also given are the calculated efficiencies. Unless stated differently, all the calculations in this section are performed for T_L = 70K, T_H = 320 K and p = 30 bar.

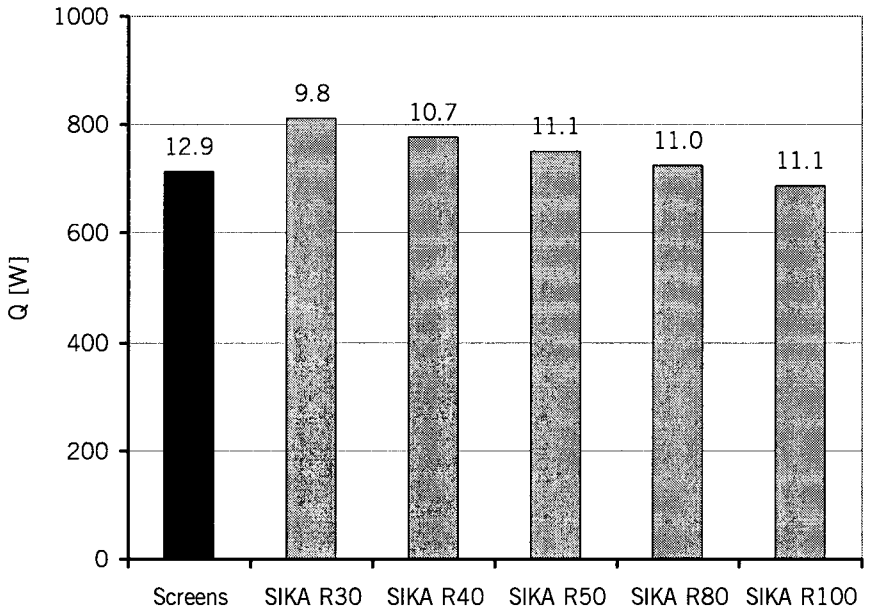

Figure 5.12: *The cooling power and efficiency (label) of a Stirling "Economy" machine as predicted by the Stirling model. The conventional regenerator with stacked screens is used, as well as a regenerator consisting of respectively SIKA-R 30, 40, 50, 80, and 100 material. The SIKA-R 30 to 80 materials predict a higher cooling power than the screen material. The efficiency (label) however is smaller for all of the modeled SIKA-R materials.*

From figure 5.12 can be seen that the SIKA-R 30 to 80 materials predict a higher cooling power than the conventional screen material. The efficiency however, is smaller for all of the modeled SIKA-R materials. Of the individual regenerator losses introduced in section 4.3, especially the conduction loss (equation 4.14) is much higher for the modeled tubes. The matrix conduction coefficient *KREG* in equation 4.33 is largely overestimated if the sintered material is modeled as cylindrical tubes. In figure 5.13 the simulations above are repeated with $KREG = 0.5f\lambda_m$.

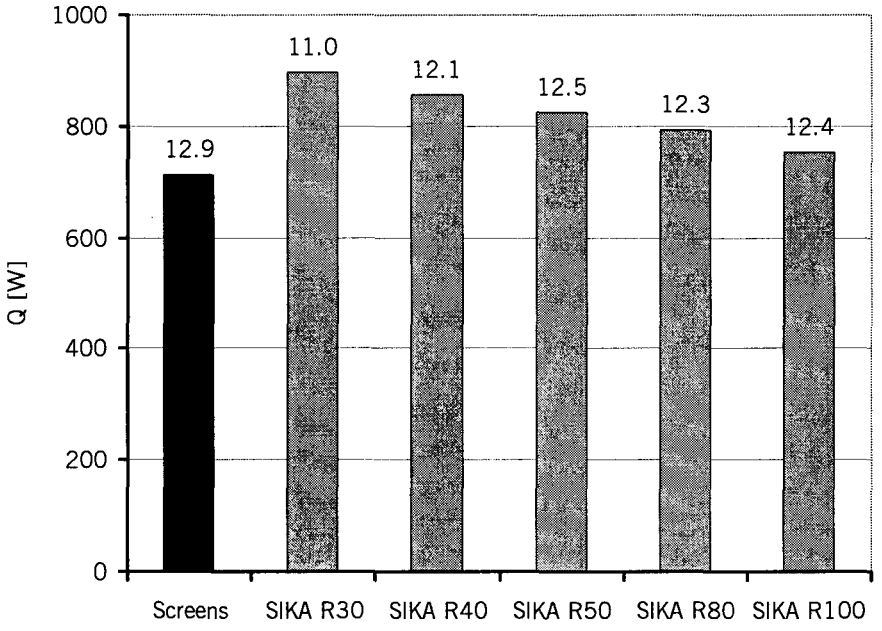

Figure 5.13: *With the Stirling model the cooling power of a Stirling "Economy" machine is modeled. As a regenerator, the conventional regenerator with stacked screens is used, as well as a regenerator consisting of respectively SIKA-R 30, 40, 50, 80, and 100 material. The axial thermal conductivity of the SIKA-R materials is now assumed to be half the value of cylindrical tubes. The SIKA-R materials predict a higher cooling power than the screen material and the cooling power is about 70W higher than in figure 5.12. The efficiency is still smaller for all the SIKA-R materials but more than 1% higher than in figure 5.11.*

As can be seen by comparing figure 5.13 to figure 5.12, the cooling power and efficiency have significantly increased by assuming a lower axial thermal conductivity. The predicted efficiencies for the SIKA-R 40 to 100 are now only a fraction lower than for the screen regenerator, and the cooling power is expected to be higher. The SIKA-R30 predicts the highest cooling power but its efficiency is lowest, so a power input of 7500W is required. This is the maximum a standard Economy-engine can deliver. The reason for this low efficiency is the relatively high flow impedance of the material, see also table 5.2. Therefore this material is not ideal for regenerator use. To derive empirical relations, as much materials as possible have to be tested. However, because the research budget is limited, only two materials will be tested in first instance. The SIKA-R 100 material is not available in the required dimensions so SIKA-R 40 and SIKA-R 80 will be tested to get the largest diversity in material properties. The tests will be described in chapter 6 and 7.

6 Experimental setup

6.1 Introduction

To determine the specific flow impedance of a regenerator, a setup is used with a static flow through the regenerator. This is described in section 6.2. To test the performance of a regenerator, a Stirling "Economy" cryogenerator is used. A standard Economy machine is fitted with temperature and pressure sensors and a heater is mounted on the cold head to measure the cooling power. After measuring with a standard stainless steel screen regenerator, different regenerators made of sintered stainless steel particles are mounted, without altering the rest of the machine. In section 6.3 a detailed description of the experimental setup is given. In section 6.4 a description is given of the regenerators made of sintered particles.

6.2 Static pressure drop

To measure the flow resistance of a regenerator in static flow conditions, the characteristic flow impedance of the regenerator is determined with the setup pictured schematically in figure 6.1. With a water column the pressure difference across the regenerator is determined. The volume flow through the system is measured with a flow meter (Brooks Instrument B.V., type G/T 1000).

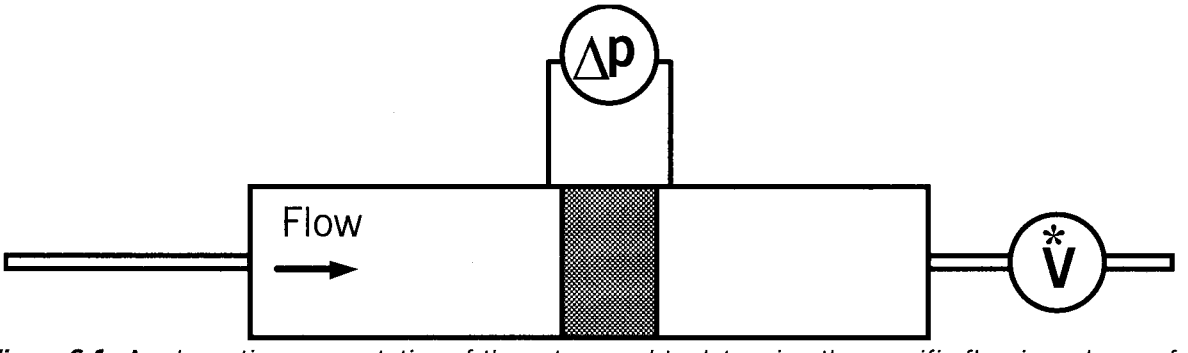

Figure 6.1: *A schematic representation of the setup used to determine the specific flow impedance of a regenerator. The regenerator is mounted into a pipe in which a flow is generated. With a water column the pressure difference across the regenerator is measured. The volume flow is measured with a flow meter.*

At low Reynolds numbers ($R_e < 1$) the characteristic flow impedance z_r of a regenerator can be determined with Darcy's law [2],

$$z_r = \frac{\Delta p A_r}{L \eta \dot{V}^*}. \tag{6.1}$$

In equation 6.1, A_r is the empty regenerator surface area, $\dot{V}^*$ the volume flow through the system, and Δp is the pressure drop over the regenerator. The flowing medium is air ($\eta = 1.8 \cdot 10^{-5}$ kg/ms; T= 293K; p = 1 bar [37]).

6.3 The Economy machine

The Economy machine is the smallest in the range of cryocoolers produced by Stirling. It has half of the cooling capacity of the standard SPC-1 machine. The Economy machine differs from the SPC-1 only at one point: the amplitude of the displacer. In figure 6.2 a schematic picture of a standard Economy machine is presented. As indicated in figure 6.2, four thermocouples and a pressure sensor are mounted at the warm side of the machine to measure the temperature of the cooling water and the temperature and pressure inside the compression space. One thermocouple is mounted at the side of the compression space where the cooling water flows into the warm heat exchanger, the other one is mounted at the opposite side. In calculations, the average value will be used.The standard cold heat exchanger (cold head), is replaced by a cold head at which a heater is mounted. To reduce conduction losses, the entire cold head is placed in vacuum. A schematic picture of the adapted cold head is given in figure 6.3. Inside the cold head, two PT-100 temperature sensors are mounted. The pressure in the expansion space is measured at room temperature through a capillary that leads through the vacuum mantle. The pressure drop and phase shift across this capillary can be estimated by modeling it as a RC-circuit. Calculations presented in Appendix F show that this additional phase shift and pressure drop can be neglected. The heater is powered with two 75 V - 15 A power supplies and can generate up to 2250 W of heat. All the data are sent to a PC and are monitored with "Labview", a software package. A schematic description of the measuring system is given in figure 6.4 and details about the different elements of the measuring system are presented in Appendix G. Because the quality of the vacuum inside the vacuum mantle influences the conduction losses inside the mantle, the vacuum is monitored with a vacuum pressure sensor.

To measure the cooling power at a certain temperature, the heater is set to a certain value. When the temperature inside the cold head has stabilized, the cooling power is equal to the applied heat if is assumed that no other thermal losses occur. The Economy machine is driven with an electro-motor. With a three-phase power meter, the power input of this motor is measured and sent to the PC. With the known cooling power and power input, the efficiency of the Economy machine at a certain temperature is known (equation 2.6).

The performance of the Economy is measured at a mean absolute pressure of 21, 26, and 31 bar. The pressure value is read at the manometer mounted inside the compression space of the machine. Actually this manometer measures relative pressure, so approximately 1 bar is added to know the absolute pressure inside the machine. At different temperatures at the cold side of the machine, a pressure signal is measured. At a sampling rate of 100.000 times per second, 2.5 periods of the oscillating pressure signal (25Hz) are measured simultaneously inside the compression space and the expansion space. The measurements described above are performed with four different regenerators, which are described in section 6.4.

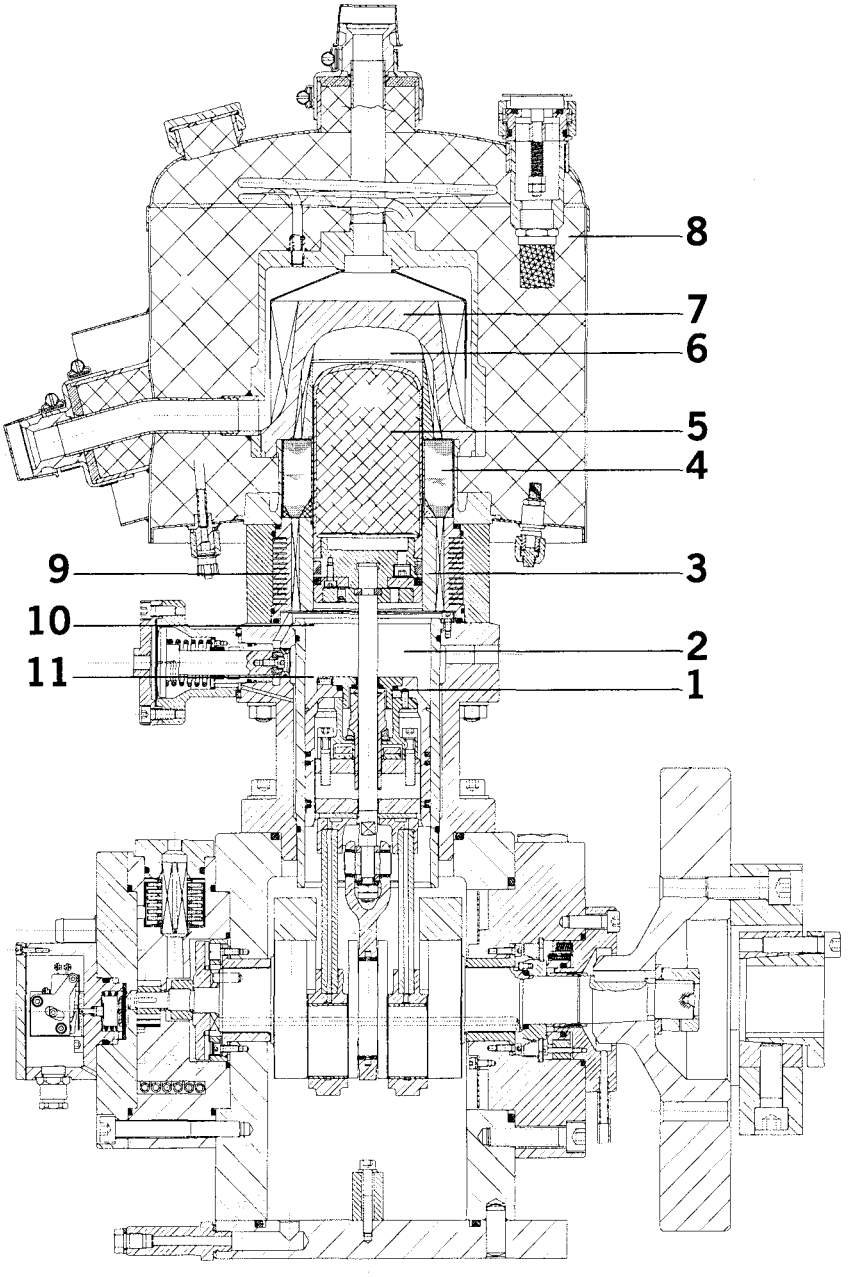

Figure 6.2: *A schematic picture of the Stirling "Economy" machine used to measure the regenerator performance. The numbers indicate some important components of the machine and the sensors that are mounted for the experiments: 1) Compression piston, 2) Compression space, 3) Warm heat exchanger, 4) Regenerator, 5) Displacer, 6) Expansion space, 7) Cold heat exchanger (cold head), 8) Isolation mantle, 9) Position of thermocouples (2x) for measuring the temperature of the cooling water inside the warm heat exchanger, 10) Position of thermocouples (2x) for measuring the temperature inside the compression space, and 11) Position of pressure sensor for measuring the pressure inside the compression space. For the experiments, the standard cold head is replaced by a cold head with a heater and the isolation mantle filled with perlite is replaced by a vacuum mantle.*

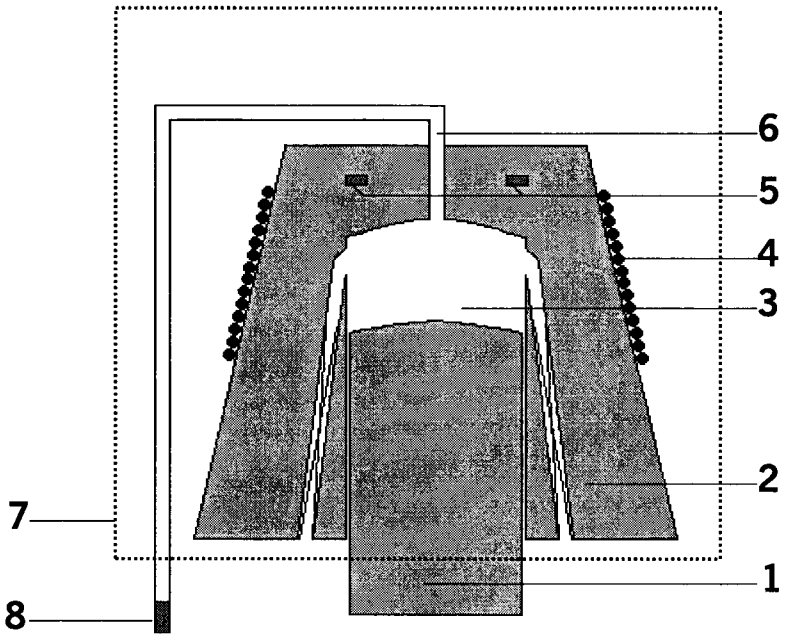

Figure 6.3: *Schematic picture of the cold head that is used in the adapted Economy machine. The cooling fins are removed and a heater is spirally wound around the cold head. The complete cold head is mounted inside a vacuum mantle. The pressure inside the expansion space is measured at room temperature at the end of a capillary. The numbers indicate the different components and the sensors used for measuring: 1) Displacer, 2) Cold head, 3) expansion space, 4) Heater (2x), 5) PT-100 Temperature sensor (2x), 6) Capillary, 7) Vacuum mantle, and 8) Pressure sensor.*

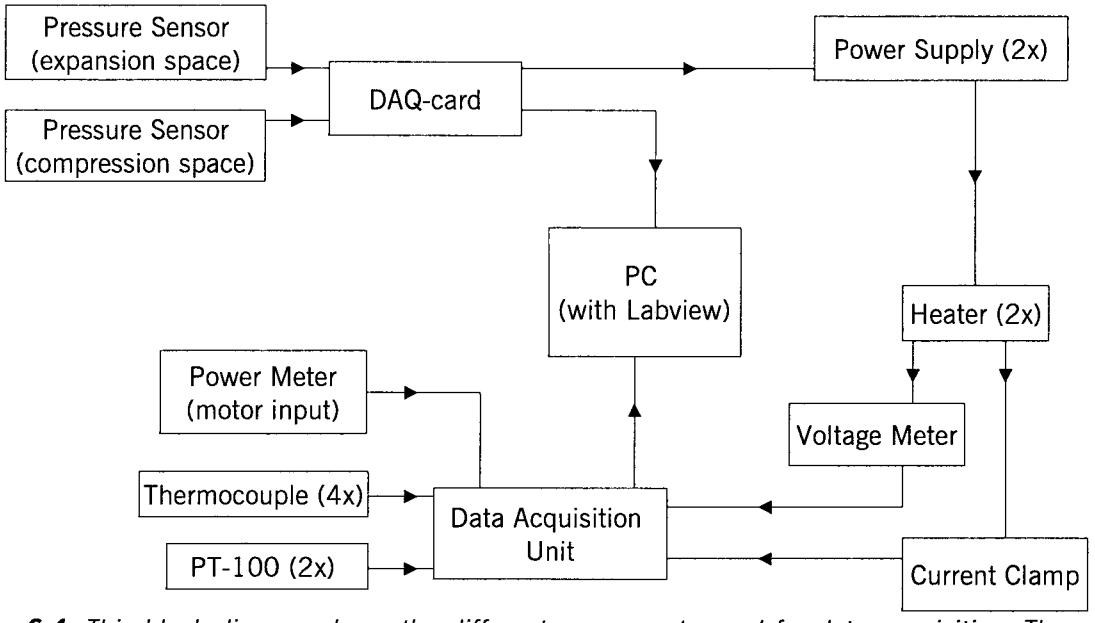

Figure 6.4: *This block diagram shows the different components used for data acquisition. The analog signals of the pressure sensors are converted to digital signals with a DAQ-card that can sample up to 100.000 times per second. With the analog output of this DAQ-card the power supply of the heaters is regulated. The signals of the power meter, the thermocouples, the PT-100 sensors, the voltage meter, and the current clamp are converted with a data acquisition unit (multimeter) that samples up to once every 10 seconds. All the data are sent to a PC and are monitored with a software package named "Labview".*

6.4 The regenerators with sintered stainless steel particles

With the experimental setup described in section 6.3, the performance of the Economy machine will be measured with a regenerator matrix that consists of sintered stainless steel particles. This performance will be compared to the performance when a stainless steel screen regenerator is used. The materials that will be tested are SIKA-R40 (f = 0.54, d = 42 μm) and SIKA-R80 (f = 0.50, d = 53 μm).

No standard size of the material is available from which a regenerator can be made out of a single piece. Therefore, the regenerators are built from three. The disks are machined to rings and the rings will be stacked and mounted between the same inner- and outer core that is used for the current SPC-1 regenerator.

Next to a screen regenerator, a SIKA-R40 regenerator, and a SIKA-R80 regenerator, a fourth regenerator will be tested. In section 5.2 it is suggested that a regenerator with a smaller d_h at the cold side and larger d_h at the warm side will produce less entropy than a uniform regenerator. Therefore a regenerator will be tested that consists of one disk SIKA-R40 material at the cold side and two disks of SIKA-R80 material at the warm side.

7 Results

7.1 Introduction

In this chapter, the results of the experiments with the sintered metal regenerators will be presented and discussed. First in section 7.2 the values of the specific flow impedance will be presented. These values are determined in steady flow conditions. In section 7.3 the performance of a Stirling Economy machine will be compared when different regenerators are used. The standard screen regenerator will be used as a reference. Flow resistance inside a regenerator causes a degradation of performance. To compare the flow resistance of the different regenerators, the dynamic pressure signal in the compression and expansion space is presented in section 7.4. Finally, in section 7.5 the difference is discussed between the measured performance and the performance predicted with the cylindrical tube model from section 5.4.

7.2 Specific flow impedance

With the experimental setup described in section 6.2, the specific flow impedance of the various regenerators is determined. In these experiments, compressed air flows through the regenerator. The Reynolds number is of order 1. The volume flow through the regenerator is varied from 0 to $1 \cdot 10^{-3}$ m^3/s from which an average value of z_r is calculated using equation 6.1. The results are presented in table 7.1.

Table 7.1: *For the stacked screens, as well for the SIKA-R40 and the SIKA-R80 material, the specific flow impedance z_r has been determined. The values of z_r are presented in the second column. In the third column, the values specified by the manufacturer are given.*

Regenerator material	**z_r (measured) [$\cdot 10^{10}$ m^{-2}]**	**z_r (specified) [$\cdot 10^{10}$ m^{-2}]**
Stainless steel screens	2.0	-
SIKA-R80	2.6	2.3
SIKA-R40	6.6	4.0

As can be seen in table 7.1, the measured z_r for the SIKA-R80 regenerator is 30% higher than z_r for the screen regenerator. For the SIKA-R40, z_r is a factor 3.3 higher than for the screens. Also the measured z_r is 13% and 65% higher than specified for the R80 and the R40 material respectively. One reason for this could be the filling factor of the material that is slightly higher than specified. For the R80 material f is 0.53 instead of 0.50 and for the R40 material f is 0.57 instead of 0.54.

The second reason could be turbulent behavior. Equation 6.1 is derived from

$$\Delta p = \frac{\overset{*}{V} L}{A_r}\left(z_r \eta + \frac{\rho \overset{*}{V}}{\beta A_r} \right). \tag{7.1}$$

In equation 7.1, β is the second order coefficient (turbulence). This β is not to be confused with the volumetric heat exchange parameter defined in section 2.3. The first part of equation 7.1 is the linear contribution to the pressure drop. In equation 6.1, the turbulent part is not

taken into account. The manufacturer of the SIKA-R materials specifies a value for β: $4.7 \cdot 10^{-6}$ m for the R80 and $3.6 \cdot 10^{-6}$ m for the R40 material. If equation 7.1 is used to calculate z_r it is 2.5 m^{-2} and 6.4 m^{-2} respectively. This small correction doesn't explain the higher value of z_r for the R40 material. Probably the specified value of β for the R40 material is too high.

7.3 Performance of the Economy machine

The screen regenerator and the regenerators with the sintered metal particles have been mounted into the modified economy machine described in section 6.3. The cooling power of the machine is measured at three different mean pressures p_m inside the machine: 21, 26, and 31 bar. The measured cooling power of the Economy is presented in figures 7.1 to 7.3. The lines in these figures have no physical meaning but are only guidelines for the eye.

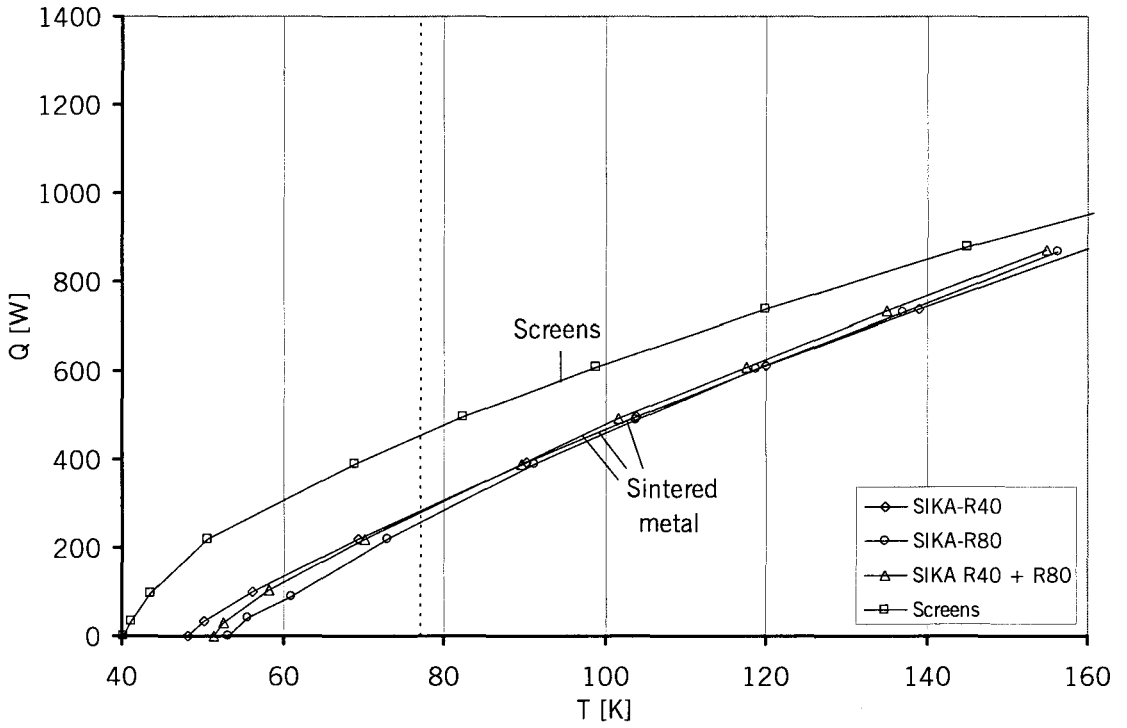

Figure 7.1 (p_m = 21 bar): *The cooling power of a Stirling Economy machine is measured as function of T. Next to a standard screen regenerator, a regenerator of SIKA-R40, SIKA-R80 and a combination of these materials are tested. As can be seen, the screen regenerator performs significantly better than the sintered materials.*

As can be seen in figures 7.1 to 7.3, the machine performs significantly better with the screen regenerator than when SIKA-R40 or R80 material is used. The higher the cold end temperature is, the smaller the difference is between the screens and the sintered materials. Of the uniform sintered materials, the R40 reaches the lowest temperature and gives the highest cooling power for $T < 130$K. At higher temperatures, the R80 performs better. The combination of both materials lies between the two curves for $T < 90$K and performs better than both uniform regenerators at higher temperatures. The main region of interest for Stirling lies around 77K, the boiling point of nitrogen.

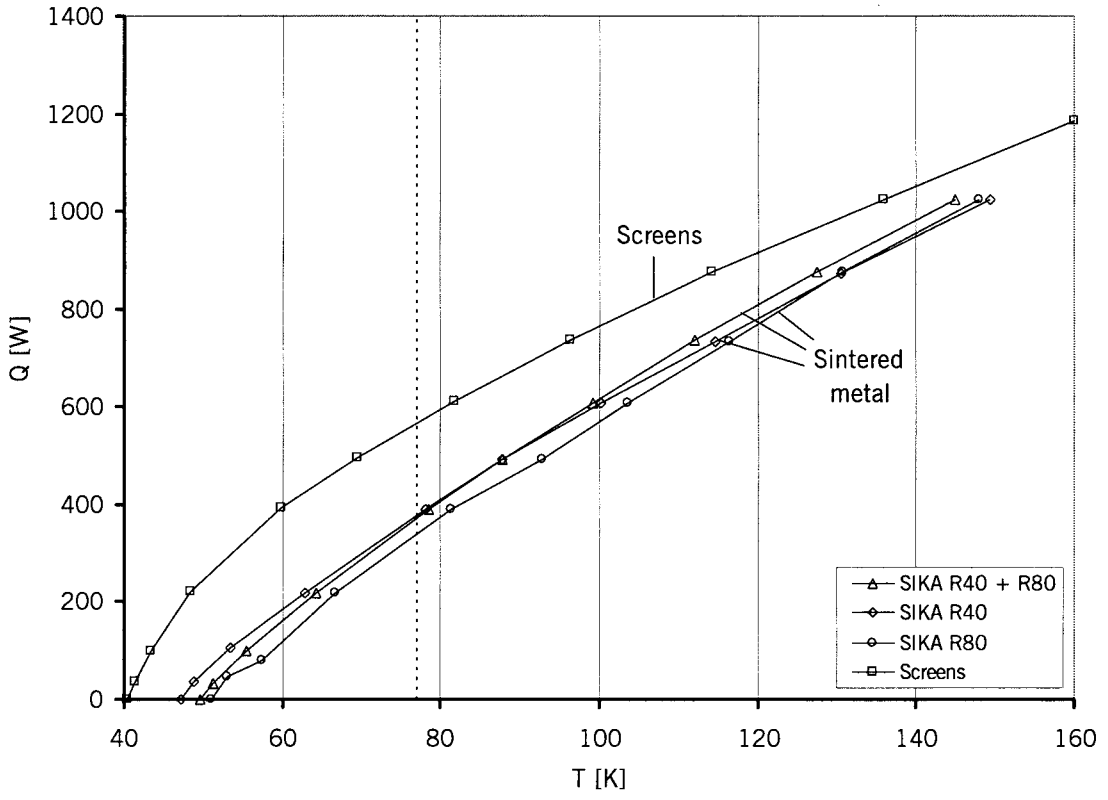

Figure 7.2 (p_m = 26 bar): *As figure 7.1.*

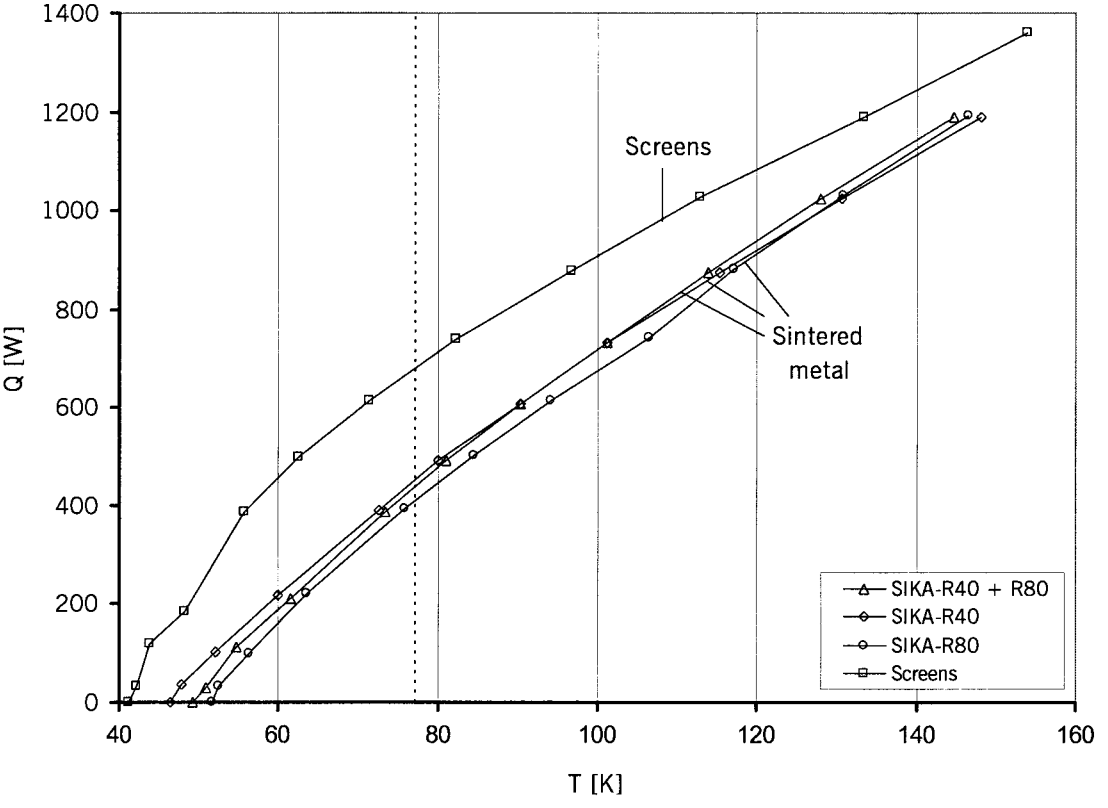

Figure 7.3a (p_m = 31 bar) : *As figure 7.1.*

The cooling power is not the only important parameter to indicate the performance of a machine. A second important parameter is the efficiency (*COP*) of the machine that can be calculated with equation 2.6. In figure 7.4 the *COP* is presented for an economy machine with four different regenerators. The mean p_m = 31 bar. For pressures of 21 and 26 bar, the plots look almost the same (Appendix H). The only difference is a slightly lower *COP* at lower pressures.

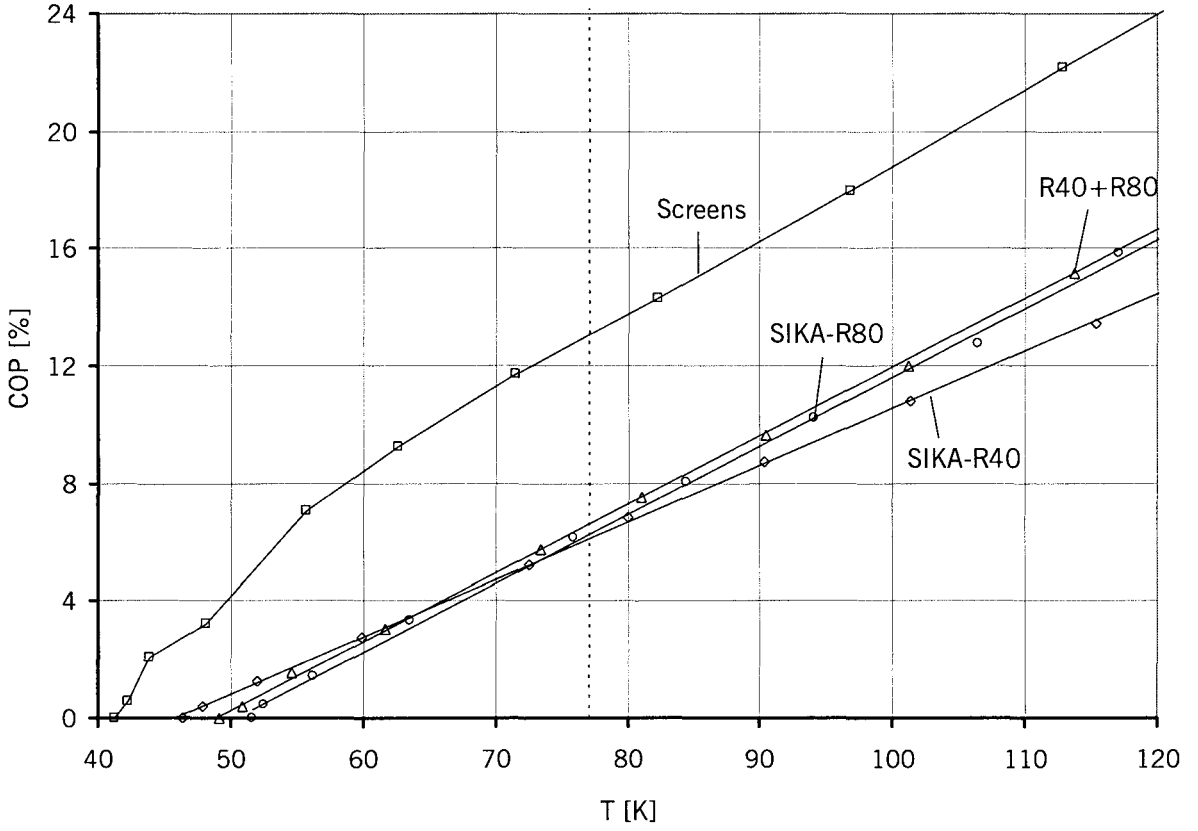

Figure 7.4: *The efficiency (COP) of the machine as function of T. At a pressure of 31 bar, the efficiency of a standard screen regenerator, a regenerator of SIKA-R40, SIKA-R80 and a combination of these materials is presented. The machine with the screen regenerator has a significantly higher efficiency than when a sintered metal regenerator is used.*

As can be seen from figure 7.4, the screen regenerator gives a much higher *COP* than the sintered metal regenerators. For the sintered metal, the *COP* depends linearly on *T*, for the screens this linear dependence occurs only for $T > 70$K. The R80 material has a steeper curve than the R40 material and has a higher COP for $T > 75$K. The *COP* of the combined regenerator has the same gradient as the R80 material, but is about 0.4% higher in the whole temperature range.

The actual cooling power of the machine is higher than the values presented in figures 7.1 to 7.3. This is due to thermal losses in the capillary that is mounted to measure the pressure in the expansion space. (Ice grows on this capillary, indicating the thermal losses) Before the capillary was mounted, the performance of the machine has been measured at a pressure of 26 bar. With the capillary, the same measurement has been repeated twice. The results are presented in figure 7.5.

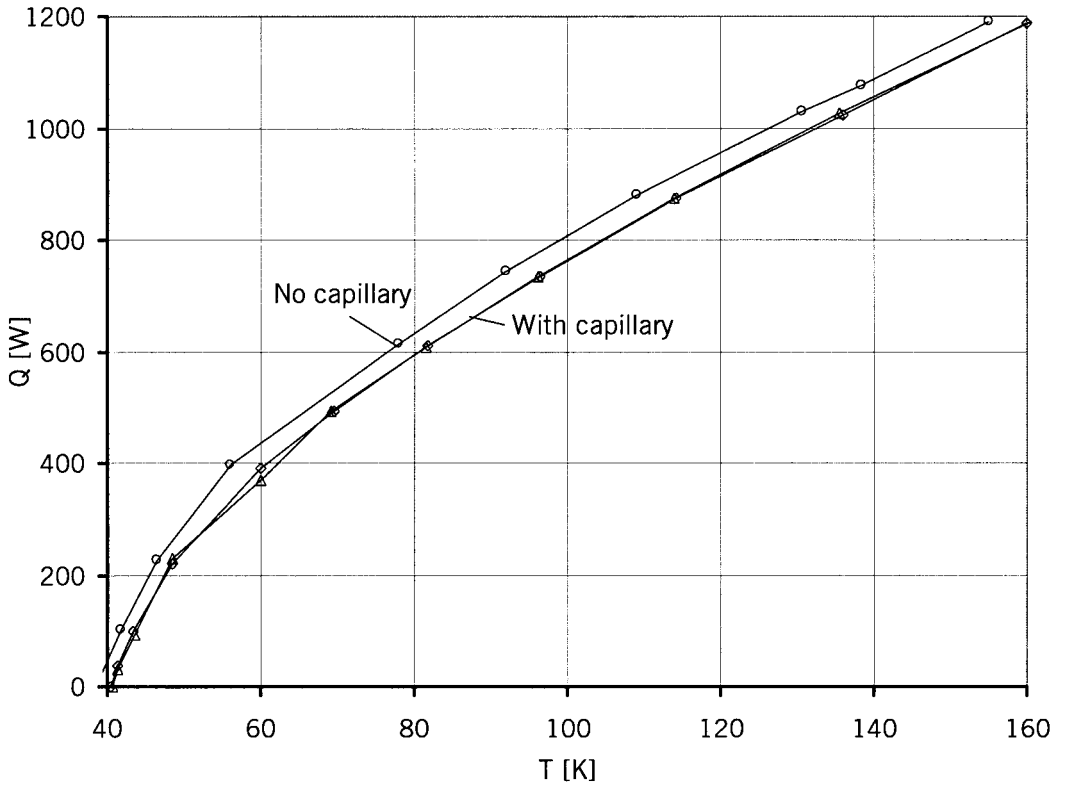

Figure 7.5: *To measure the pressure in the expansion space, a capillary is used that leads from the cold head to a pressure sensor outside the vacuum mantle. At a pressure of 26 bar, the cooling power of the machine is measured before the capillary is mounted, as well as with the capillary (2x). Due to a heat pump effect, a thermal loss occurs. At 26 bar and 60 K < T < 100 K, this loss is about 45 W.*

As can be seen in figure 7.5, the cooling power with capillary is about 45 W smaller than without capillary for 60 K < T< 100 K. From the two measurements with the capillary can be seen that the cooling power delivered by the machine is very reproducible.

From figure 7.1 to 7.4, the cooling power and the efficiency at a cold end temperature of 77 K can be interpolated. In table 7.2, the cooling power and the efficiency are presented at 77 K for p_m = 21, 26 and 31 bar. The efficiency at 21 and 26 bar is presented in Appendix H. The values for Q and COP in table 7.2 are corrected with the extra 45 W that is lost in the capillary.

Table 7.2: *For an Economy machine, the cooling power and the efficiency (COP) is determined at T_L = 77 K. This is the temperature at which nitrogen liquefies at atmospheric pressure, the main application of the machines produced at Stirling.*

Material	**Q (T_L = 77 K) [W]**			**COP (T_L = 77 K) [%]**		
p_m [bar]	**21**	**26**	**31**	**21**	**26**	**31**
Screens	515	615	735	11.5	13.1	14.1
SIKA-R80	305	385	465	5.7	6.6	7.0
SIKA-R40	335	425	495	5.9	6.5	6.7
R40 + R80	335	425	490	6.4	6.9	7.3

In table 7.2 it can be seen that compared to the screen regenerator, the Economy machine delivers 30-40% less cooling power with the sintered metal. The *COP* is 50% lower. The cooling power with the screen regenerator is consistent with prior measurements at Stirling [39].

7.4 Dynamic pressure drop

The pressures in the compression and expansion space, respectively p_C and p_E, are measured. At a sampling rate of 100.000 per second, 1.5 periods of the oscillating pressure signal are measured. The pressure signal contains some noise that is filtered out by fitting the data points to [34]

$$p(t) = \frac{p_m}{(1 + 0.5\varepsilon \sin(\omega t + \tau))^2}. \tag{7.2}$$

Because the pressure oscillations are caused by two pistons that oscillate with a phase difference, the actual pressure signal is described by equation 7.2. For small ε, equation 7.2 can be approximated by the cosine signal presented in equation 4.3. In equation 7.2, ω is the angular frequency, which is about 157 s^{-1}. The phase is given by τ and can be defined as zero for the compression space. Then τ for the expansion space is the phase difference between p_C and p_E. For the curve fitting, software called "Mathcad 2000" is used. For screens, p_m = 21 bar and T = 40K, the pressure data and a fit to equation 7.2 are pictured in figure 7.6.

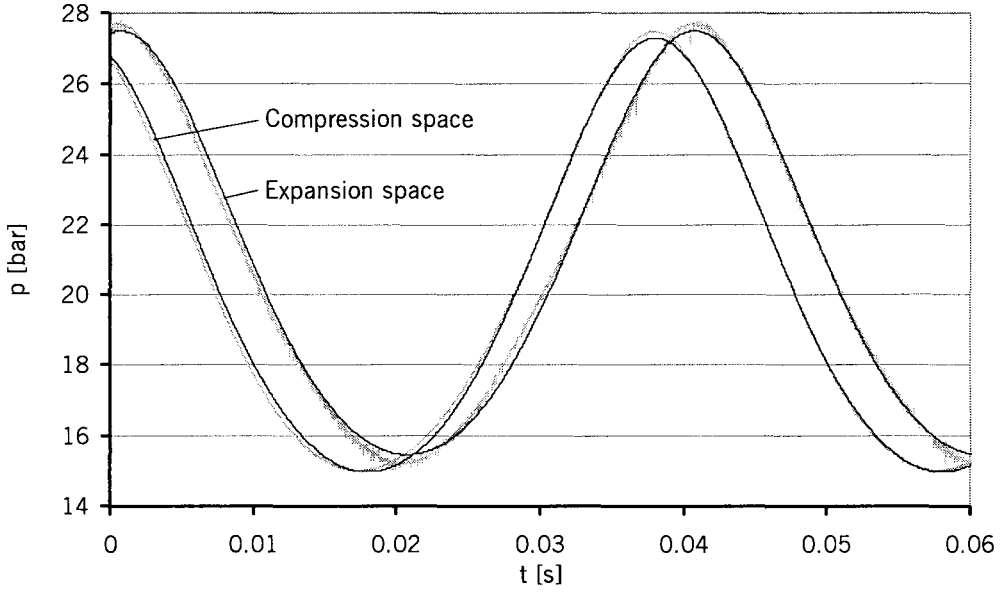

Figure 7.6: *For p_m = 21 bar and T_L = 40 K, the measured pressure data (grey line) are fitted to equation 7.2 (black line). The pressure in the compression and the expansion space is presented. The fitted curve has a slightly lower amplitude. A small offset is noticed between the two curves.*

From the measured data in figure 7.6, it can be seen that p_E has a slight offset compared to p_C. This is due to a small offset between the two pressure sensors. The curve fitting causes a small decrease in amplitude and therefore very small differences between p_C and p_E are difficult to measure. To get a picture of the pressure drop across the various regenerators, in figure 7.7 (screens) and figure 7.8 (SIKA-R40), fitted curves are shown for p_m = 31 bar.

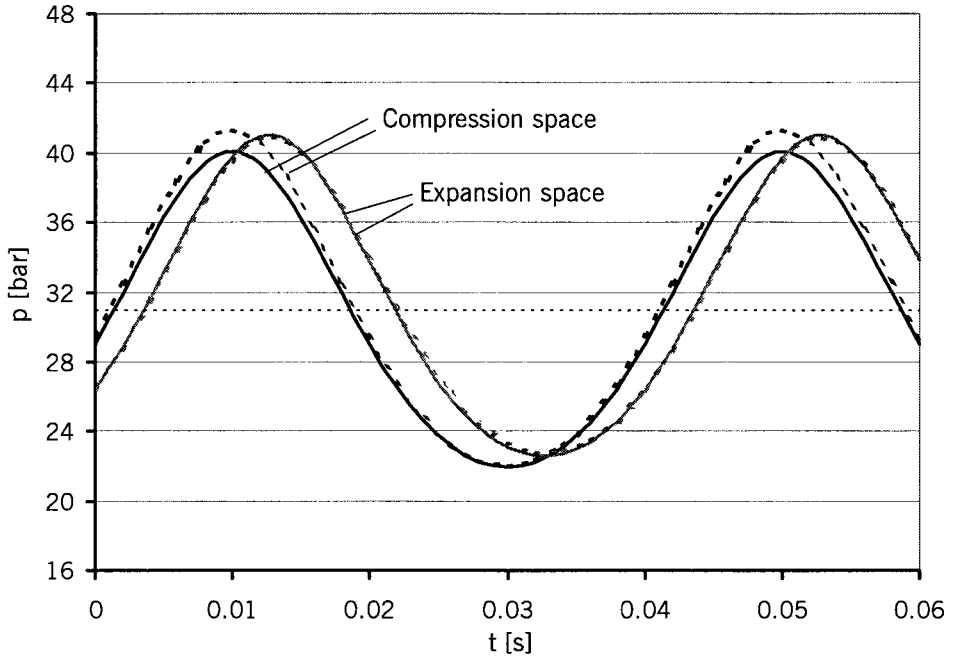

Figure 7.7 (Screens)

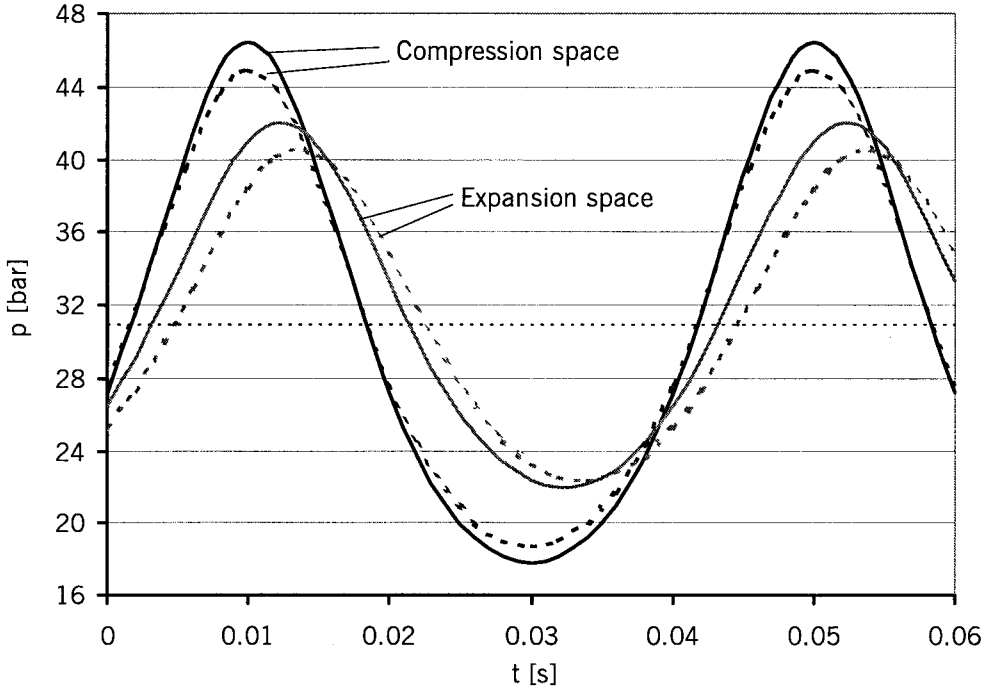

Figure 7.8 (SIKA-R40)

Figure 7.7 and 7.8: *For p_m = 31 bar, p_C and p_E are measured and fit to equation 7.2. In figure 7.7 this is presented for a machine with a screen regenerator at T_L = 41 K(solid line) and 154 K (dotted line). In figure 7.8, SIKA-R40 is used and T_L = 46 K (solid line) and 147 K (dotted line). The R40 material causes a significantly higher pressure amplitude in the compression space than the screens. For the screens the difference in pressure amplitude between p_C and p_E is very small, for the R40 material it is 3.2 bar. For both materials, a phase shift of 25-30 degrees is seen between p_C and p_E.*

In figure 7.7 it can be seen that for screens at T_L = 41 K, the pressure amplitude in the compression space is about the same as the pressure amplitude in the expansion space: about 8.7 bar. This pressure amplitude is approximated by εp_0 in equation 7.2. Because the pressure signal in the expansion space has a slightly different shape, it is shifted upwards a little bit by fitting it to equation 7.2. For T_L = 154 K, the pressure amplitude in the expansion space is about 9.2 bar and a drop in pressure amplitude of about 0.5 bar is seen across the regenerator. This indicates a temperature dependence of the pressure drop that is caused by the higher viscosity at higher temperatures. At both values of T_L, a phase shift of about 25 degrees is seen between p_C and p_E.

In figure 7.8 it can be seen that the pressure amplitude in the compression space is much higher for the SIKA-R40 material than for the screens. This pressure amplitude is 12.8 bar and 11.9 bar for T_L = 46 K and 147 K respectively. At both temperatures, a drop of about 3.2 bar is seen between the amplitudes of p_C and p_E. This indicates that the pressure drop shows no significant temperature dependence. The phase shift between p_C and p_E is 21 and 33 degrees for T_L = 46 K and 147 K respectively.

For all the measurements presented in section 7.3, the pressure drop and the phase shift across the regenerator have been determined at several different temperatures. In figure 7.9 and 7.10 this is presented as a function of the temperature at the cold side for p_m = 31 bar.

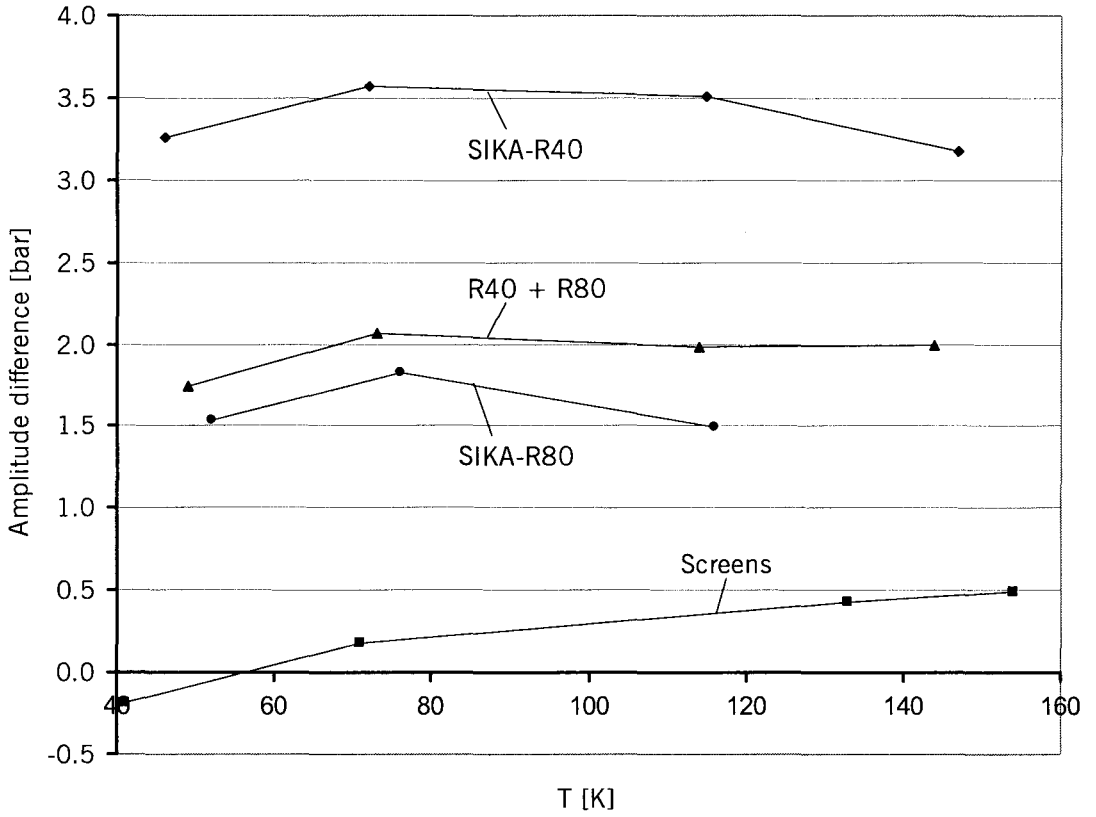

Figure 7.9: *The drop in pressure amplitude across the regenerator at p_m = 31 bar and several cold end temperatures. The screen regenerator causes the lowest pressure drop, the SIKA-R40 the highest. The pressure drop across the screens is temperature dependent, the sintered metal materials don't show such behavior.*

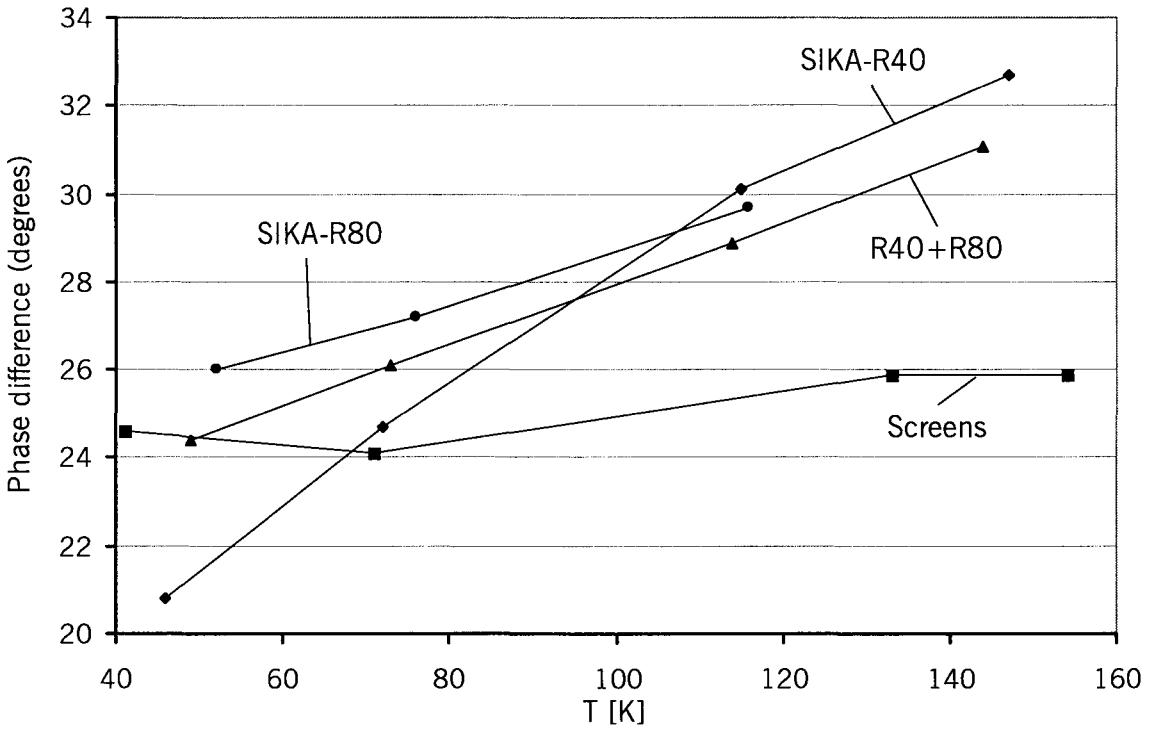

Figure 7.10: *The phase difference between p_C and p_E at p_m = 31 bar and several cold end temperatures. The phase difference is temperature dependent for all materials, the screens showing the smallest and the SIKA-R40 material showing the largest temperature dependence.*

From figure 7.9 it can be seen that the screen regenerator causes a very low amplitude drop across the regenerator. It is not measurable for $T_L < 60$ K and increases with temperature to 0.5 bar at $T_L = 150$ K. The amplitude drop across the sintered metal regenerators is not significantly temperature dependent and is 1.7 bar and 3.3 bar for the SIKA-R80 and R40 respectively. If a combination of 1/3 R40 and 2/3 R80 is used, the average amplitude drop is 1.9 bar, while a linear combination of both materials would predict 2.2 bar. This indicates that the largest part of the pressure drop is caused at the warm side of the regenerator.

Another conclusion from figure 7.9 is that the pressure drop across the sintered metal regenerators is not temperature dependent, while the pressure drop across the screens does show a small temperature dependence. In section 7.5 this will be discussed.

From figure 7.10 it can be seen that the phase difference between p_C and p_E is temperature dependent. The largest temperature dependence occurs for the R40 material, the material with the largest pressure drop. Because the compression piston and the displacer are out of phase, the phase difference is partially forced. In addition, it depends on the flow resistance and the void volume inside the regenerator [34]. The void volume is not temperature dependent, the linear part of the flow resistance is, because it is dependent on η (equation 7.1). The higher z_r is, the larger the temperature dependence of the linear component of the flow loss is. This causes a larger gradient for the phase difference as function of the temperature like is seen in figure 7.10.

For mean pressures of 21 and 26 bar, the amplitude drop and phase shift across the regenerator are presented in Appendix H.

7.5 Discussion

The Economy machine with the sintered metal regenerators performs much less than predicted with the cylindrical tube model used in section 5.4. This can be seen in figure 7.11 that presents the model prediction and the measured cooling power for the screens and the SIKA-R40 regenerator for p_m = 31 bar.

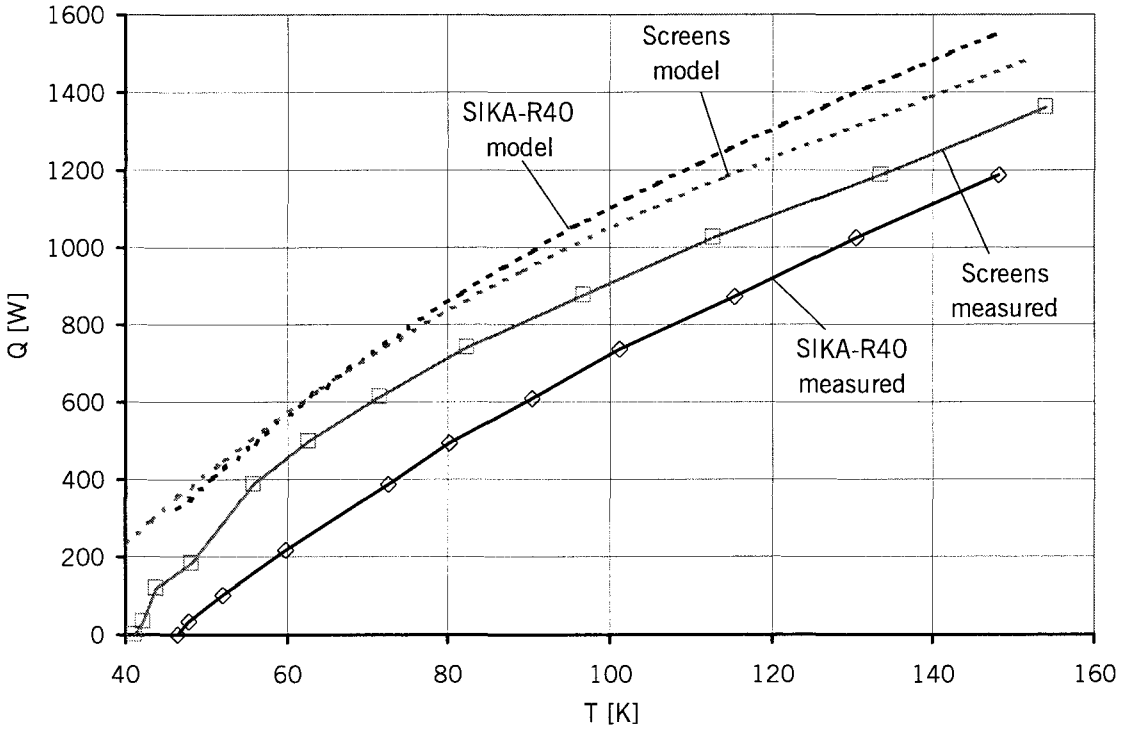

Figure 7.11: *With the Stirling model (chapter 4), the cooling power is calculated for an Economy machine with a screen and a SIKA-R40 regenerator. The average pressure is 31 bar. The R40 regenerator is modeled as cylindrical tubes with laminar flow, like is described in section 5.4. The modeled cooling power is compared to the measured cooling power. For the screens and for 60 < T< 150 K, the model calculates a cooling power that is 110-150 W higher than is measured. For the R40 material, the difference between the model and measurements is 350-385 W.*

In figure 7.11 it can be seen that for 60 < T < 150 K, the modeled cooling power for the screen regenerator is 110-150 W higher than measured. This is an overestimation of 11-26%. If the thermal loss of 45 W in the capillary is taken into account, the overestimation is even less, 7-16%. In addition to this very accurate prediction, the modeled curve shows about the same temperature dependence as the measured one.

The modeled cooling power for the SIKA-R40 material is 350-380 W higher than measured (figure 7.11). Even if the thermal loss in the capillary is taken into account, this is an overestimation of 30-140% for 60 < T < 150 K. Although the absolute difference is very large, the cylindrical tube model predicts about the same temperature dependence as is measured.

In section 7.4 and in Appendix H, it can be seen that the drop in pressure amplitude across the regenerator is much higher for the sintered metal regenerators than for the screen one. The specific flow impedance determined in laminar flow (section 7.2) does not indicate such a large difference in flow loss. From this, the suspicion rises that turbulent effects in the sintered metal

regenerators under normal operating conditions of the Economy machine, play a larger role than was assumed in section 5.4.

Another reason for additional flow losses might be caused by the oscillation of the flow. Under oscillating flow conditions, the flow changes direction twice every period of oscillation. After each change in direction, it takes the flow some time to stabilize. If this stabilization time is relatively small compared to half a period of oscillation, the flow can be considered as quasi-steady. The Womersley number W_o gives an indication for this [40]:

$$W_o = \frac{d_h}{2}\sqrt{\frac{\omega}{2\eta}}. \tag{7.3}$$

For the screen regenerator and p_m = 30 bar, W_o varies from 0.14 at the warm side to 0.47 at the cold side. For the sintered metal materials it is about a factor 2 lower. If $W_o < 1$, an oscillating flow can be regarded as quasi-steady [40]. So in the regenerator under normal operating conditions, the flow is considered quasi-steady.

To determine the influence of turbulence on the pressure drop, equation 7.1 can be used. As stated before, it consists of two parts, a laminar part linearly dependent on the volume flow and a turbulent part, dependent on the square of the volume flow. For the sintered metal materials, the values of z_r are measured and specified by the manufacturer. For the screens, the value is only determined by measurement. For the sintered metal materials the values of β are specified by the manufacturer, but no value of β is known for the screens. However, a value of C_w has been determined empirically for the screens (equation 4.24) and this C_w also consists of a laminar part $\sim R_e^{-1}$ and a constant turbulent part. For the pressure drop across the regenerator, equation 4.23 can be used and if the specified C_w is used, this equation also consists of a laminar part linearly dependent on the volume flow and a turbulent part, dependent on the square of the volume flow. Now equations 4.23 and 7.1 can be combined to get

[confidential]. (7.4)

If equations 7.4 and 4.24 are combined, $z_r = 1.7 \cdot 10^{10}$ m^{-2} and $\beta = 3 \cdot 10^{-5}$ m. This z_r is only 15% lower than the measured value presented in section 7.2. Now, for all the materials z_r and β are known. In the steady flow experiments presented in section 7.2, the volume flow is varied from 0 to $1 \cdot 10^{-3}$ m^3/s. In figure 7.12 the expected pressure drop is presented for these volume flows. To compare the different materials, R_e is used instead of the volume flow. For the SIKA-R materials, the values of z_r and β specified by the manufacturer are used (table 7.1). For the screens, $z_r = 1.7 \cdot 10^{10}$ m^{-2} and $\beta = 3 \cdot 10^{-5}$ m are used.

In figure 7.12 it can be seen that at low Reynolds numbers, the expected pressure drop is mainly dependent on the part caused by laminar flow. R_e is calculated with equation 2.23 in which the average velocity is calculated with equation 2.27. For screens d_h = 68 μm, for SIKA-R80 d_h = 42 μm, and for SIKA-R40 d_h = 32 μm. The last two values are the average pore diameters specified by the manufacturer. At a flow of $1 \cdot 10^{-3}$ m^3/s, R_e = 2.5, 1.2, and 1.0 for the screens, the R80 and the R40 material respectively. The expected pressure drop at these Reynolds numbers is about 0.031 bar, 0.046 bar and 0.076 bar for the screens, the R80 and the R40 material respectively. The pressure drops for the screens and the R80 material, are consistent with the measurements presented in section 7.2. The measured value for the R40 material is about 50% higher than expected. This is consistent with the results in section 7.2.

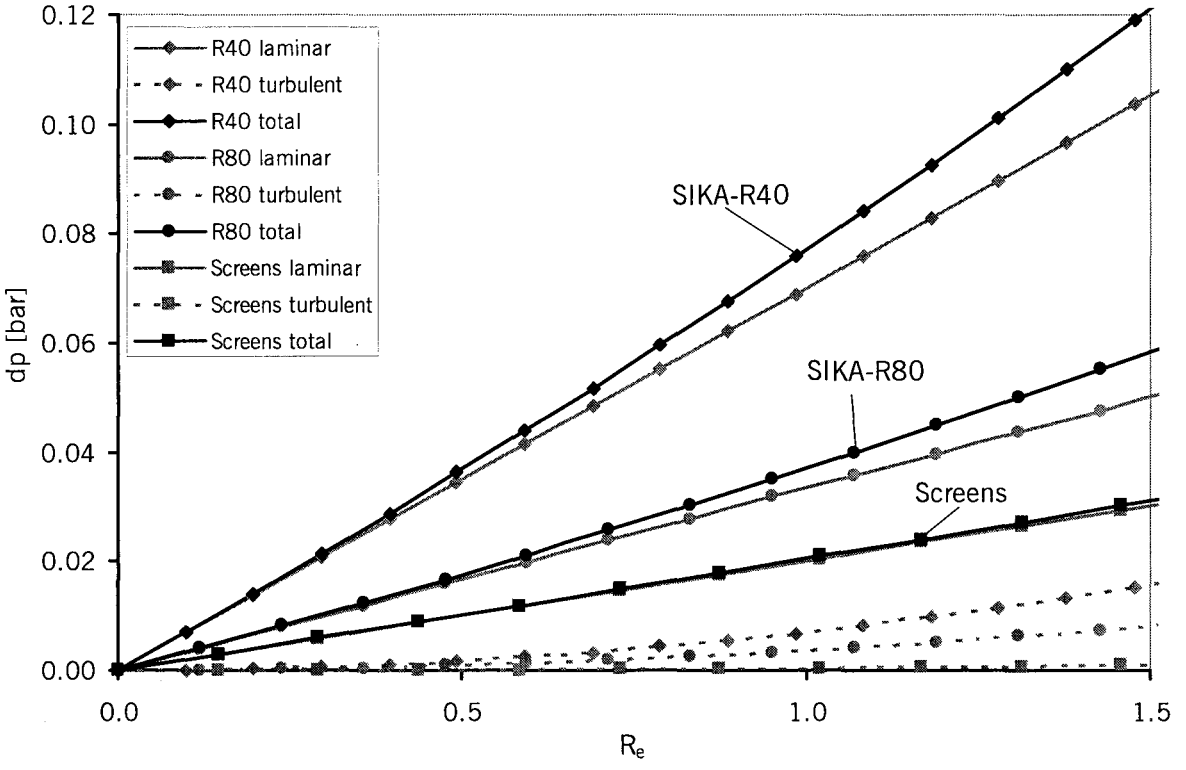

Figure 7.12: *With equation 7.1, the pressure drop across three different regenerators is calculated, one with screens, one with SIKA-R80 and one with SIKA-R40 material. The gas used for flow is compressed air, the pressure is atmospheric (1 bar) and the temperature is 293 K. For all three materials, the main part of the pressure drop is caused by laminar flow. At a flow of 1·10^{-3} m^3/s, the pressure drop is 0.031 bar, 0.046 bar and 0.076 bar for the screens, the R80 and the R40 material respectively (R_e = 2.5, 1.2 and 1.0).*

To get an impression of the pressure drop in an Economy machine at actual operating conditions, the same calculations are performed for an Economy operating at 25 Hz, filled with helium at a pressure of 30 bar. The regenerator is considered isothermal at respectively 70 K and 320 K, typical temperatures of the cold and the warm side of a regenerator. The calculated pressure drops are presented in figures 7.13 and 7.14.

The flow is considered quasi-steady. With the amplitude of the displacer and the frequency, the average volume flow is estimated to be 3·10^{-3} m^3/s at the cold side of the regenerator. With this volume flow and for T = 70 K, R_e=148, 121, and 100 for the screens, the R80 and the R40 material respectively. Because the molar flow is supposed to be constant within the regenerator and the molar volume at 320 K is roughly four times the molar volume at 70 K, the typical volume flow at the warm side of the regenerator is about 12·10^{-3} m^3/s. With this volume flow and for T = 300 K, R_e = 52, 43, and 35 for the screens, the R80 and the R40 material respectively.

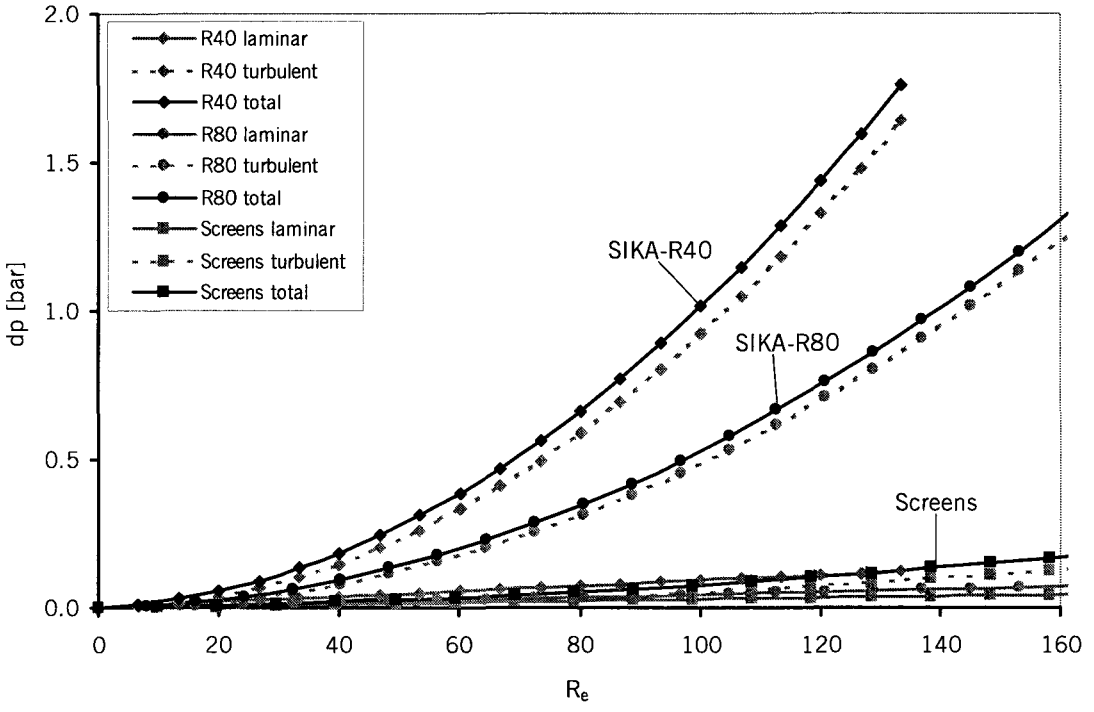

Figure 7.13 (T = 70 K)

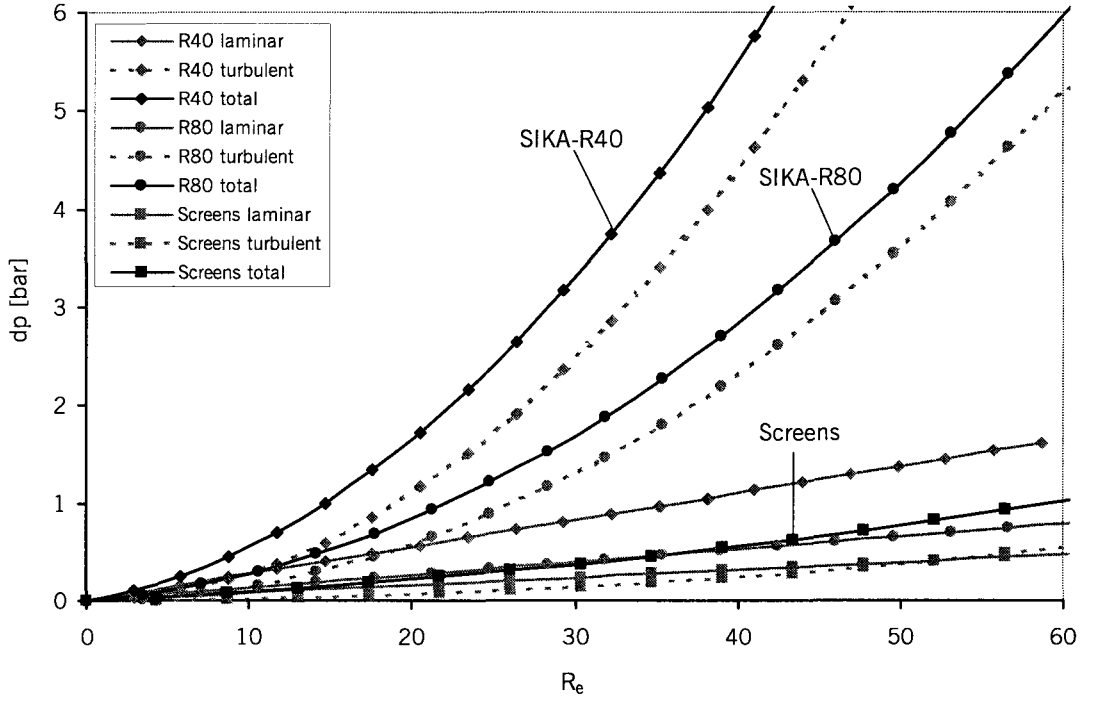

Figure 7.14 (T = 320 K)

Figure 7.13 and 7.14: *With equation 7.1, the pressure drop across three different regenerators is calculated, one with screens, one with SIKA-R80 and one with SIKA-R40 material. The gas used for flow is helium, the pressure is 30 bar. The temperature is 70 K (7.13) and 320 K (7.14) respectively. The Reynolds numbers presented are for typical volume flows at the cold and the warm side of the regenerator respectively. Total pressure drop is significantly higher for the SIKA-R materials because the turbulent part is significantly larger than for the screens.*

From figure 7.13 it can be seen that at a volume flow of $3 \cdot 10^{-3}$ m^3/s, the pressure drop across an isothermal regenerator at 70 K, would be 0.15 bar, 0.76 bar, and 1.0 bar for the screens, the R80 and the R40 material respectively. At a temperature of 320 K and a volume flow of $12 \cdot 10^{-3}$ m^3/s, it would be 0.85 bar, 3.2 bar, and 4.4 bar for the screens, the R80 and the R40 material respectively (figure 7.14).

To get an idea of the order of magnitude of the pressure drop, the regenerator is divided into 26 isothermal sections of T = 70, 80,..., 320 K. The volume flow is supposed to be linear with temperature, from $3 \cdot 10^{-3}$ m^3/s at 70 K to $12 \cdot 10^{-3}$ m^3/s at 320 K. Equation 7.1 is used to calculate the pressure drop across each section and for η and ρ, the values in Appendix D are used. The total pressure drop across the regenerator calculated in this way is presented in table 7.3.

Table 7.3: *For a regenerator with stacked screens, one with SIKA-R80 and one with SIKA-R40 material, the pressure drop is calculated under real operating conditions. Quasi-steady flow is assumed, the gas is helium and the average pressure is 30 bar. The calculations are performed for T_L=70K and T_H=320K. In the third column, the measured values are presented.*

Regenerator material	**Δp (calculated) [bar]**	**Δp (measured) [bar]**
Stainless steel screens	0.46	-
SIKA-R80	1.9	1.7
SIKA-R40	2.6	3.3
1/3 SIKA-R40 and 2/3 SIKA-R80	2.0	1.9

As can be seen in table 7.3, the pressure drop across the SIKA-R80 material is calculated to be about 4 times higher than across the screens. For the R40 material this is almost a factor 6. For the combination of both materials, the calculated pressure drop is 2.0 bar while a linear combination of both materials would give 2.1 bar. The reason for this difference is that the main part of the pressure drop is caused at the warm side of the regenerator (figure 7.13 and 7.14). A reduction of flow resistance in this part therefore causes a more than linear decrease in total pressure drop. As can be seen in the third column of table 7.3, the measured values are close to the calculated values. If for the SIKA-R40 material the measured value of z_r=$6.6 \cdot 10^{10}$ m^{-2} is used instead of the specified value of $4.0 \cdot 10^{10}$ m^{-2}, the calculated Δp is 2.9 bar, which is even closer to the measured value.

For the screens, no measurable pressure drop occurs at T_L = 70K. From the calculations above, the pressure drop is expected to be 0.46 bar. This difference might be caused by fitting the pressure data to equation 7.2. By doing this, the peak in the pressure signal is somewhat flattened. Therefore small differences between p_C and p_E are barely measurable.

The measured pressure drop across the screens shows a small temperature dependence (figure 7.9). The higher the temperature, the larger the relative contribution of the laminar term of the flow resistance is (figures 7.13 and 7.14). This term is dependent on the temperature by means of the viscosity.

The measured pressure drop across the sintered metal regenerators is not temperature dependent (figure 7.9). This can be explained by the fact that in these materials the main part of the pressure drop is caused by the turbulent part of equation 7.1 (figures 7.13 and 7.14). If the temperature increases, the density will decrease. This would decrease the pressure drop. In the

mean time however, the volume flow will increase. Apparently this compensates the effect of the decreasing density and the total pressure drop remains constant with temperature.

From the discussion above is concluded that turbulence plays a very important role in the pressure drop across a regenerator of sintered metal material. With equation 7.4, a more accurate estimation of C_w can be made for these materials. For d in equation 7.4, the specified average pore diameter of the SIKA-R materials can be used. The flow resistance now is given by:

$$C_w = \frac{109}{R_{ef}} + 17.7 \quad \text{(SIKA-R40) and} \tag{7.5}$$

$$C_w = \frac{108}{R_{ef}} + 17.9 \quad \text{(SIKA-R80).} \tag{7.6}$$

As can be seen from equations 7.5 and 7.6, the equations for C_w are almost the same for both materials. The modeled pressure drop however, will be different because d occurs in R_{ef} and in equation 4.23 to calculate Δp. Equation 7.5 is inserted into the Stirling model and the heat exchange still is supposed to be the same as in a cylindrical tube with $d = 32\ \mu m$. From now on this model will be called "model 2". The cooling power for an Economy with a R40 regenerator calculated with model 2, is pictured in figure 7.15 (dotted line). In figure 7.16, the same is pictured for $p_m = 21$ bar.

As can be seen in figure 7.15, model 2 predicts a 9% lower cooling power than the cylindrical tube model (55-135 W for $60 < T < 140$ K). In figure 7.16 (dotted line) can be seen that compared to the cylindrical tube model, the decrease in modeled cooling power with model 2 is larger at $p_m = 21$ bar than at $p_m = 31$ bar. Compared to the cylindrical tube model it is 16-27% lower for $p_m = 21$ bar (85-150 W for $60 < T < 140$ K). This indicates that one of the regenerator losses depends more on the pressure inside the system than is assumed in model 2. A first guess might be that the heat exchange loss in the real system at higher pressures is larger than assumed. In equation 4.32, the heat exchange coefficient Λ used in the cylindrical tube model is presented. It is dependent on R_{ef}^{-1} and R_{ef} is dependent on the mass flow, which is linearly dependent on the average pressure. The heat exchange loss is linear with Λ^{-1}. To increase the influence of the average pressure on the heat exchange loss, it is assumed that $\Lambda \sim R_{ef}^{-1.5}$. This model will be called "model 3".

In figure 7.15 it can be seen that especially at low temperatures, model 3 is a better approximation of the measured values than model 2. Model 3 overestimates the measured data at $p_m = 31$ bar only by 120-190 W for $60 < T < 140$ K. When for the measured values the loss in the capillary (45 W) is taken into account, the overestimation is only 12-28% in this temperature region. Compared to the overestimation of 30-140% with the cylindrical tube model, this is a large improvement.

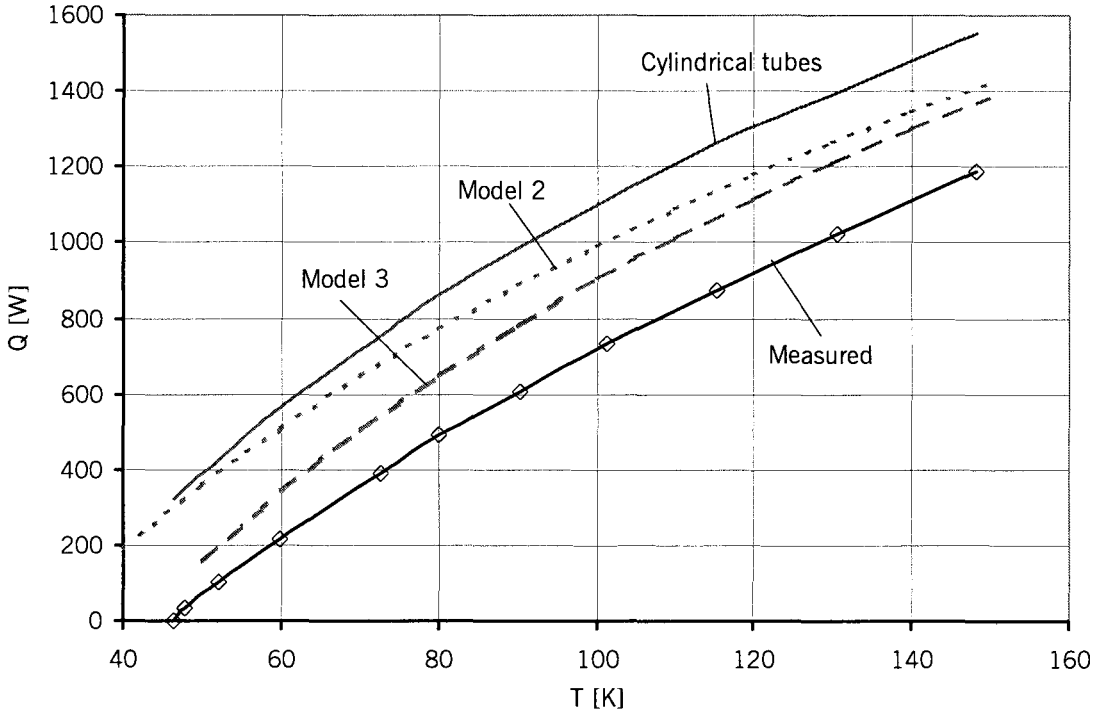

Figure 7.15: *For SIKA-R40 material, the measured values of the cooling power are compared to the values calculated with the Stirling model for p_m = 31 bar . Three different models are used: cylindrical tubes (solid gray line), model 2 (dotted gray line) and model 3 (dashed gray line). Model 3 is the closest approximation of the measured values.*

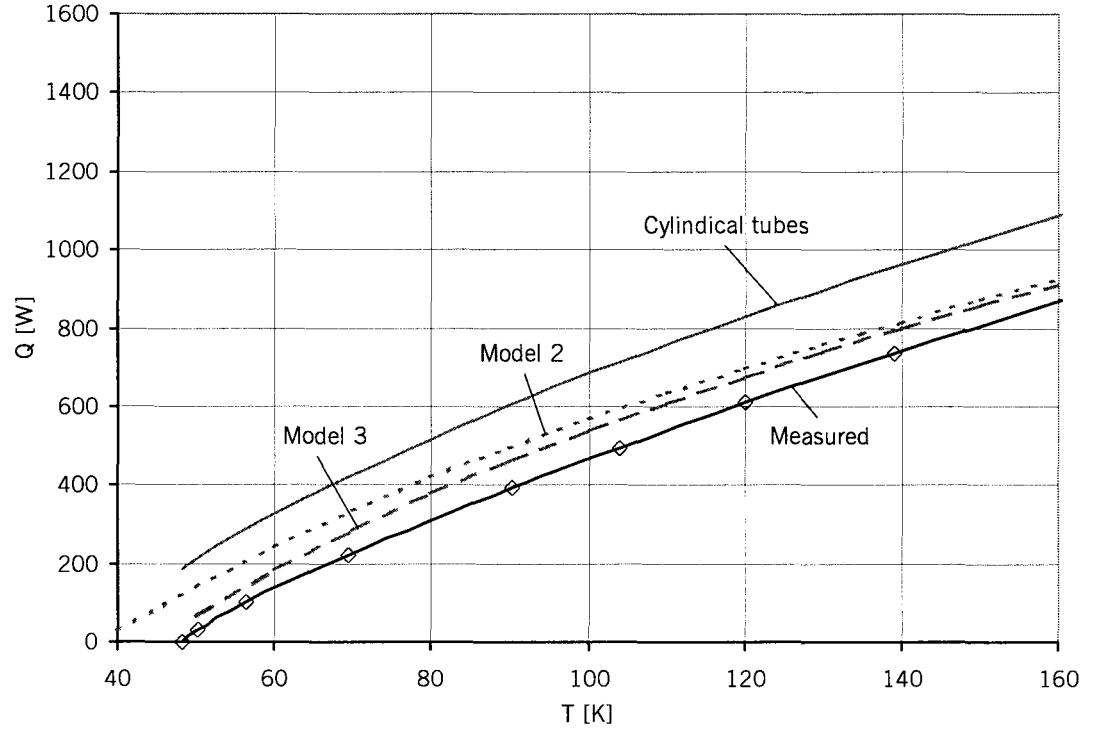

Figure 7.16: *The same as figure 7.15, only p_m = 21 bar. Compared to figure 7.15, model 2 gives a closer approximation of the measured values.*

At p_m = 21 bar (figure 7.16), the overestimation of model 3 is only 45-70 W for 60 < T < 140K, which is only 16-32%. If for the measured values the loss in the capillary (45 W) is taken into account, the overestimation is only 0-6% in this temperature region. If figure 7.15 and 7.16 are compared, it can be seen that model 3 still does not predict the right pressure dependence, but that it is a better approach of the measured values than model 2, as well for p_m = 21 bar as for p_m = 31 bar.

Another important feature for a model is that it predicts the correct values of both the SIKA-R40 and the SIKA-R80 material. In figure 7.17 R40 and R80 material is modeled for p_m = 21 bar. Model 2 and 3 are compared to the measured values.

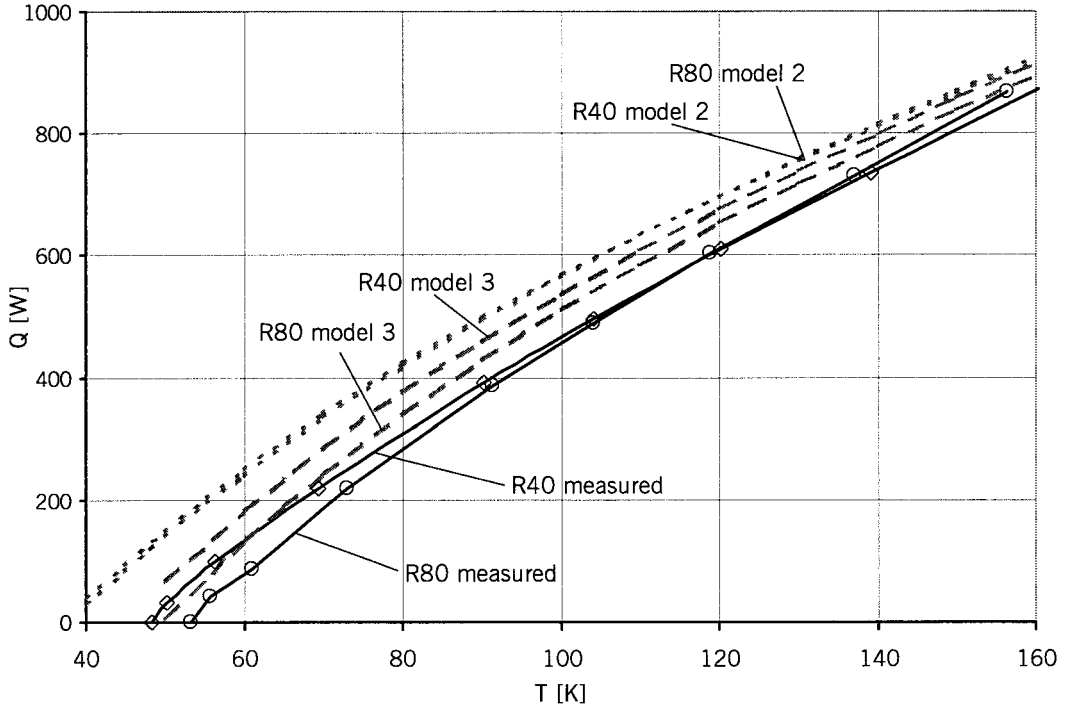

Figure 7.17: *Model 2 (dotted gray line) and model 3 (dashed gray line) are compared to the measured values for p_m = 21 bar. SIKA-R40 and SIKA-R80 material are modeled. The difference between the R40 and the R80 material calculated with model 3, gives a better agreement with the measurements.*

In figure 7.17 it can be seen that model 2 predicts almost the same cooling power for both materials. The measured values however, differ for the R40 and the R80 material. For T < 110 K, the R40 material performs better, for T > 110K the R80 material. Model 3 predicts a better performance for the R40 material in the whole temperature range, but a decreasing difference in cooling power between both materials at higher temperatures. This still is not corresponding with the measurements, but a better approach than model 2.

To further improve model 3, a better approximation for the heat exchange has to be determined empirically. Next to the heat exchange, a better approximation for the heat conduction has to be found. This can be done by measurement of the heat conduction.

8 Conclusions and recommendations

8.1 Conclusions

Tests are performed with a new type of regenerator matrix. The new matrix consists of sintered stainless steel particles. Two materials are tested: SIKA-R40 and SIKA-R80. The number presents the typical particle size. Compared to the current regenerator matrix with sintered stainless steel screens, the SIKA-R materials have a significantly higher filling factor. The tests are performed with a Stirling Economy machine. With a heater the cooling power at a certain cold end temperature is determined. The machine is filled with helium and the tests are performed at three different mean pressures inside the machine: 21, 26, and 31 bar.

At 77 K, the boiling point of nitrogen, the Economy with the screens delivers cooling powers of 515, 615, and 735 W, at pressures of 21, 26, and 31 bar respectively. With the R40 material, the cooling powers are 335, 425, and 495 W at these pressures. The R80 material performs slightly less. The reduction in cooling power with the SIKA-R materials is 30-40 %. Of the SIKA-R materials, the R40 performs slightly better for $T < 130$ K and the machine can reach a lower absolute minimum temperature. At higher temperatures, the R80 material performs slightly better.

In addition to the cooling power, the efficiency is an important parameter to define the performance of a machine. With the screens, the Economy has efficiencies of 11.5, 13.1, and 14.1 % at 77 K, at pressures of 21, 26, and 31 bar respectively. With the R40 material, the efficiency is 5.9, 6.5, and 6.7 % at these pressures. The R80 gives a comparable efficiency. Compared to the screens, the efficiency is reduced by 50 % with the SIKA-R materials. Of the SIKA-R materials, the R80 material has the highest efficiency for $T > 75$ K.

Inside a regenerator, the entropy production has to be minimized to give the best performance. From calculations it is concluded that a regenerator with non-uniform hydraulic diameter will perform better than a uniform regenerator. Therefore, next to two uniform matrices of sintered metal particles, a combination is tested. At the cold side (1/3 of the length), R40 material is used, which has a finer structure. At the warm side (2/3 of the length), R80 material is used, which has a more open structure. For $T > 90$ K, this combination gives a slightly higher cooling power than the individual materials. In addition to this, the combination of both materials gives a slightly higher efficiency than the R80 material and has the highest efficiency for $T > 70$ K.

During the experiments, the pressure in the compression and the expansion space is measured. From this, the drop in pressure amplitude across the regenerator can be determined. For the screens this drop is 0 to 0.5 bar, dependent on the cold end temperature. For the R40 material it is 2.6, 2.9, and 3.3 bar, at a pressure of 21, 26, and 31 bar respectively. The R80 material causes a pressure amplitude drop of 1.5 to 1.7 bar at these pressures. This significantly higher amplitude drop, is the main reason for the lower performance of the SIKA-R materials compared to the screens.

Compared to the screens, turbulence plays a much larger role in the SIKA-R materials. This causes higher flow losses and is the main reason for the higher pressure drop across the SIKA-R regenerators, compared to the screens. The main part of the flow resistance is caused at the warm side of the regenerator. A reduction in flow resistance in this part of the regenerator therefore gives a more than linear decrease of the total pressure drop. If the flow resistance is

decreased, the heat exchanging surface probably will decrease as well. Therefore the cooling power will not increase linearly with a reduction of flow resistance at the warm side. From the combination of both material is seen that the increase is only very small. The increase in efficiency is larger.

A powerful design tool for the machine and all its components, is the Stirling model. This model combines theory with empirical coefficients for flow resistance, heat exchange, and heat conduction. For the screen regenerator, the model is in very good agreement with the experiments. Because the SIKA-R materials have not been used before, no empirical coefficients are known. Therefore, for simplicity the SIKA-R materials are modeled as cylindrical tubes with laminar flow. For this geometry the coefficients for flow resistance, heat exchange, and heat conduction are known and can be added to the Stirling model. For the cylindrical tubes, a better performance is predicted than for the screens.

The cylindrical tube model overestimates the cooling power of the Economy by 30-140 %, dependent on the temperature. The model ignores turbulent effects and because these are very large in the SIKA-R materials, it is not correct. If the model is adapted for turbulent behavior, it is in much better agreement with the measurements. If also a better estimation for the heat exchange is used, the overestimation is only 12-28%. To further improve the model, a better approximation for the heat exchange has to be determined empirically. Next to the heat exchange, a better estimation of the heat conduction has to be found.

8.2 Recommendations

The SIKA-R materials perform less than the sintered screens if they are used in a regenerator matrix. Therefore this new type of regenerator is not suitable as a drop-in substitute for the screen regenerator in the current Economy machine. However, a new type of machine could be developed by Stirling. If this new machine is equipped with a SIKA-R40 regenerator and operated at a mean pressure of 26 bar, it will deliver 425 W of cooling power at 77 K. The efficiency will be 6.5%. The cooling power will be 30% less than with the current Economy and the efficiency will be half the current value. As a compensation for this, the machine will have significantly lower production costs. Not only will the regenerator cost less, the part of the machine that separates and liquefies the nitrogen is allowed to be less powerful and therefore will cost significantly less. For some customers this will be an interesting option.

The new type of regenerator is used in a machine that has been optimized for a screen regenerator. To further improve the performance of the SIKA-R regenerators, experiments are recommended with a regenerator with an altered geometry, e.g. shorter. Because the materials have a higher filling factor than the screens, for the same length, more material is present to store the heat. Therefore the length can be reduced, which will result in a lower pressure drop. Also the void volume inside the regenerator will be smaller. Disadvantages of a shorter regenerator are less heat exchanging surface and a higher axial conduction. An optimum combination has to be found. In addition to changing the regenerator geometry, the phase difference between the compression piston and the displacer can be further optimized.

Another recommendation is to produce a regenerator in which the screens are rolled instead of stacked. A regenerator like this is expected to perform the same as the current regenerator. Production costs are expected to be significantly lower.

A uniform regenerator always performs less than a regenerator with a larger hydraulic diameter at the warm side and a smaller hydraulic diameter at the cold side. Therefore it is recommended to perform tests with a stacked screen regenerator in which a combination is used of various wire diameters.

A regenerator geometry with cylindrical tubes predicts a better performance for the regenerator. A recommendation is to look for a method to create such a geometry. Companies that can be contacted are "Mercorp" and "Mezzotech" (Appendix A). A disadvantage of a cylindrical tube geometry could be higher production costs.

The last recommendation is an alternative method for the production of the current stacked screen regenerator. The current production method is cutting out the screens first, than stacking them and finally sintering them together. Instead, the screens can be stacked and sintered first in such a way that a plate of sintered screen material is produced. From this plate the individual regenerator matrices can be cut. With modern cutting techniques like laser cutting, wire electrical discharge machining or water cutting this should be possible. This alternative production method will save time in the production process and therefore probably will cost less.

9 References

[1] A.T.A.M. de Waele; Dictaat Cryogene Technieken; Technische Universiteit Eindhoven; 2004.

[2] P.P. Steijaert; Thermodynamical aspects of pulse-tube refrigerators (thesis); Technische Universiteit Eindhoven; 1999.

[3] M.E. Will and A.T.A.M. de Waele; Heat exchanger versus regenerator: a fundamental comparison; Accepted for Cryogenics; 2004.

[4] R. A. Ackerman; Cryogenic Regenerative Heat Exchangers; Plenum Press; New York; 1997.

[5] I. Rühlich and H. Quack; Investigations on Regenerative Heat Exchangers; Cryocoolers 10, p. 265-274; 1999.

[6] K. Nam and S. Jeong; Measurement of cryogenic regenerator characteristics under oscillating flow and pulsating pressure; Cryogenics 43, p. 575-581; 2003.

[7] K. Yuan, L.Wang, Y.K. Hou, Y. Zhou, J.T. Liang and Y.L. Ju; Oscillating Flow Characteristics of a Regenerator under Low Temperature Conditions; Cryocoolers 12, p. 539-545; 2003.

[8] S. Choi, K. Nam and S. Jeong; Investigation on the pressure drop characteristics of cryocooler regenerators under oscillating flow and pulsating pressure conditions; Cryogenics 44, p. 203-210; 2004.

[9] K. Nam and S. Jeong; Experimental study on the regenerator under actual operating conditions; Advances in Cryogenic Engineering 47, p. 977-984; 2002.

[10] M.A. Lewis and R. Radebaugh; Measurement of Heat Conduction through Bonded Regenerator Matrix Materials; Cryocoolers 12, p. 517-522; 2003.

[11] U. Bin-Nun and D. Manitakos; Low cost and high performance screen laminate regenerator matrix; Cryogenics 44, p. 439-444; 2004.

[12] T.W. Wysokinski, I.G. Spearing, P.G. Reedeker and J.A. Barclay; Improvement in the second-stage cooling power of a two-stage GM refrigerator through modification of the first stage regenerator; Advances in Cryogenic Engineering 45, p. 229-236; 2000.

[13] W. Kays and A.L. London, Compact Heat Exchangers, 3rd Edition; New York; McGraw-Hill; 1985.

[14] I. Rühlich and H. Quack; Wound profile-wire regenerators – Fabrication and test; Advances in Cryogenic Engineering 45, p. 365-372; 2000.

[15] W. Rawlins and K.D. Timmerhaus; Measurement of the performance of a spiral wound polyimide regenerator in a pulse tube refrigerator; Advances in Cryogenic Engineering 37; p. 947- 953; 1992.

[16] J.N. Chafe and G.F. Green; Neodymium-ribbon-regenerator cooling performance in a two-stage Gifford-Mcmahon refrigerator; Advances in Cryogenic Engineering 43, p. 1589-1596; 1998.

[17] L. Tuchinsky, R. Loutfy and B.J. Tomlinson; Innovative Technology for Low Temperature Regenerators; Cryocoolers 11, p. 427-432; 2001.

[18] J.B. Hendricks; Predicted Performance of a Low-Temperature Perforated Plate Regenerator; Cryocoolers 12, p. 483-487; 2003.

[19] J.B. Hendricks; A new method for producing perforated plate recuperators; Advances in Cryogenic Engineering 41, p. 1329-1337; 1996.

[20] K. Kelly, A. McCandless and S. Motakef; LIGA-Fabricated High-Performance Micro-Channel Regenerators for Cryocoolers; Cryocoolers 12, p. 489-497; 2003.

[21] R. Yaron, S. Shokralla, J. Yuan, P.E. Bradley and R. Radebaugh; Etched Foil Regenerator; Advances in Cryogenic Engineering 41, p. 1339-1346; 1996.
[22] M. P. Mitchell and D. Fabris; Improved Flow Patterns in Etched Foil Regenerator; Cryocoolers 12, p. 499-505; 2003.
[23] M. P. Mitchell; Assembly methods for etched foil regenerators; Advances in Cryogenic Engineering, p. 1592-1597; 2004.
[24] Internal document at Stirling Cryogenics & Refrigeration BV about the Stirling model. (handwritten)
[25] Y.S. Touloukian and E.H. Buyco; Specific Heat; Metallic Elements and Alloys; New York: IFI/Plenum; 1970.
[26] A. Kashani, B. P. M. Helvensteijn, J. R. Maddocks, P. Kittel, J. R. Feller, K. A. Gschneider, V. K. Pecharsky and A.O. Pecharsky; Performance of a new regenerator material in a pulse tube cooler; Advances in Cryogenic Engineering 47; 2002.
[27] A. Kashani and B. P. M. Helvensteijn; New Regenerator materials for use in Pulse Tube Coolers; Cryocoolers 11; 2001.
[28] K. A. Gschneidner Jr., A. O. Pecharsky and V. K. Pecharsky; Ductile, High Heat Capacity, Magnetic Regenerator Alloys for the 10 to 80 K Temperature Range; Cryocoolers 11; 2001.
[29] S. A. Miller, J. D. Nicholson, K. A. Gschneider JR., A. O. Pecharsky and V.K. Pecharsky; Manufacturing Considerations for Rare Earth Powders Used in Cryocooler and Magnetic Refrigerator Applications; Cryocoolers 11; 2001.
[30] W. R. Mérida and J. A. Barclay; Monolithic regenerator technology for low temperature (4 K) Gifford-McMahon cryocoolers; Advances in Cryogenic Engineering 43; 1998.
[31] C. M. Hargreaves; The Philips Stirling Engine; Elsevier Science Publishers B.V.; 1991.
[32] D. W. J. Willems; Internal document at Stirling Cryogenics & Refrigeration BV about the Stirling model.
[33] V. Backx; Aanpassingen aan een model en inleidende metingen aan een testopstelling voor een hoogvermogen pulsbuis; Internal document Stirling Cryogenics & Refrigeration BV;2002.
[34] F. Gärtner; Programm H001S, Berechnung des Stirlingprozesses, Chapter XI; Internal document Stirling Cryogenics & Refrigeration BV;1969.
[35] Allprops version 6/4/96; Center for Applied Thermodynamic Studies; University of Idaho.
[36] A. Castelijns; Internal document at Stirling Cryogenics & Refrigeration BV about the different regenerators used in the past.
[37] Verein Deutsche Ingenieure; VDI-Wärmeatlas; Düsseldorf, Germany; 1984.
[38] S.C.M. Aerts; Comparison of the orifice, inertance and double inlet pulse tube refrigerator (graduation report); Technische Universiteit Eindhoven; 1999.
[39] V. Backx; Meetrapport 5-litermachine (R0085); Internal document at Stirling Cryogenics & Refrigeration BV, Rapport no. TB-20020280; 2003.
[40] C. Loudon, A. Tordesillas; The use of the dimensionless Womersley number to characterize the unsteady nature of internal flow; Journal of Theoretical Biology; 1998; 191(1):63-78.

Appendix A: List of contacted companies

[confidential]

Appendix B: Typical input file for the Stirling model (SPC-1 machine)

[confidential]

Appendix C: Typical output file for the Stirling model (SPC-1 machine)

[confidential]

Appendix D: Input values for the entropy production calculations

In the table below the temperature dependent input values for the entropy production calculations in section 5.2 are given for temperatures between 70 and 320K. The matrix material is stainless steel and the gas data for Helium are taken at 30 bar and are derived from [24] and [34]. The assumptions for the other parameters are explained in section 5.2.

T [K]	λ_m [W/mK]	λ_g [W/mK]	C_p [J/molK]	ρ [kg/m^3]	R_e	N_u	$V_m \cdot 10^4$ [m^3/mol]	$\eta \cdot 10^5$ [kg/sm]
70	6.6	0.053	21.2	19.5	289.7	18.1	2.06	0.78
80	7.3	0.059	21.1	17.1	265.7	17.2	2.34	0.86
90	7.9	0.065	21.0	15.3	246.2	16.4	2.61	0.92
100	8.5	0.070	20.9	13.8	230.0	15.8	2.89	0.99
110	9.1	0.076	20.9	12.6	216.2	15.2	3.17	1.05
120	9.6	0.081	20.9	11.6	204.4	14.7	3.45	1.11
130	10.1	0.086	20.9	10.7	194.1	14.2	3.73	1.17
140	10.5	0.091	20.8	10.0	185.0	13.8	4.00	1.23
150	10.9	0.095	20.8	9.4	176.9	13.5	4.28	1.28
160	11.3	0.100	20.8	8.8	169.7	13.1	4.56	1.34
170	11.7	0.104	20.8	8.3	163.1	12.8	4.83	1.39
180	12.0	0.109	20.8	7.8	157.2	12.6	5.11	1.45
190	12.3	0.113	20.8	7.4	151.8	12.3	5.39	1.50
200	12.6	0.117	20.8	7.1	146.9	12.1	5.66	1.55
210	12.9	0.121	20.8	6.7	142.3	11.8	5.94	1.60
220	13.1	0.125	20.8	6.4	138.1	11.6	6.22	1.65
230	13.3	0.128	20.8	6.2	134.2	11.4	6.49	1.69
240	13.6	0.132	20.8	5.9	130.5	11.2	6.77	1.74
250	13.8	0.136	20.8	5.7	127.1	11.1	7.05	1.79
260	14.0	0.139	20.8	5.5	123.9	10.9	7.32	1.83
270	14.2	0.143	20.8	5.3	120.9	10.7	7.60	1.88
280	14.3	0.146	20.8	5.1	118.1	10.6	7.88	1.92
290	14.5	0.150	20.8	4.9	115.5	10.4	8.15	1.97
300	14.7	0.153	20.8	4.7	113.0	10.3	8.43	2.01
310	14.8	0.157	20.8	4.6	110.6	10.2	8.71	2.06
320	15.0	0.160	20.8	4.5	108.4	10.0	8.98	2.10

Appendix E: Construction of the current regenerator (in Dutch)

[confidential]

Appendix F: Pressure drop and phase shift across a capillary

To measure the pressure in the expansion space, a pressure sensor is mounted at the end of a long capillary like pictured in figure F1.

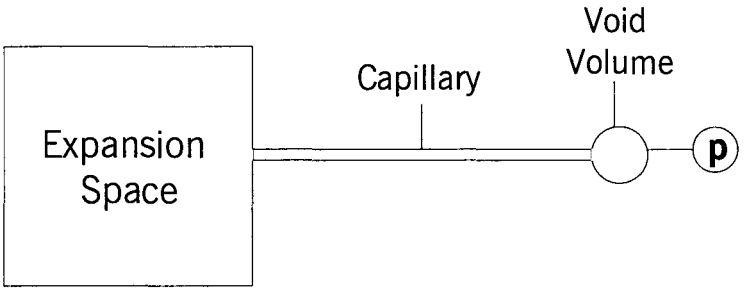

Figure F1: *To measure the pressure in the expansion space, a pressure sensor is mounted at the end of a long capillary. At the end of the capillary a small void volume exists in which the sensor is mounted.*

To verify if the flow through the capillary leads to a pressure drop or a phase shift, the capillary and the void volume are modeled like an electrical RC-circuit. This is allowed because the dimensions of the capillary are much smaller than the wavelength of the pressure oscillation. The pressure is equivalent to an electric voltage and the volume flow to an electric current. The capillary has a total impedance Z, consisting of a flow resistance represented by a resistance R and a void volume at the end of the capillary, represented by a capacity C. Schematically the electrical analogue of the capillary is represented in figure F2.

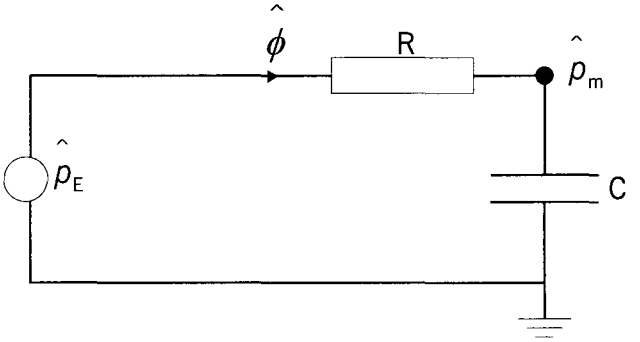

Figure F2: *The capillary can be represented by its electric analogue. In this analogue, the capillary is represented by a resistance and a capacity. The pressure amplitude is represented by an electric voltage and the volume flow by an electric current.*

The pressure amplitude in the expansion space $\hat{p}_E$ can be represented as

$$\hat{p}_E = Z\hat{\phi}. \tag{F1}$$

In equation F1, $\hat{\phi}$ is the amplitude of the volume flow through the capillary. The capacity of a void volume is defined by [38]

$$C = \frac{V}{\gamma p_0}. \tag{F2}$$

In equation F2, V is the void volume, consisting of the volume of the capillary and the volume of the small space in which the pressure sensor is mounted. The average pressure inside the capillary is p_0 and γ is the ratio of isobaric to isochoric specific heat ($\gamma = 1.67$ for helium at 293K and 1 bar). For laminar flow, the flow resistance of a capillary is represented by [38]

$$R = \frac{128\eta l}{\pi d^4}. \tag{F3}$$

In equation F3, l is the length and d is the diameter of the capillary.

The pressure amplitude $\hat{p}_m$, measured by the pressure sensor at the end of the capillary is now calculated with

$$\hat{p}_m = \frac{1}{j\omega C}\hat{\phi}, \tag{F4}$$

in which ω is the frequency of the pressure oscillation. The volume flow is calculated with

$$\hat{\phi} = \frac{\hat{p}_E}{R + \frac{1}{j\omega C}}. \tag{F5}$$

$$\hat{p}_m = \frac{\hat{p}_E}{1 + j\omega RC} = \frac{\hat{p}_E(1 - j\omega RC)}{1 + (\omega RC)^2} \rightarrow \left|\frac{\hat{p}_m}{\hat{p}_E}\right| = \sqrt{\frac{1 + (\omega RC)^2}{(1 + (\omega RC)^2)^2}} \text{ and} \tag{F6}$$

$$\arg(\hat{p}_m) = \arctan(-\omega RC). \tag{F7}$$

Across the capillary, the temperature is not constant, but varies from room temperature to 50K. Therefore the value of the viscosity is an average estimation. The input parameters for equation F1 to F7 are chosen as below.

$\eta = 1{\cdot}10^{-5}$ kg/ms (He at 30 bar)

$l = 1$ m
$d = 1$ cm
$V = 1\,\text{cm}^3$

$\hat{p}_E = 6{\cdot}10^5$ Pa (6 bar)
$p_0 = 3{\cdot}10^6$ Pa (30 bar)
$\omega = 157\ \text{s}^{-1}$ (25 Hz)

With these values, the value of $\hat{p}_m$ can be calculated:

$\hat{p}_m = 5.999 \cdot 10^5 - 7.663 \cdot 10^3 j$ Pa.

$$\left| \frac{\hat{p}_m}{\hat{p}_E} \right| \approx 1$$

This indicates that the pressure drop across the capillary can be neglected.

The phase shift across the capillary equals the argument of $\hat{p}_m$, which is –0.7 degrees. The phase difference between the pressure in the compression and the expansion space is about 25 degrees, so this small extra phase shift can also be neglected.

Appendix G: Characteristics of the measurement system

In this appendix the characteristics of the different components of the measurement system are given. If known, the company that produces the sensor, as well as the sensor type is given.

Sensor	Company	Type
Thermocouples (4x)	Thermocoax	Type K
PT-100 sensors (2x)	Thermocoax	
Pressure sensors (2x)	Druck	PMP4070-60bar-A
DAQ-card	National Instruments	Multifunction DAQ-200kS/s, 16-Bit, type NI 6035E
Data acquisition unit	Agilent	Data acquisition/Switch unit, type 34970A
Vacuum pressure sensor	Leybold	TTR 90
Power supply heater (2x)	Philips	PE1647 DC Power Supply 75V-15A
Current clamp	LEM	LTS 15-NP
Power meter (motor input)	Hioki	Clamp-on power Hi tester, type 3135
Vacuum pump	TRIVAC	D4B
Flow meter cooling water	Brooks instruments	10-1120 (not calibrated)

Appendix H: Figures used in chapter 7

In this appendix some figures are presented that are used for the discussion in chapter 7. In figures H1 and H2, the efficiency (*COP*) at 21 and 26 bar is plotted. Figures H3 and H4 present the measured pressure amplitude drops and figures H5 and H6 the phase shifts across the regenerator at respectively 21 and 26 bar.

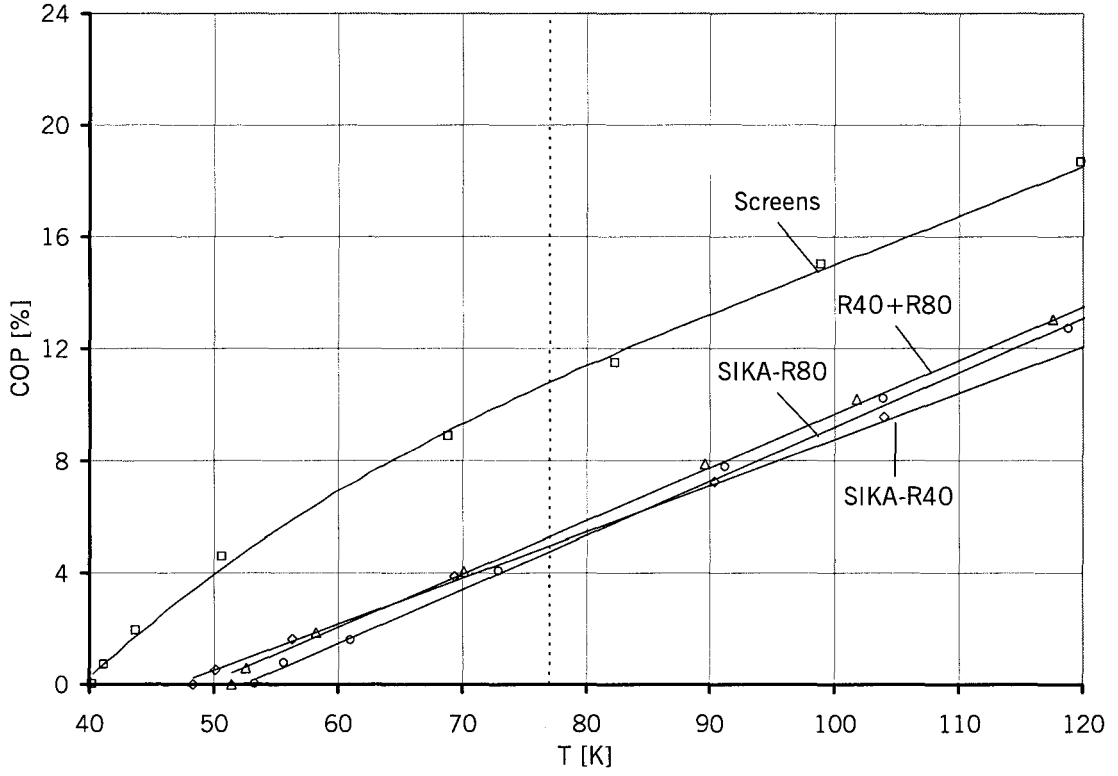

Figure H1 (p_m = 21 bar)

Figure H1 and H2: *The efficiency (COP) of the machine at a mean pressure of 21 bar (H1) and 26 bar (H2). A standard screen regenerator, a regenerator of SIKA-R40, SIKA-R80 and a combination of these materials are used. As can be seen, the Economy with the screen regenerator has a significantly higher efficiency than when a sintered metal regenerator is used.*

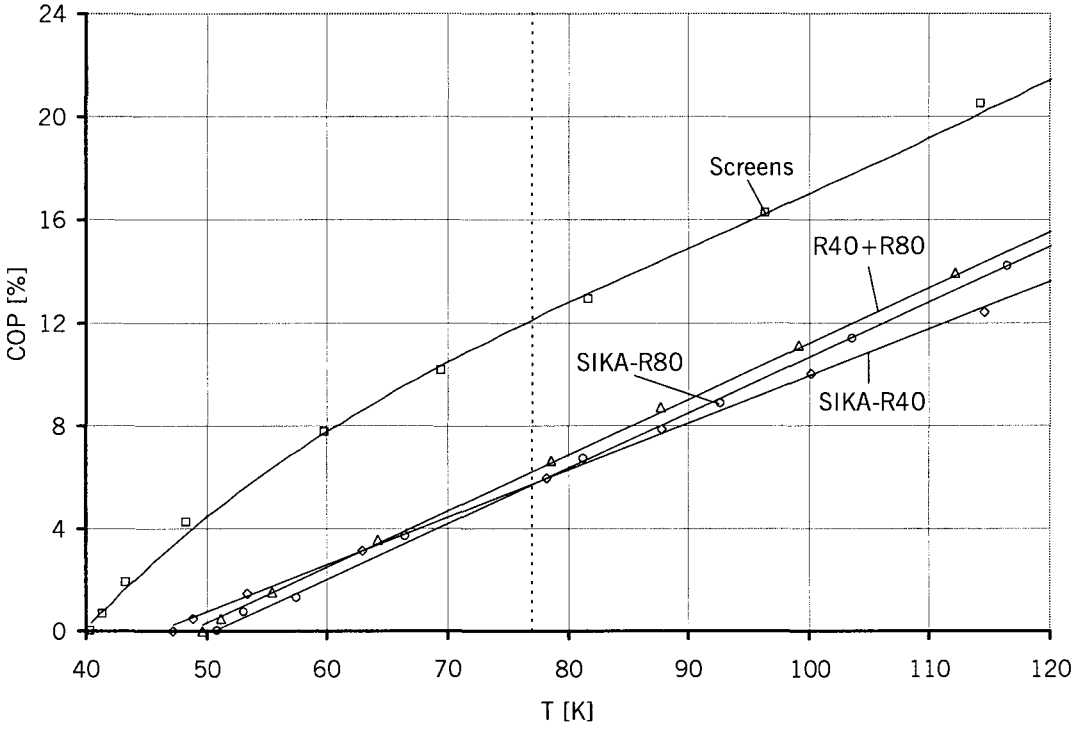

Figure H2 (p_m = 26 bar)

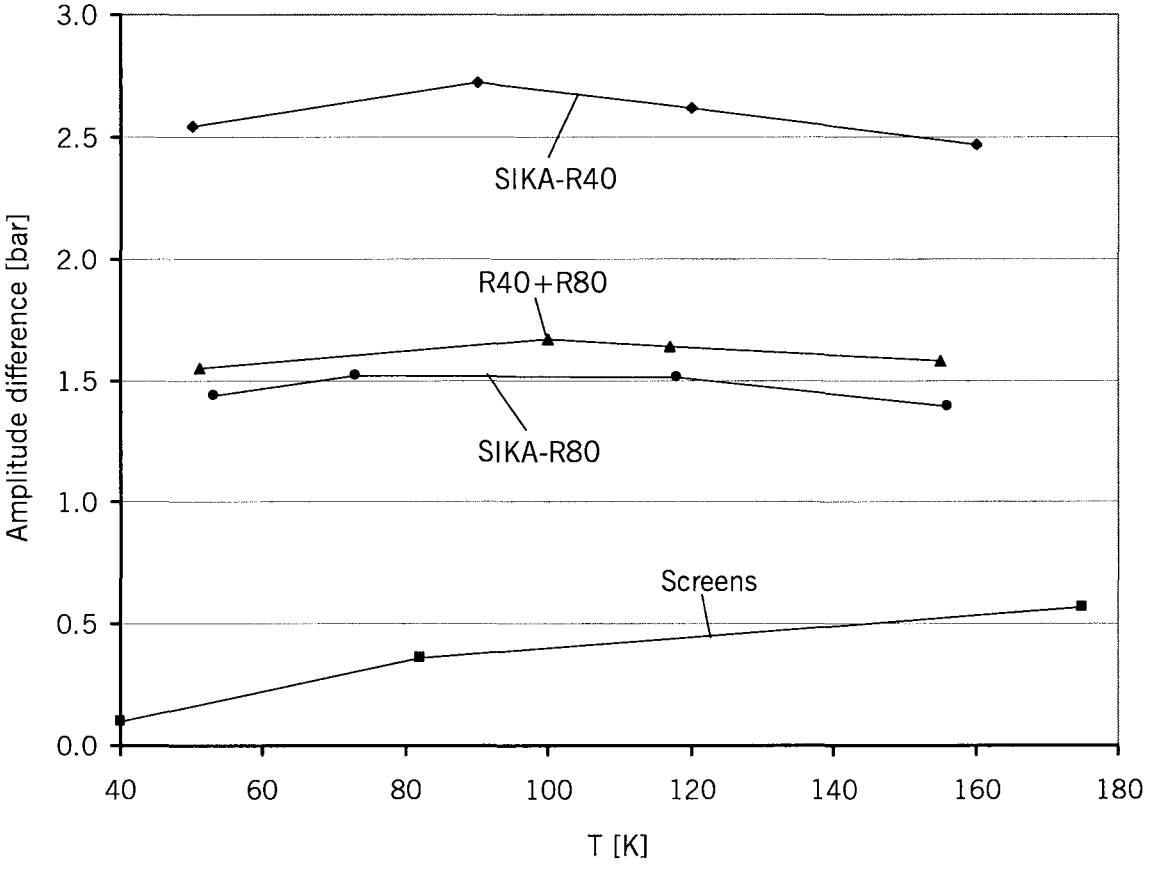

Figure H3 (p_m = 21 bar)

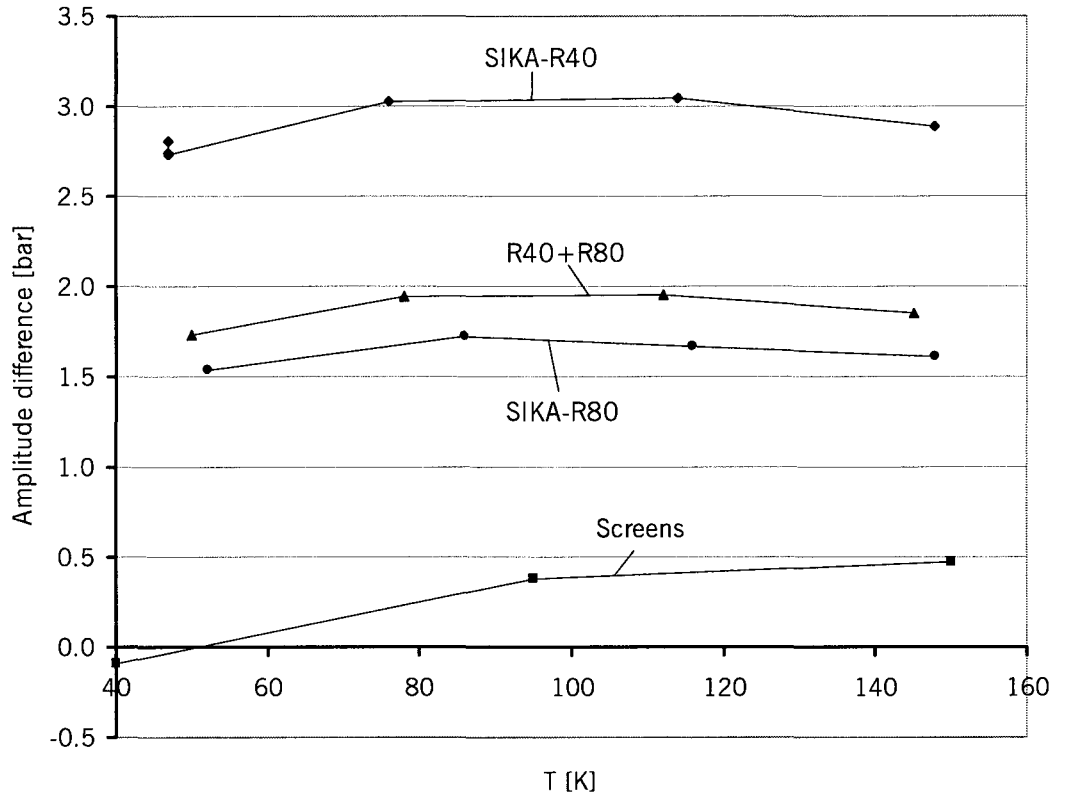

Figure H4 (p_m = 26 bar)

Figure H3 and H4: *The drop in pressure amplitude across the regenerator. The mean pressure is 21 bar (H3) and 26 bar (H4). The screen regenerator causes the lowest pressure drop, the SIKA-R40 the highest. The pressure drop across the screens is temperature dependent, the sintered metal materials don't show such behavior.*

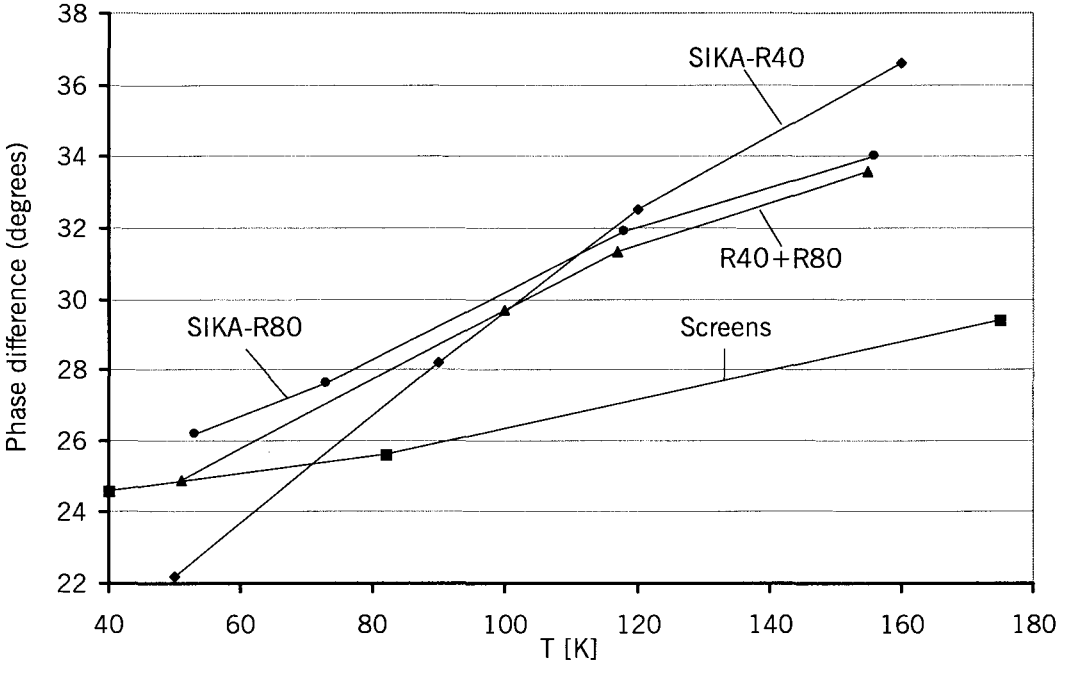

Figure H5 (p_m = 21 bar)

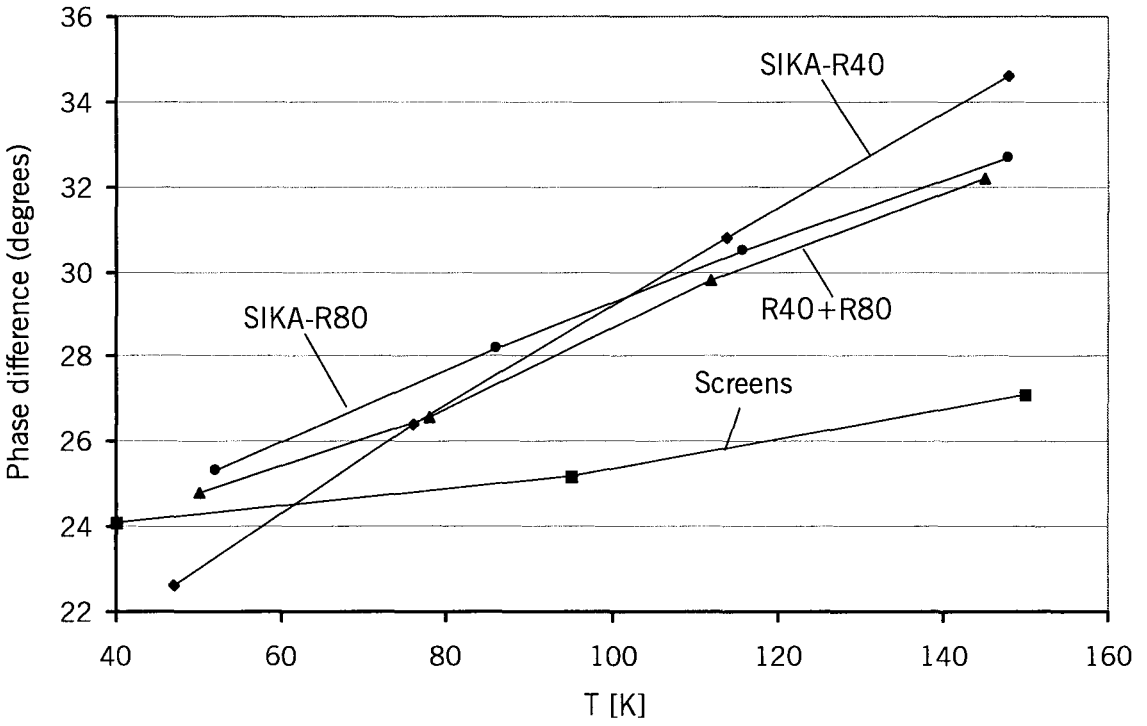

Figure H6 (p_m = 26 bar)

Figure H5 and H6: *The phase difference between p_C and p_E. The mean pressure is 21 bar (H5) and 21 bar (H6). The phase difference is temperature dependent for all materials, the screens showing the smallest and the SIKA-R40 material showing the largest temperature dependence.*